Fleetwide Models of Lane Departure Warning and Prevention Systems in the United States

Taylor Robert Johnson

Thesis submitted to the faculty of the Virginia Polytechnic Institute and State University in partial fulfillment of the requirement for the degree of

Master of Science
In
Biomedical Engineering

Hampton C. Gabler, Chair
Shane B. McLaughlin
Steven Rowson

December 7, 2016

Blacksburg, Virginia

Keywords: vehicle safety, active safety, road departure, lane keeping

Fleetwide Models of Lane Departure Warning and Prevention Systems in the United States

Taylor Robert Johnson

ABSTRACT

Road departure crashes are among the deadliest crash modes in the U.S. each year. In response, automakers have been developing lane departure active safety systems to alert drivers to impending departures. These lane departure warning (LDW) and lane departure prevention (LDP) systems have great potential to reduce the frequency and mitigate the severity of serious lane and road departure crashes. The objective of this thesis was to characterize lane and road departures to better understand the effect of systems such as LDW and LDP on single vehicle road departure crashes.

The research includes the following: 1) a characterization of lane departures through analysis of normal lane keeping behavior, 2) a characterization of road departure crashes through the development and validation of a real-world crash database of road departures (NCHRP 17-43 Lite), and 3) develop enhancements to the Virginia Tech LDW U.S. fleetwide benefits model.

Normal lane keeping behavior was found to vary with road characteristics such as lane width and road curvature. Consideration of the dynamic driving behaviors observed in the naturalistic driving study (NDS) data is important to avoid LDW false alarms and driver annoyance. Departure characteristics computed in normal driving were much less severe than the departure parameters measured in real-world road departure crashes.

The real-world crash data collected in NCHRP 17-43 Lite database was essential in developing enhancements to the existing Virginia Tech LDW fleetwide benefits model. Replacement of regression model predictions with measured crash data and improvement of the injury criteria resulted in an 11-16% effectiveness for road departure crashes, and an 11-15% reduction in seriously injured drivers.

Fleetwide Models of Lane Departure Warning and Prevention Systems in the United States

Taylor Robert Johnson

GENERAL AUDIENCE ABSTRACT

Road departure crashes account for nearly one-third of the roughly 30,000 automobile traffic fatalities in the U.S. each year. Lane departure warning (LDW) and lane departure prevention (LDP) systems are two safety systems developed to reduce the large number of fatalities resulting from road departures. The safety systems warn drivers if the vehicle begins to drift out of the intended lane of travel, and automatically steer the vehicle back into the lane of travel if it continues to drift. While LDW and LDP systems have potential to lower the number of fatal lane and road departure crashes, the technology is not yet a standard feature in production vehicles. There has been a lower than expected acceptance rate, and real-world benefits of the systems have not been published.

The research objective for this thesis was to characterize lane and road departures to investigate the effect of these safety systems on road departure crashes. The first section of this thesis analyzed large amounts of time series data recorded from people in normal driving scenarios to model lane keeping behavior in non-crash, drift out of lane departures. We found driving behavior varied with road characteristics such as lane width and road curvature. These dynamic driving behaviors may lead to LDW false alarms and contribute to driver annoyance with the systems.

The second portion of this research involved the development and validation of a real-world road departure crash database. The database included key departure parameters such as angle, speed, and road curvature. These parameters were used in the third section of the thesis to enhance the Virginia Tech LDW U.S. fleetwide benefits model, which is a mathematical trajectory simulation model that determines whether or not these road departure crashes could have been prevented if every vehicle in the U.S. was equipped with LDW. We found an effectiveness of 11-16% prevention for road departure crashes, and an 11-15% reduction in serious driver injury.

ACKNOWLEDGEMENTS

This research was funded by Toyota Motor Corporation and Toyota Engineering & Manufacturing North America, Inc.

I would like to start by thanking my advisor Dr. Clay Gabler for bringing me into the research group. You have been a great mentor throughout my time in grad school. I have gained experience, knowledge, and skills that I know will be useful in my career as an engineer. Also, thank you to Dr. Shane McLaughlin and Dr. Steven Rowson for agreeing to be on my committee and provide feedback.

I would also like to acknowledge Rini Sherony, Hiroyuki Takahashi, and Katsuhiko Iwazaki from Toyota for their helpful feedback on these studies.

Thank you Jackey, Nick, John, Whitney, Grace, David, Kay, Daniel, and Kaitlyn for helping on this research and providing feedback. You all have been a great group to work with over the past year. Also, thanks to all of my classmates, peers, and professors who I have had the pleasure to learn from during my time at Virginia Tech. I am proud to be a part of the Hokie community.

Finally, a big thank you to my family and mentors from NC for the continued support throughout my life. I could not have made it this far without you. You always encouraged me to live life, find something I enjoy, and work hard at it.

TABLE OF CONTENTS

List of Figures

List of Tables

1 INTRODUCTION

1.1 ROAD DEPARTURE FATALITIES

Motor vehicle traffic fatalities in the United States (U.S.) have declined over the past 40 years thanks to improved safety technology, stricter driving law enforcement, and educational efforts on issues such as drunk driving or texting while driving. Figure 1 illustrates the decrease in fatal crashes using the National Highway Traffic Safety Administration (NHTSA) Fatality Reporting System (FARS) data collected from 1975-2014. The FARS database is a nationwide census that records detailed information on fatal vehicle crashes each year. Although the number of fatal crashes has decreased, there are still about 30,000 per year [1].

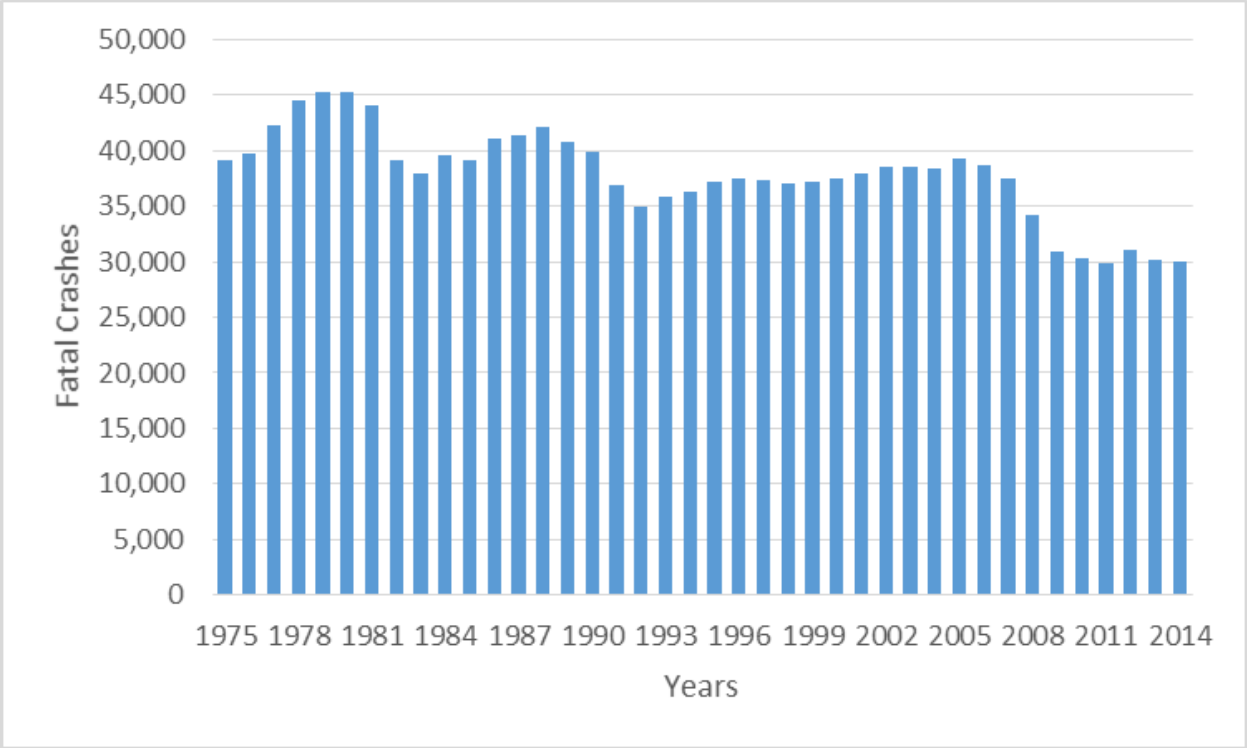

Figure 1. Traffic Fatalities from 1975-2014 [1]

Road departures account for a large portion of traffic fatalities each year and are among the deadliest crash modes in the United States. A previous study [2] reviewed departure crashes

occurring from 2010-2011 recorded in the National Automotive Sampling System (NASS) General Estimates System (GES) and FARS databases collected by NHTSA. Similar to FARS, the NASS/GES database is a nationally representative collection of police reported automobile crashes. However, GES contains crashes of all severity while FARS only contains fatal crashes. The review of these two databases found that for all crashes involving at least one passenger vehicle from 2010-2011, only 12% were single passenger vehicle ran off road departure crashes. However, single vehicle ran off road departures comprised nearly 1/3rd of all fatal crashes involving at least one passenger vehicle [2]. Ran off road crashes exclude cases where the driver experienced control loss or swerved to avoid an animal or object in the road. More recent FARS data shows nearly 5,500 single vehicle ran off road departure crashes occurred in 2014—a slightly lower 26% of all fatal passenger vehicle crashes. Regardless, road departures remain a highly harmful crash mode that needs to be addressed.

When vehicles depart the roadway, there is high potential to strike fixed roadside objects such as trees, poles, and traffic barriers. Some of these roadside safety features such as guardrails and crash cushions are designed to provide a more forgiving roadside environment [3]. However, collisions with these fixed objects can result in significant occupant compartment intrusion and high magnitude decelerations causing serious injury to the driver and passengers. Departure crashes involving factors such as control loss due to weather or swerving to avoid an animal or pedestrian in the road are difficult to predict with current technology. Electronic stability control (ESC) is one advanced technology, mandated in the U.S. since model year 2012, that mitigates control loss crashes. ESC detects when traction is compromised and automatically applies braking to individual wheels to assist the driver in regaining control [4]. These systems have great potential to reduce traffic fatalities [5][6], but ESC is unable to predict non-control loss road departures or drift out of lane departures. However, emerging lane departure safety systems promise to avoid drift out of lane departures induced by distracted driving, impairment, or driver error.

1.2 Lane Departure Warning and Prevention Systems

Most drivers are occasionally guilty of minor lane infractions. These events are generally corrected quickly and are either unnoticed, or have no consequence. However, in busy everyday lives, drivers can easily be distracted. In 2014, there were 3,179 occupants killed, 520 non-occupants killed, and over 400,000 occupants injured in distraction-influenced crashes [7]. A study on distracted driving performed by the Virginia Tech Transportation Institute (VTTI) found that when drivers were text messaging, they spent an average of 4.6 out of a 6 second interval looking at the device [8]. Driving at 89 kph, that is the equivalent of traveling further than the length of a football field without looking at the road [8]. During this time, a minor lane infraction can lead to a serious crash if the vehicle trajectory is not promptly corrected.

While distractions such as texting, reaching, or eating pose a prominent threat to automobile safety, there are other reasons drivers depart the road. A previous study [2] identified non-performance errors such as falling asleep, medical conditions (e.g., seizure), and other critical non-performance incidences as the cause for 22% of lane departure scenarios. As with distracted driving, it only takes a brief moment of falling asleep to significantly deviate from the lane of travel. Lane departure warning (LDW) and lane departure prevention (LDP) systems are two safety technologies that are becoming more prevalent in the vehicle fleet to help address lane and road departures.

LDW and LDP are often referred to as active safety systems. While passive safety systems, such as seatbelts and airbags, aim to reduce injury during a crash, active safety systems aim to predict and prevent crashes from ever occurring. Intersection Advanced Driver Assistance Systems (I-ADAS), for example, aim to predict when an intersection crash may occur and alert the driver or automatically perform evasive action [9][10][11][12]. Similarly, LDW systems detect impending lane departures and provide the driver with either a visual, audible, or tactile alert. If the driver fails to acknowledge the alert or does not make appropriate corrections, LDP can provide an automatic

steering input to guide the vehicle back into the initial lane of travel. The progression of LDW and LDP intervention is illustrated in Figure 2. These active safety systems have promising potential to reduce the number of crashes and injury severity [13][14][15][16][17][18]. In lane departure scenarios, even if drivers are unable to avoid a crash, the systems will help mitigate the outcome by alerting the driver before impact or automatically steering to reduce the lateral excursion.

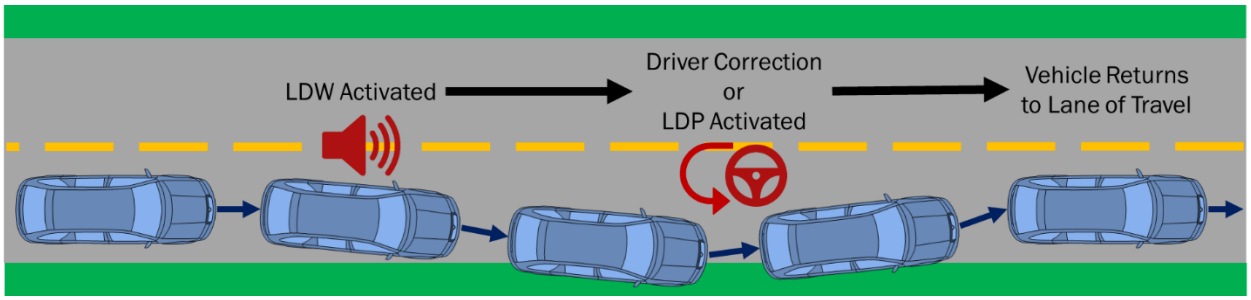

Figure 2. Progression of LDW and LDP System Intervention

Despite these promising benefits, driver acceptance has been lower than expected for lane departure systems. Other active safety systems such as forward collision warning (FCW) have also been challenged by driver acceptance [19][20][21][22]. However, a study performed by the Insurance Institute for Highway Safety (IIHS) monitored the usage of active safety systems in Honda vehicles being serviced at dealerships and found a significant difference between LDW and FCW acceptance rates [23]. The investigation found FCW was activated in nearly all vehicles, while LDW was disabled in 66% of the study sample. LDW appears to be plagued by nuisance alarms, triggering warnings when drivers feel they do not need one [23]. Drivers who maintain close proximity to the lane boundary or move at high lateral rates within the lane may experience false alarms. This low acceptance rate of LDW is also thought to be largely influenced by failure to use turn signals. Turn signals are one of the key triggers for LDW and LDP systems in distinguishing accidental from intentional lateral maneuvers and determining when to intervene. Drivers did not use turn signals in

about 50% of lane changes observed in a 2011 study [24]. In addition to low driver acceptance, another IIHS study [25] found no reduction in insurance claims for vehicles with LDW.

Driver behavior also plays a large role in the challenges engineers face when designing LDW and LDP systems. Studies have shown driving behavior changes with factors such as vehicle type, time of day, weather/road surface conditions, and driver age [26][27]. Every driver has different driving characteristics. A single driver may even have multiple driving behaviors depending on traffic, time of day, and road demographics. The systems are prone to false positive alarms, where warnings are delivered to the driver when the driver feels there is no risk of departure. Current production systems, including the Toyota Lane Departure Alert (LDA), permit drivers to change the warning sensitivity level preference [28]. However, drivers who constantly drive or drift close to the lane boundary may not find a setting that avoids false positive warnings. The concern is that drivers may completely disable the system if these false alarms become an annoyance, resulting in no potential benefits.

1.3 New Car Assessment Program Lane Departure Confirmation Testing

One method with which lane departure systems are currently being evaluated is the New Car Assessment Program (NCAP) performed by NHTSA. The NCAP was designed in 1979 to examine the crashworthiness of new vehicles entering the U.S. fleet. NCAP evaluates crash performance in frontal, side, and overlap tests using fully instrumented vehicles and crash dummies. Ratings from one to five stars are assigned so consumers have a way to quantify vehicle safety. Since consumers are more likely to purchase highly rated vehicles, there is incentive for manufacturers to invest in building safer vehicles [29].

In addition to testing crashworthiness, the NCAP more recently began to evaluate crash avoidance technology in an effort to recommend standard safety features for future vehicle models.

The confirmation testing includes forward collision warning (FCW) and LDW/LDP. The LDW component of NCAP testing introduced in 2011 requires the following [30]:

- Forward speed of 72 kph
- Lateral velocity of 0.5 m/s
- Testing of departures on both the left and right side of the lane
- Testing of continuous white, discontinuous yellow, and discontinuous raised markers
- Each combination of test conditions replicated five times

Each trial involves an induced lane departure. After the vehicle passes through the start gate at the appropriate speed, the test driver steers the vehicle towards the desired departure side. The driver releases the steering wheel prior to departure and the distance to lane boundary (DTLB) is recorded at the instant the LDW is delivered. A positive DTLB indicates the vehicle is still within the lane boundary. The warning DTLB must be between -0.3 m and 0.75 m to receive a passing grade, and must pass 3 of the 5 replicated trials [30]. Figure 3 illustrates the test configuration. The goal of this testing is to confirm these systems work and provide reasonable warnings for consumer use. However, this is an idealized test setup that does not include variation in factors such as lighting condition, road curvature, or vehicle forward and lateral speed [31].

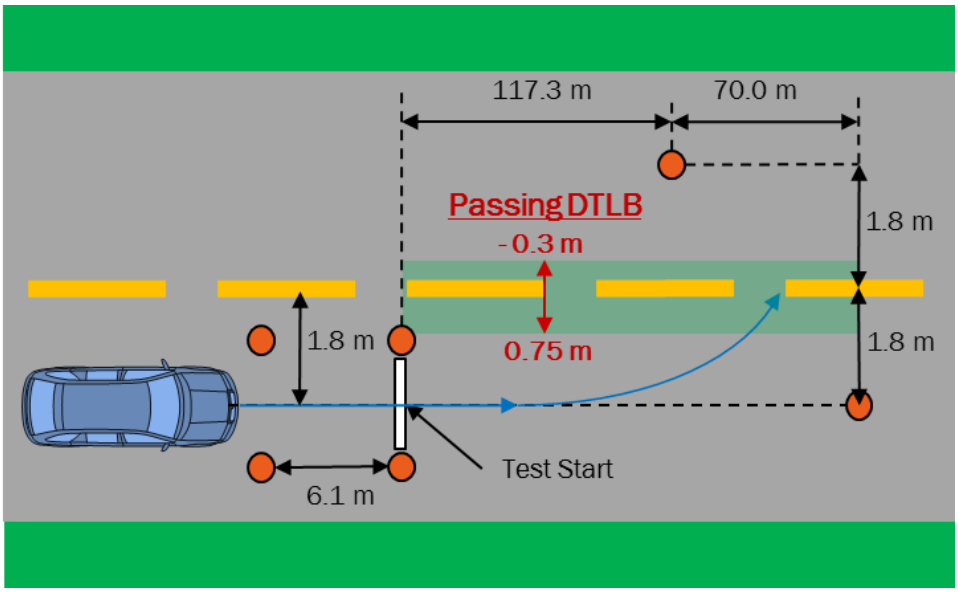

Figure 3. NCAP LDW Confirmation Test Setup for Left Side Departure

1.4 European New Car Assessment Program Lane Support Systems Testing

The European version of the NCAP (Euro NCAP) is similar to the NHTSA NCAP in that it provides safety ratings for consumers. The Euro NCAP also tests additional active safety systems such as lane departure warning and prevention. The general process for LDW confirmation is the same as the NHTSA NCAP. A driver steers the vehicle towards the lane boundary, and the point of LDW delivery is recorded. The Euro NCAP was modeled after the NHTSA NCAP and still uses specifications such as a forward speed of 72 kph and testing of both left and right side departures. The main differences, however, are that the Euro NCAP defines a target turning maneuver radius of 1,200 m and performs tests at both 0.3 and 0.5 m/s lateral velocities. The NHTSA NCAP only tested one lateral rate. The Euro NCAP also only tests solid and dashed lane markings. [32]

1.5 Research Objective

Although automakers are rapidly deploying active safety systems to reduce the number of serious lane and road departure crashes in the U.S. in recent years, road departures remain an

extremely harmful and prevalent crash mode. The LDW and LDP systems are still fairly new technology and are not yet widely accepted by drivers. The goal of this research was to characterize lane and road departures to better understand how lane departure safety systems can reduce the number and severity of single vehicle road departure crashes. The study contains a characterization of normal lane keeping behavior through naturalistic driving study data, a characterization of road departure crashes using real-world crash data, and models for predicting the potential fleetwide benefits of LDW systems.

2 CHARACTERIZING LANE DEPARTURES THROUGH NATURALISTIC DRIVING STUDY DATA

2.1 BACKGROUND

To reduce the number and severity of lane and road departure crashes, as well as increase driver acceptance of LDW/LDP systems, it is important to first understand normal driving behavior. Naturalistic driving studies (NDS) are a unique resource that can provide valuable realistic insight into everyday driving [33][34]. In a typical NDS, a large number of vehicles are instrumented with cameras and sensors to record data. Individuals are recruited to drive these instrumented vehicles in their day to day activities over the duration of the NDS. This allows researchers to monitor driver behavioral characteristics such as braking, turn signal use, and acceleration profiles for a sample population. Researchers can also collect information on driver distractions such as texting or eating.

The data collected in NDS is a valuable tool for characterizing lane departures. One application this research aimed to explore was to build a simple driver model of lane departure and recovery behavior. Using vehicle kinematic data and lane tracking technology, the movement of the vehicle with respect to the lane of travel was analyzed. Lane keeping behavior models developed using NDS data has potential to be used for enhancement of current LDW/LDP systems, improving intervention timing and minimizing false alarms.

Commercial LDW and LDP systems are proprietary and the algorithms governing intervention timing are not publicly available. However, it is believed that lateral distance to lane boundary (DTLB) and lateral velocity are two key components in determining if the departure systems should intervene. As previously discussed in the outline of the NCAP assessment for LDW systems, DTLB is a commonly used metric in lane tracking analyses. DTLB is defined as the lateral distance between the leading edge of the vehicle and the lane boundary. A positive DTLB indicates

the vehicle is still within the lane of travel. A negative DTLB indicates the vehicle has crossed the lane boundary.

The inclusion of a rate dependent term, lateral velocity, has the potential to be a better method for determining intervention timing than relying on DTLB alone. The NCAP evaluation, for example, assumes a single constant lateral velocity. Combining lateral velocity and DTLB allows for a better predictive measure of driver intent with respect to lane keeping behavior. There is opportunity with NDS data to build a simple model of lane keeping because both lateral velocity and DTLB, along with other roadway characteristics, are derived from data recorded by the instrumented forward facing cameras and lane tracking algorithms. To be consistent with previous research and established conventions, the sign conventions used throughout this thesis for DTLB and lateral velocity are illustrated in Figure 4. Lateral velocity is the time derivative of DTLB, where a positive value indicates the vehicle is departing further from the lane center, and a negative value indicates the vehicle is recovering back towards the lane center. Data elements were always taken from whichever side of the lane the vehicle was closer to, so sign conventions remained consistent regardless of whether the vehicle was approaching a left or right side departure.

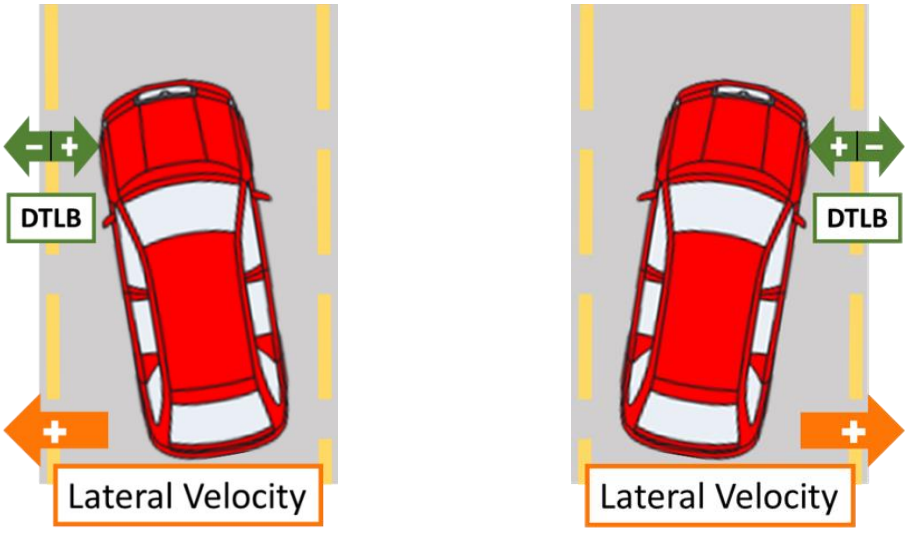

Figure 4. Conventions for DTLB and lateral velocity

Fujishiro and Takahashi (2015) conducted a NDS in Japan to characterize and visualize lane keeping behavior. This study generated a methodology to quantify normal driving behavior through the relationship of DTLB and lateral velocity. It was hypothesized that this normal driving distribution would change with road characteristics such as lane width and road radius of curvature [35]. Fujishiro and Takahashi found that as lanes became narrower and roads became more sharply curved, drivers tended to deviate further from the lane of travel. They also found that lateral velocity decreased as drivers approached the lane boundaries.

The objective of this chapter was to characterize the problem of common drift out of lane departures through the analysis of NDS data. Adopting the approach established by [35], two U.S. NDS datasets were analyzed to quantify normal lane keeping behavior and determine how behavior changes with lane width and road curvature. Understanding normal driving behavior is believed to be essential in identifying the limitations of lane departure active safety systems, especially in terms of driver acceptance.

2.2 DATA SOURCES

Two studies were performed using different NDS data sources: the Integrated Vehicle-Based Safety Systems (IVBSS) NDS conducted by the University of Michigan Transportation Research Institute (UMTRI) [36] and the Virginia Tech Transportation Institute (VTTI) 100-Car NDS [37]. The two data sources are outlined in the following discussion

2.2.1 UMTRI IVBSS DATA SELECTION

The goal of the IVBSS NDS was to investigate the effectiveness of vehicle safety systems and monitor driver behavior. IVBSS assessed a number of active safety technologies including forward collision warning (FCW), lane change/merge (LCM) warning, blind spot monitoring (BSM), curve speed warning (CSW), and lane departure warning (LDW). The lane departure portion of the IVBSS

study consisted of 108 drivers randomly selected to participate in a 40 day test period. During the testing phase, each driver was provided a 2006 or 2007 Honda Accord retrofitted with sensors, cameras, and LDW. The drivers were instructed not to change their daily driving routing and proceed as they normally would in their own car. [36]

For the first 12 days, a baseline was established where data was collected while vehicles were driven, but the LDW system was disabled and no warnings were delivered if a lane or road departure was detected. The remaining 28 days acted as a treatment period where drivers did receive warnings from the LDW system when departures were detected. Over 147,000 km of driving data was collected in the testing period and 12,760 unintentional drift out of lane departure events were collected by UMTRI. To be classified as an unintentional lane departure, the following criteria had to be met [36]:

- Known lane boundary type (no virtual boundaries)
- 100% lane tracking software confidence
- No braking, lane change, or turn signal use during the departure event
- Buffer time of 5 seconds before/after any intentional maneuver
- Vehicle returned to lane in 20 seconds or less
- Vehicle speed above 40.2 kph

For each of the lane departure events identified by UMTRI, time series data was provided including the duration of the departure event, plus 30 seconds before the leading wheel first crossed the lane boundary and 30 seconds after the vehicle fully returned to the initial lane of travel. The time series lane tracking data was the basis for generating the population driving behavior models in this thesis.

Figure 5 illustrates the two phases of LDW data collection in IVBSS. Note that the ratio of number of lane departure events per day was roughly doubled for the baseline period when LDW

was disabled. For the treatment period when LDW was enabled, drivers may have become more cautious in nature due to the warnings, or the LDW system may have been effective at warning drivers and preventing lane departures. Regardless of the reason, the LDW clearly had a significant influence on lane keeping behavior. Since the goal of this chapter was to characterize and understand normal driving behavior, only data from the baseline period subset of 5,833 lane departure events was used. Sampled at 10 Hz, there were nearly 2 million valid time series data points for analysis of normal lane keeping behavior.

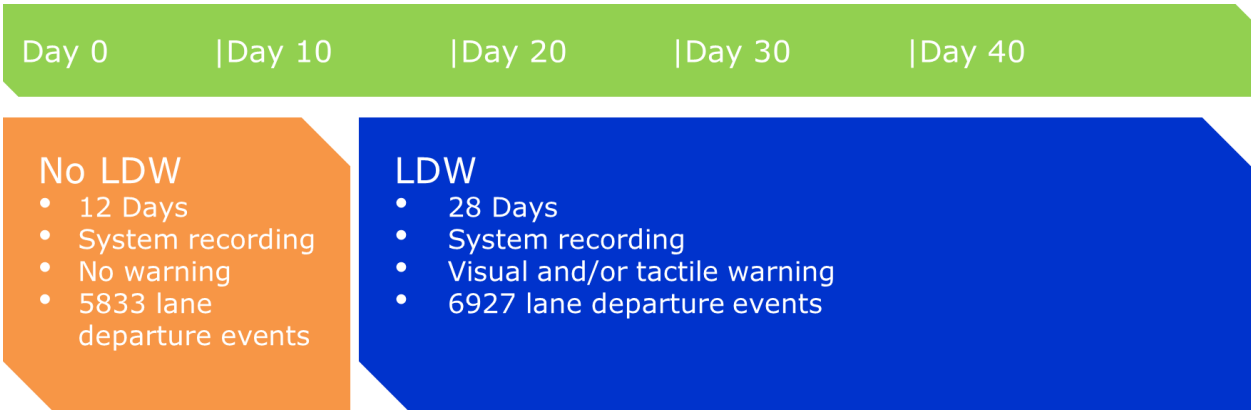

Figure 5. IVBSS Timeline for LDW Data Collection

2.2.2 VTTI 100-Car Data Selection

The VTTI 100-Car study was another NDS with a goal of collecting a large quantity of normal driving data from vehicles equipped with inertial sensors and cameras. The study [37] was conducted in the Northern Virginia/Washington, DC area and consisted of roughly one year of data collection from 100 vehicles. Over the duration of the study, nearly 43,000 hours and over 3.2 million kilometers of naturalistic driving data was collected from the vehicle Controller Area Network (CAN) bus, accelerometers, and video cameras installed in each car [37]. Data provided for this thesis from VTTI was a subset of the 100-Car dataset—133,000 full-trip time series data files. The benefit of having full-trip files, compared to the flagged lane departure segments provided by UMTRI for the

IVBSS study, was that the dataset contained much more normal in-lane driving data. However, it also meant that data quality checks and strict filters were required to ensure lane tracking data used for the study was accurate and consistently reliable.

The first round of data processing identified drivers with consistently high quality lane tracking data and working instrumentation. This step excluded drivers who were not primary drivers, drove less than 100 days, or had invalid lane tracking data in more than 40% of all trips or 40% of total driving distance. The resulting subset contained 45 unique drivers. The second pass of data quality check applied some of the same criteria used to identify lane departures in the IVBSS NDS including 100% lane tracking confidence, known and real lane boundaries, and vehicle speed above 40.2 kph [36]. Additionally, a minimum 60 second window of meeting these criteria was required to be included in the analysis. This window ensured adequate segments of time series data were available to perform computations and model driving behavior. The second round of data processing removed an additional three drivers due to noisy lane tracking confidence signals. Two additional drivers were manually removed due to obstructions to the camera view resulting in physically unrealistic lane measurements such as negative lane widths.

The final subset for this 100-Car lane keeping behavior analysis contained data from 40 drivers and 6,109 trips. Unlike with IVBSS data, VTTI did not identify and validate unintentional drift out of lane departure events. Therefore, an algorithm was developed to identify lane departures based on lane tracking data. To be considered a valid lane departure, the DTLB had to be negative for more than one time step (> 0.1 s) and the departure could not last more than 20 s. In the 6,109 trip files, 4,506 lane departure events were identified. Over 16 million time series points sampled at 10 Hz accompanied these departures to generate the normal driving distribution.

2.2.3 *Removal of Artifacts in Lane Tracking Data*

Lane tracking technology is still relatively new and is not without issues. The accuracy of these systems is highly dependent on factors such as roadway surface conditions, weather, and lighting. If lane markings are not present or covered by snow, the forward facing camera will struggle to track boundaries. If the sun is at a low angle flooding the camera with light, the system may experience camera washout and be unable to distinguish the contrast of lane lines. Both IVBSS and 100-Car datasets contained these artifacts of machine vision. While many of the issues with surface conditions and lighting were likely caught by the 100% lane tracking confidence filter used while processing IVBSS and 100-Car data, the more problematic artifacts were ones where the lane tracking system had high confidence that it was tracking a lane boundary, but it may not have been the correct lane line. Instances like these appeared when there were intentional lane changes, vehicles traveled through intersections, or there was a merging lane. Artifacts were discovered when deriving lateral velocity from DTLB inflated the error and produced unrealistic (> 5 m/s) values.

Figure 6 shows an example case in the IVBSS data that had two lane changes prior to the first lane departure event. When a vehicle intentionally changes lanes, the lane tracking systems have to transition and jump to the new boundaries. For intersections and lane merges, the system often loses sight of the true lane boundaries and scrambles to find the next closest one. These situations generate rapid spikes and other abnormal characteristics in the DTLB signal. The majority of these artifacts in IVBSS and 100-Car were the product of lane changes resulting in spikes similar to the two shown in Figure 6. NDS data typically has a turn signal record, but since signal use is low in the U.S. and is not always used for the full duration of the maneuver it is not a reliable lane change flag. The approach for removal of invalid IVBSS data was to identify prominent peaks with DTLB values beyond the specified maximum excursion assigned to each departure event by UMTRI, and remove a 10 second window surrounding the peak. The typical duration of a lane change has been found to be between

1.0 and 13.3 seconds, with an average of 4.6 seconds [38]. Manual inspection of a sample of these lane change spikes in IVBSS data showed good agreement with these durations, averaging between 5 and 6 second peak widths. Therefore, the selected 10 second window of removal was found to be a conservative approach.

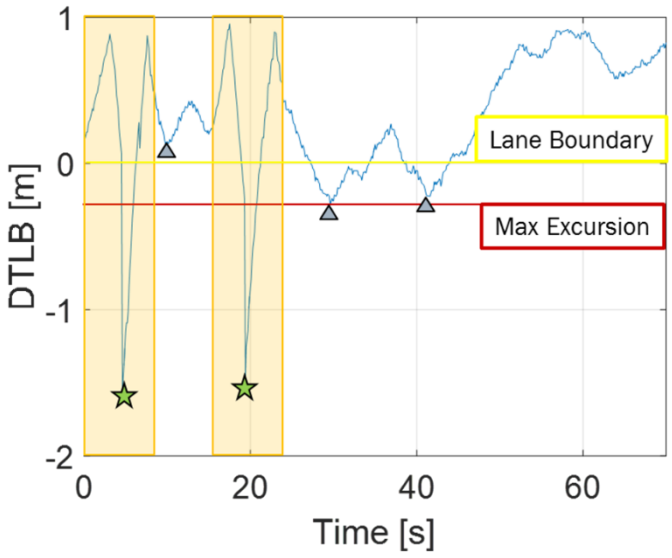

Figure 6. Removing Artifacts in Lane Tracking Data

For the 100-Car data artifacts, a previous study [39] identified lane change events based on a similar method of detecting steep changes in DTLB for the subset of 45 drivers from the first pass of data processing. Any data in the remaining 6,109 trips that fell between the start and end of a flagged lane change event was excluded. Although some abnormalities in the DTLB signal remained, this greatly reduced the amount of data with unrealistic lateral velocities above 5 m/s. Less than 0.5% of the millions of time series data points in both the IVBSS and 100-Car studies had these high lateral velocities after removing the majority of these lane tracking artifacts.

2.3 METHODS

As previously discussed, the methodology for quantifying normal lane keeping behavior in the U.S. was motivated by and adopted from [35]. Characterizing the normal driving behavior centers around the distribution of lateral velocity and DTLB. This section will outline the visualization techniques and equations used to generate plots of normal lane keeping behavior.

For an overall view of the normal driving distribution based on time series data, a scatter density plot was generated for each NDS dataset of lateral velocity and DTLB. Figure 7 shows a sample plot. The scatter density plot of lateral velocity and DTLB show where the majority of data fall based on the color coded frequency scale. From this figure, it is easy to identify a high frequency yellow center encompassing a lateral velocity of 0 m/s and a DTLB within the lane of travel. The lower frequency dark blue data model less common driving behaviors. The grey arrows indicate the clockwise direction of flow if you were to trace vehicle trajectories. Starting from the center of the distribution, as drivers increase lateral velocity the vehicle moves closer to the lane boundary—sometimes crossing the boundary. Lateral velocity approaches zero as drivers reach a minimum DTLB. Drivers then recover with a negative lateral velocity as the vehicle shifts back up to a more positive DTLB.

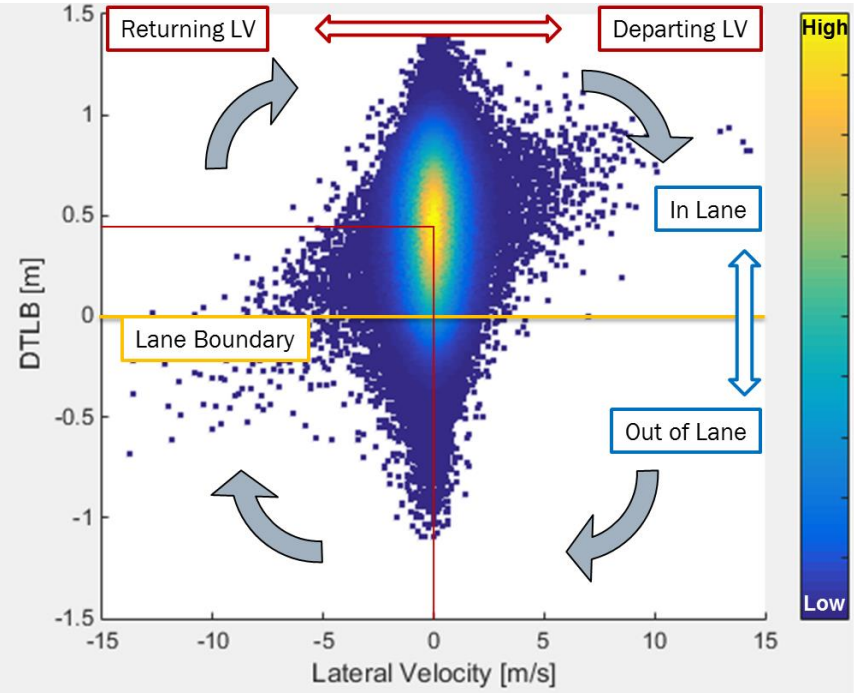

Figure 7. Sample Scatter Density Plot of Normal Driving Distribution

In Figure 7, several ellipsoidal color bands are visible towards the center of the distribution. To more cleanly define boundaries in the normal driving distribution, Fujishiro and Takahashi (2015) derived ellipsoidal isopleths from the 2D normal distribution probability density function shown in Equation 1. Here, V is lateral velocity, D is DTLB, and the mean and standard deviation for each parameter are μ and σ, respectively.

$$f(V,D) = \frac{1}{2\pi\sigma_V\sigma_D}\exp\left[-\frac{1}{2}\left(\frac{(V-\mu_V)^2}{\sigma_V^2}+\frac{(D-\mu_D)^2}{\sigma_D^2}\right)\right] \qquad \textbf{Equation 1}$$

Integrating Equation 1 over an ellipse, S, gives the probability, P, that data falls within the ellipse region. Equation 2 shows the derivation of this relationship, where $-c^2/2$ is set equal to the exponent portion of Equation 1.

$$P = \iint_S f(V,D)dS = \iint_S \frac{1}{2\pi\sigma_V\sigma_D}\exp\left[-\frac{c^2}{2}\right]dVdD = 1 - \exp\left[-\frac{c^2}{2}\right] \quad \textbf{Equation 2}$$

Simplifying and substituting the exponent back in for $-c^2/2$ results in Equation 3, an ellipse equation associated with the lateral velocity – DTLB relationship and the corresponding means and standard deviations. For the IVBSS and 100-Car studies, as well as [35], a P of 99% was selected to capture as much of the driving data as possible and represent the normal driving region. Data that falls outside the 99% ellipsoidal isopleth is considered irregular driving behavior where the driver should be warned and the trajectory corrected.

$$\ln(1-P) = -\frac{1}{2}\left(\frac{(V-\mu_V)^2}{\sigma_V^2} + \frac{(D-\mu_D)^2}{\sigma_D^2}\right) \quad \textbf{Equation 3}$$

To investigate how the normal lane keeping ellipsoidal isopleths change with road demographics, such as lane width and road curvature, two more variables were defined. Lane width was simply measured by the lane tracking system as the distance between the left and right lane boundaries. However, *CurveG* was a derived variable equivalent to centripetal acceleration used to help classify curve severity [35]. *CurveG* is defined by Equation 4, where *Speed* is the vehicle instantaneous forward travel velocity and *ROC* is the road radius of curvature. High *CurveG* values indicate more sharply curved roads, while low *CurveG* values represent straighter roads.

$$CurveG = \frac{Speed^2}{ROC} \quad \textbf{Equation 4}$$

Equation 4 was used for the 100-Car study and [35] because *ROC* was computed and recorded by the instrumented lane tracking systems. For IVBSS, the roadway radius of curvature data element was not provided with the subset of lane departure time series data. An alternate form of *ROC* was computed for IVBSS shown in Equation 5, where *YawRate* is the yaw rate of the vehicle. Note this method relies on vehicle yaw rate, which has potential to bias roadway *ROC* due to inherent noise in

angular rate sensors and the dependence on vehicle lateral motion. However, the overall dataset for IVBSS showed small lateral departure distances and low lateral velocities, so the lane departures were considered minor events. The vehicle curvature characteristics in IVBSS were assumed to reasonably follow roadway curvature characteristics.

$$ROC = \frac{Speed}{YawRate} \qquad \textbf{Equation 5}$$

Substituting the *ROC* equivalent from Equation 5 into Equation 4, *CurveG* for IVBSS is defined in Equation 6.

$$CurveG = \frac{Speed^2}{\left(\frac{Speed}{YawRate}\right)} = Speed * YawRate \qquad \textbf{Equation 6}$$

2.4 RESULTS

Although the two NDS data sources used in this chapter differed in duration, location, and driving population, the following distributions show the data population statistics are generally in agreement. Figure 8 shows the cumulative distribution for vehicle travel speed for all time points. The median speed for the 100-Car data was 102.0 kph, while IVBSS had a slightly higher median at 113.6 kph. These speeds indicate the majority of the valid lane departure data were likely captured on highways where speed limits are above 90 kph.

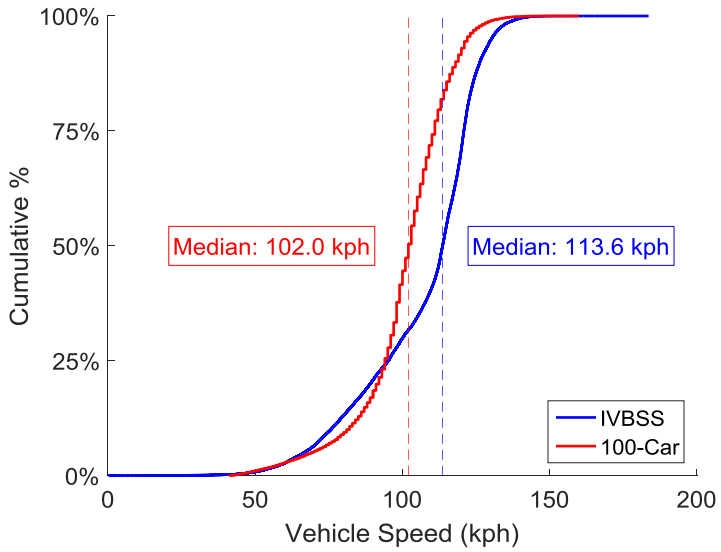

Figure 8. Distribution of Vehicle Travel Speed

The cumulative distribution for departure angle is shown in Figure 9. The median departure angle for IVBSS drift out of lane departures was 0.6 degrees. The median angle for 100-Car was 0.4 degrees. These angles are extremely small and confirm the lane departures in the two NDS were primarily minor lane infractions that were easy to recover from.

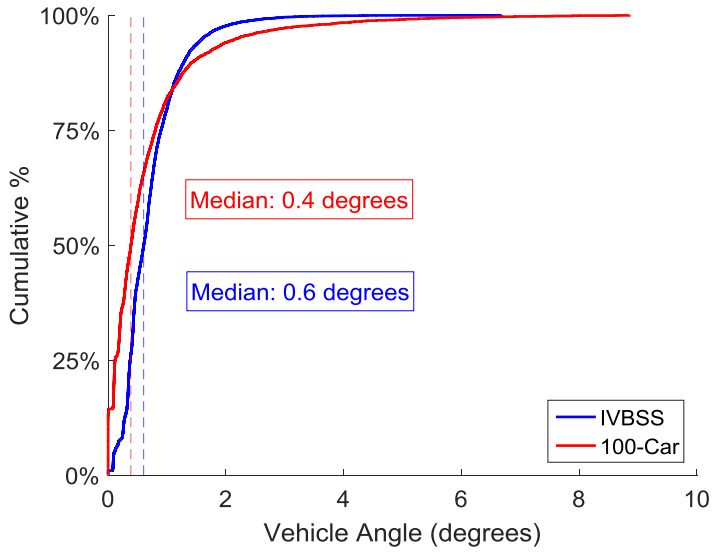

Figure 9. Distribution of Vehicle Departure Angle

Figure 10 illustrates the cumulative distribution for lane width in the two datasets at all valid data points. IVBSS had a lower median at 3.4 m compared to 100-Car with a median width of 3.8 m. The standard lane width for primary roads in the U.S. is 3.6 m [40], which lies between these two median values. The 100-Car data did appear to have more unusually high lane widths than IVBSS, but lane widths above 4 m were typically found to be lane tracking artifacts when additional width was added as vehicles entered or exited a merge or turn lane.

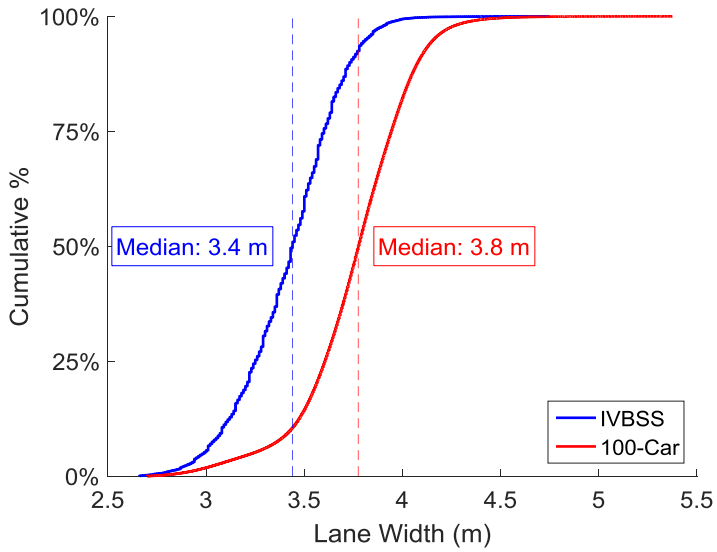

Figure 10. Distribution of Roadway Lane Width

The cumulative distribution of *CurveG* is shown in Figure 11. Both NDS data had medians of 0.2 m/s^2. This relatively low *CurveG* median indicates most of the lane keeping and departure data used in these studies occurred on fairly straight roads. Again, primary highway roads are unlikely to have sharply curved roads with higher speed limits. Also note that the *CurveG* distributions are very similar, indicating the assumptions made to derive *ROC* from vehicle yaw rate was reasonable.

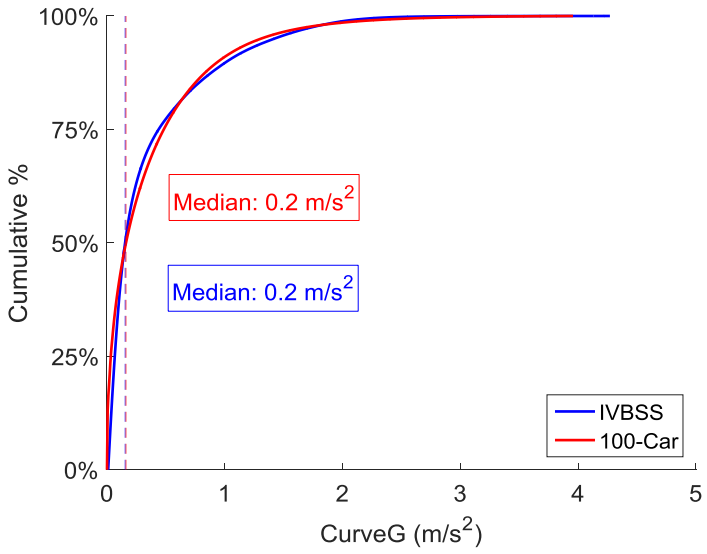

Figure 11. Distribution of Roadway Curvature (*CurveG*)

The maximum lateral excursion for each lane departure event in the two studies is illustrated in the cumulative distribution of Figure 12. The median for both NDS was 0.1 m. The drift out of lane departures in IVBSS and 100-Car were very minor and resulted in no crashes.

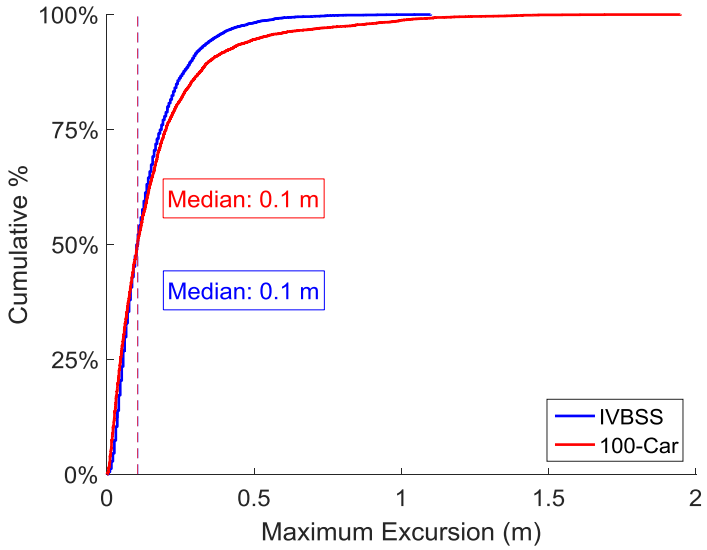

Figure 12. Distribution of Maximum Excursion Out of Lane

Figure 13 shows the departure duration for each lane departure event in the two NDS. The median time out of lane for IVBSS was 1.5 s. The median departure duration for 100-Car was slightly lower at 1.1 s. Again, this distribution of departure duration shows drivers recovered quickly back into the lane of travel and did not experience significant lane departures. Some drivers did remain over the lane boundary for longer durations, but it was found that many of these infractions were committed by drivers who consistently drive close to or on the lane boundary.

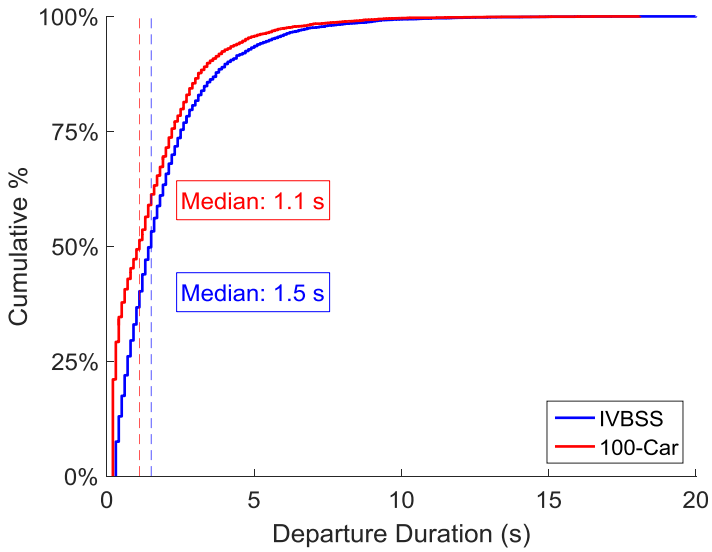

Figure 13. Distribution of Departure Duration

These cumulative distributions show similarities between the two NDS used in this chapter to characterize normal lane keeping behavior. The majority of the valid data used in these analyses was likely collected on highways consisting of wider lanes and straight to moderately curved roads. It is important to note, however, the ratio of time series data used to departures. In IVBSS, there was about 55 hours of valid data used in the normal driving distribution and 5,833 lane departure events. In 100-Car, there was about 463 hours of valid lane keeping data used and 4,506 identified lane departure events. The 100-Car data likely captured more in-lane driving, as previously mentioned, compared to IVBSS, which specifically targeted data immediately surrounding a departure event. It

is also important to note the distribution of departures per driver. Figure 14 and Figure 15 show the number of departure events per driver for the IVBSS and 100-Car datasets, respectively. In IVBSS, 20% of the drivers committed 63% of the drift out of lane departures. In 100-Car, 20% of the drivers committed 72% of the lane departures. In both NDS datasets, at least one driver did not experience any lane departures.

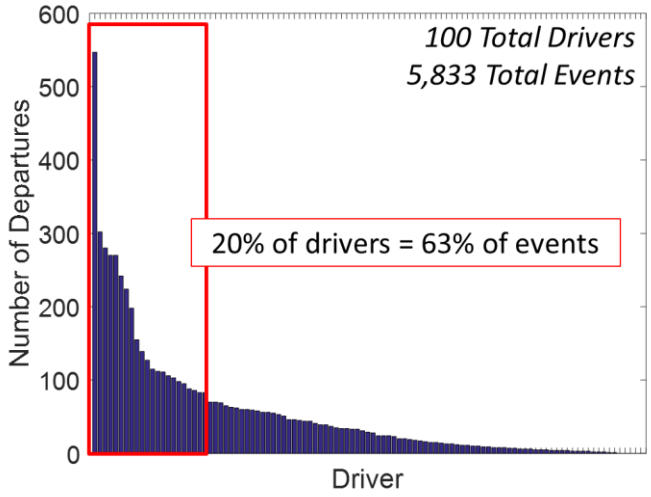

Figure 14. Distribution of Departures Committed Per Driver in IVBSS

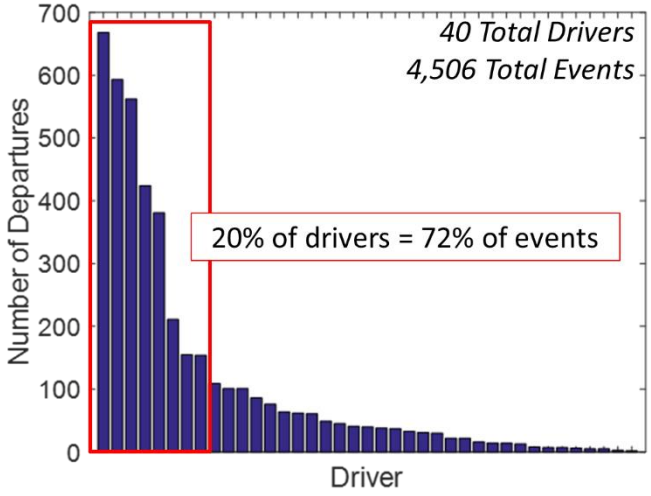

Figure 15. Distribution of Departures Committed Per Driver in 100-Car

These distributions illustrate the need for a dynamic LDW system, as normal lane keeping behavior varies widely among drivers. The normal driving distributions for each study are displayed and compared in sections 2.4.1 and 2.4.2.

2.4.1 IVBSS NORMAL DRIVING DISTRIBUTION

The normal lane keeping distribution generated for the IVBSS NDS is shown in Figure 16. The left portion of Figure 16 displays the overall driving distribution. Here, the scatter density plot shows a high frequency center around a lateral velocity of 0 m/s and just under a 0.5 m DTLB. This means drivers in the IVBSS NDS most commonly maintained a straight trajectory with respect to the lane markings, about 0.5 m from the lane boundary. The right side of Figure 16 is a zoomed in window to more easily view the 99% normal driving behavior boundary. Nearly all of the data except for the dark blue low frequency data falls within the pink ellipse. The key characteristic points of interest in the ellipsoidal isopleths are the right most boundary (highest lateral velocity), the lower boundary (furthest deviation from lane center), and the intersection with the lane boundary (0 m DTLB). These three characteristics can be used to define and understand limits of normal driving behavior in the sample population. It is important to note that some of the dark blue data points fall outside realistic ranges (> 5m/s) for lateral velocity. As previously discussed, this was found to be caused primarily by machine vision artifacts in the lane tracking data from multiple drivers and trips. A large portion of these artifacts were removed using the algorithm previously described. However, some of these jumps in DTLB were not caught by the algorithm and could not be validated with video because video was only available for 10 seconds before and 10 seconds after the departure event. These remaining outliers were assumed to be machine vision artifacts. Regardless, they account for a small percentage of the nearly 2 million data points and were not found to significantly affect the normal lane keeping boundary.

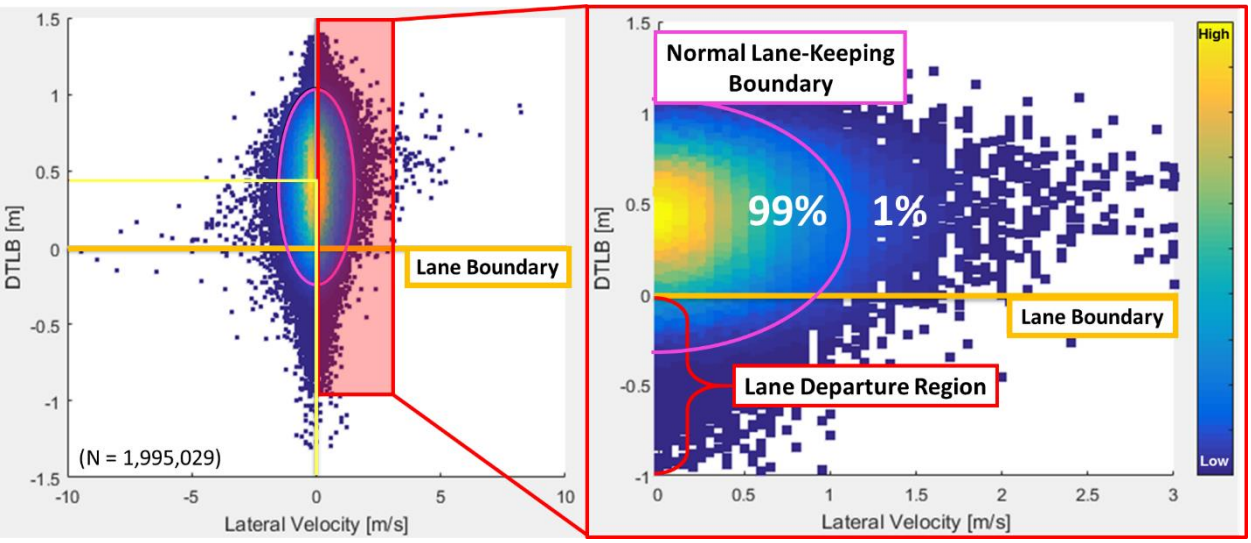

Figure 16. Normal Driving Distribution for the IVBSS NDS

The ellipse methodology was applied to various subsets of the IVBSS data to investigate the effects of lane width and road curvature on normal lane keeping behavior. Lane width and *CurveG* divisions were established based on the cumulative distributions previously discussed. Figure 17 shows the effect of road curvature on driving behavior. The IVBSS data was first divided into three lane width groupings—wide, median, and narrow—and then into three *CurveG* levels within each lane width group. In each lane width group of Figure 17, it is clear that as *CurveG* increases, or roads become more sharply curved, the ellipses grow in size. The right side limit and the lower limit both increase, demonstrating that drivers reach higher lateral velocities with respect to lane boundaries and deviate further from the lane center as road curvature increases. Note that the lower limit for all of the ellipses is well below the lane boundary at a DTLB of 0m, which means minor lane departures are still within the normal driving region for this sample population. It is also apparent from the intersection of the normal lane keeping ellipse and the lane boundary that lateral velocity decreases as drivers approach the lane boundary. This is intuitive, as drivers attempt to minimize the time and distance traveled out of lane.

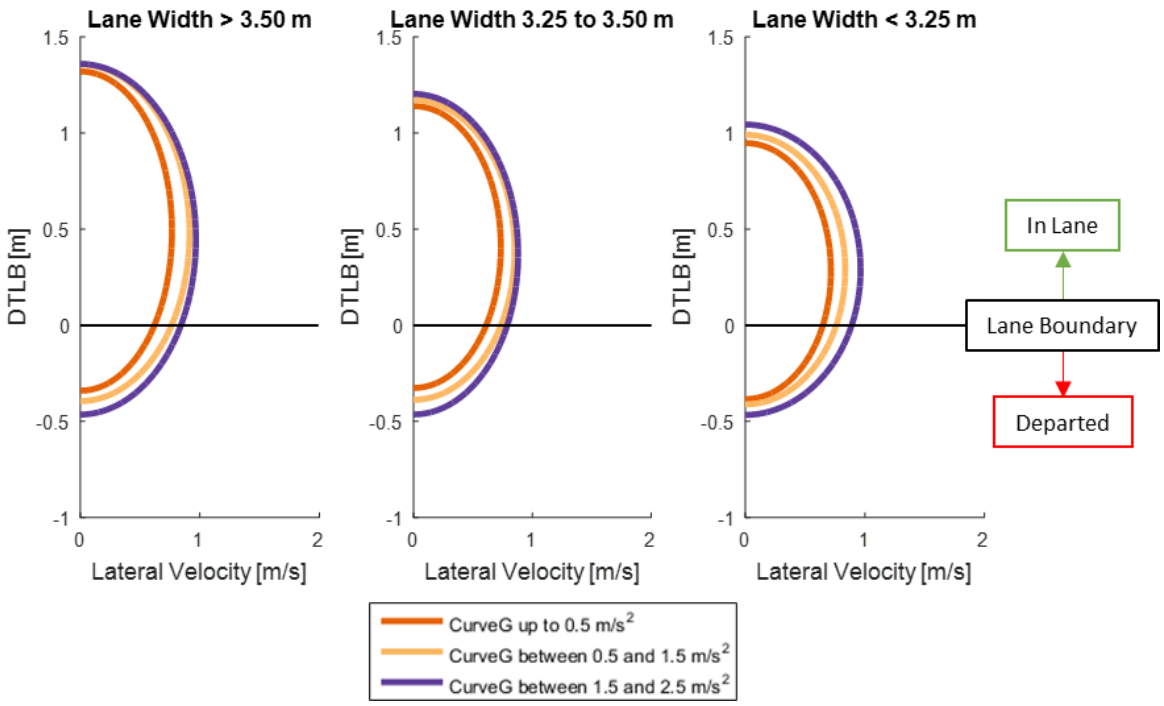

Figure 17. The Effect of Road Curvature on Normal Driving Behavior Distribution in IVBSS

Reversing the order of data subsets, the influence of lane width on driving behavior can be investigated. The resulting 99% ellipses are shown in Figure 18. The IVBSS data was divided first by *CurveG*, and then three lane width levels within each *CurveG* group. The sets of driving boundaries in these three subplots do not exhibit the same characteristics as Figure 17. The maximum lateral velocity for each subgroup is roughly the same, and the minimum DTLB appears to converge to a common value. This means that as lane width varied in the IVBSS NDS, driving behavior remained relatively constant. This is not consistent with what Fujishiro and Takahashi (2015) found in the Japan dataset [35]. However, it is important to recall that the IVBSS data is biased towards lane departure events and did not contain a large variety of road demographics.

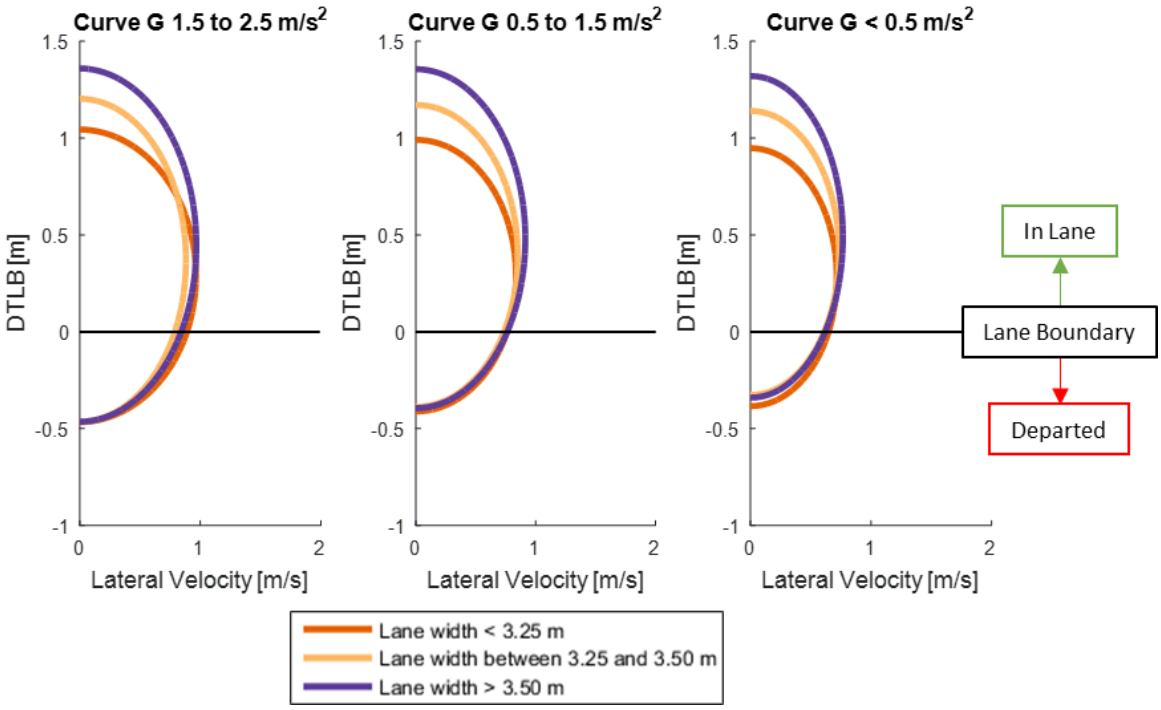

Figure 18. The Effect of Lane Width on Normal Driving Behavior Distribution in IVBSS

2.4.2 100-Car Normal Driving Distribution

The normal lane keeping distribution generated for the 100-Car NDS is shown in Figure 19. The left portion of Figure 19 displays the overall driving distribution. The 100-Car distribution appears different in several aspects compared to the IVBSS distribution. The distribution center is higher and there is a wider spread of data points. The 100-Car scatter density plot shows a high frequency center at a lateral velocity of 0 m/s as IVBSS did, but the DTLB centers around 0.75 m. This means drivers in the 100-Car NDS primarily drove about 0.75 m from the lane boundary with minimal lateral movement. The DTLB center of 0.75 m is closer to the distribution distance reported in [35] and is likely higher than IVBSS because the 100-Car data contained more in-lane normal driving data. It was not restricted to only data surrounding lane departures. The right side of Figure 19 is a zoomed in window of the normal driving distribution and clearly illustrates the 99% ellipse boundary. Although the dark blue region appears very large and dense in Figure 19, it only accounts

for about 1% of the data collected. As with IVBSS, the majority of this dark blue region with unrealistic (> 5 m/s) lateral speeds was generated by machine vision artifacts. Since there was significantly more time series data in the filtered 100-Car dataset compared to the IVBSS dataset, this region appears denser. A sample of trip files with these high magnitude lateral velocities and jumps in DTLB were identified. Generating a normal driving distribution for each individual file proved these outliers were simply artifacts and not from a single driver with an abnormal lane keeping profile. Regardless, these outliers had a negligible impact on the overall distribution and normal lane keeping boundary.

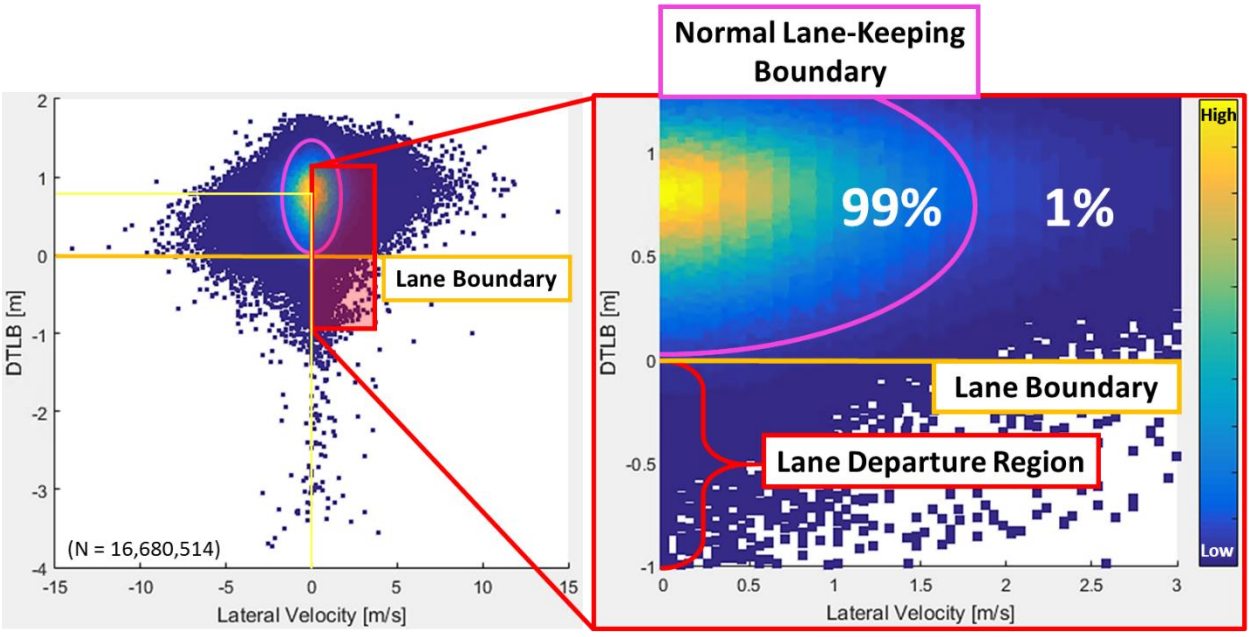

Figure 19. Normal Driving Distribution for the 100-Car NDS

As with the IVBSS study, various subsets of the 100-Car data were defined based on the cumulative distributions previously shown to explore the effects of lane width and road curvature on lane keeping behavior. Figure 20 shows the effect of road curvature on normal driving behavior. Similar to the IVBSS plots, it is clear that within each lane width group, the ellipses increase in size as *CurveG* increases. This means drivers displayed higher rates of lateral motion and deviated further from the lane center as roads became more sharply curved. In the narrowest lane grouping, the lower

boundaries were in the negative DTLB portion of the subplot demonstrating lane departures were possibly within normal lane keeping behavior for these conditions in 100-Car. IVBSS data had lower limits below 0 m DTLB for all three lane width groups. It is also apparent that lateral velocity decreased as drivers approached the lane boundary in 100-Car.

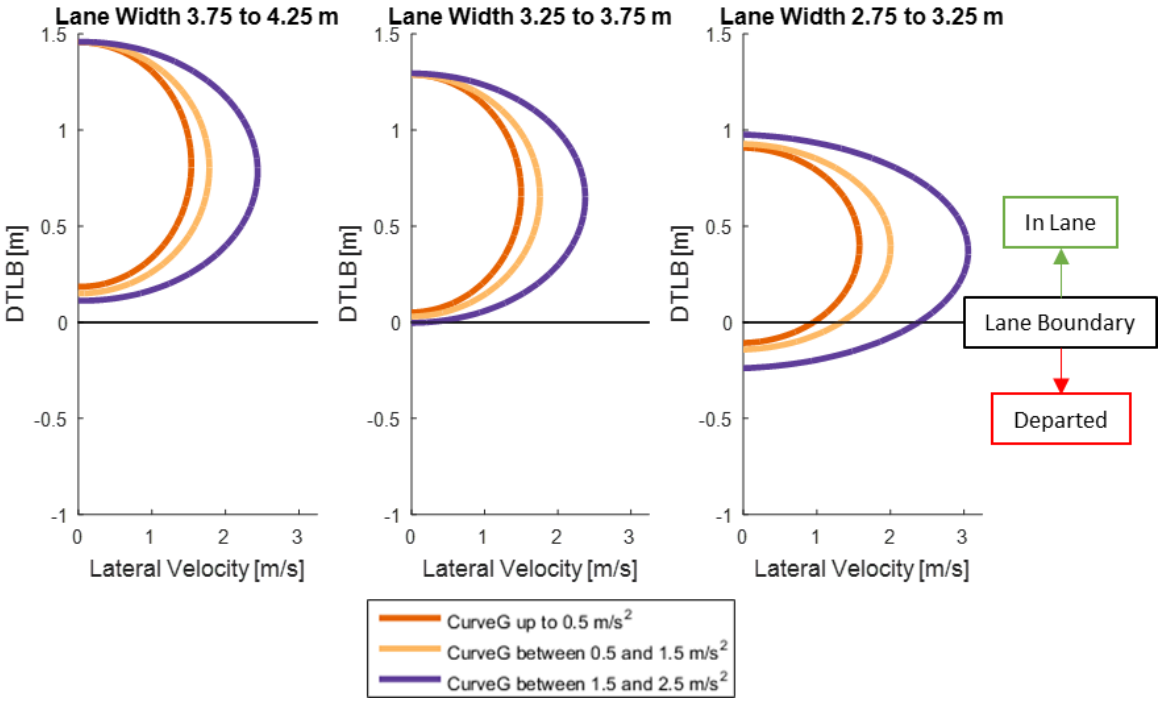

Figure 20. The Effect of Road Curvature on Normal Driving Behavior Distribution in 100-Car

Figure 21 shows the effects of lane width on normal driving when the subset order is flipped. The 100-Car data was first subset by *CurveG* groups, and then three lane width levels within each *CurveG* group. In contrast to the lack of patterns seen with IVBSS data, there does appear to be a trend with lane width on normal lane keeping. Although the maximum lateral velocity for each subgroup is roughly the same, the lower DTLB limit moves further from the lane center as lane width decreases. This means that as lanes became narrower in the 100-Car NDS, drivers tended to deviate further from the lane center. This is the conclusion Fujishiro and Takahashi (2015) found in the Japan dataset [35]. Again, only the most narrow lane width group had a lower ellipse limit in the departure region.

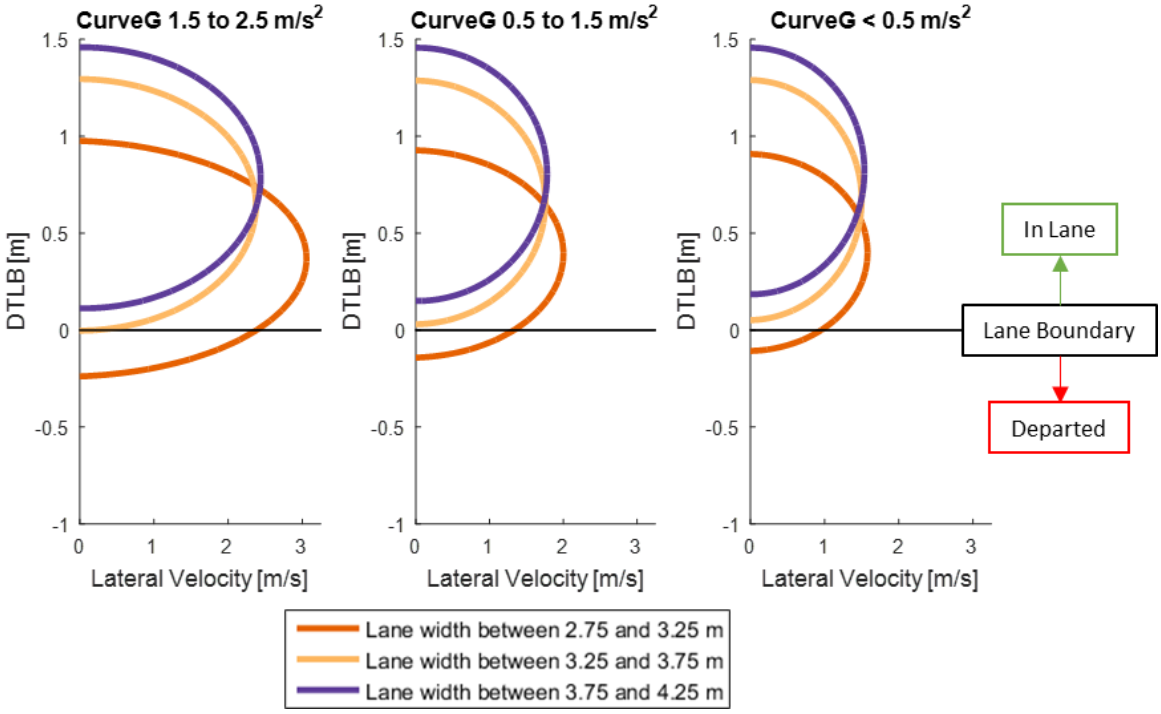

Figure 21. The Effect of Lane Width on Normal Driving Behavior Distribution in 100-Car

2.5 DISCUSSION

The IVBSS and 100-Car data arrived at conclusions similar to those drawn by Fujishiro and Takahashi (2015) in the study using a Japan NDS. Although road and population demographics vary between the three datasets, there are several key components of normal lane keeping behavior that can be stated from the studies. For example, lane widths in the U.S. NDS were found to be much wider than the lanes in Japan [35]. However, Fujishiro and Takahashi (2015) found much lower lateral velocity limits and none of the studies had lower DTLB limits past 0.5 m out of lane. Therefore, it could be concluded that the wider U.S. lane widths allow for more lateral motion without departing, while Japan drivers are forced to be more cautious and disciplined with lane keeping trajectories since there is a smaller margin for error. Table 1 outlines findings from each study.

Table 1. Summary of Findings from Normal Driving Distributions from 3 NDS

Conclusion	IVBSS	100-Car	Japan [35]
Normal driving centered near lane center with minimal lateral velocity	√	√	√
Lateral deviation increases as lanes become narrow		√	√
Lateral deviation increases with road curvature	√	√	√
Lateral velocity decreases as vehicle approaches lane boundary	√	√	√

The main disagreement in the results besides IVBSS showing no influence of lane width was the distribution DTLB center. IVBSS had an overall central DTLB of 0.45 m. 100-Car and the Japan data both had a central DTLB closer to 0.8 m. This alludes to some of the limitations in the datasets and methodology. As previously mentioned, the only data provided from the IVBSS NDS besides the time out of lane was 30 seconds before and 30 seconds after a lane departure event. Therefore, for roughly every 60 seconds of data, there was guaranteed to be a segment of negative DTLB values. This overestimation of time spent out of lane in normal driving is likely the main cause for the entire lane keeping distribution shifted down closer to the lane boundary at 0 m DTLB. The full-trip files of 100-Car allowed for much longer continuous segments of normal in-lane driving behavior without the lane departure bias. More unprocessed data, however, made it more difficult to differentiate valid lane tracking data. Since nearly every data element used in these studies relied on the forward facing lane tracking data, it was essential to extract quality data. There remained some artifacts of the machine vision software in 100-Car where the DTLB jumped rapidly when odd road characteristics were encountered. These abnormal data can be seen in the high lateral velocities seen in the normal driving distribution up to 10 and 15 m/s and the DTLB values of several car widths over the lane.

Another point that can be made with regards to the distribution centers is how they relate to the NCAP LDW Confirmation test. As previously discussed, in order to receive a passing grade for the NCAP LDW test, the system must provide a warning between a DTLB of 0.75 and -0.3 m. It could be

argued that the window for a LDW system to pass is too large, as the normal driving distribution centers for 100-Car and the Japan NDS were around 0.8 m DTLB. If LDW systems pass and are implemented into the vehicle fleet providing warnings at 0.75 m DTLB, drivers will likely experience false alarms and become annoyed if they deviate much from a central position.

Other limitations include the age of the NDS data. The 100-Car NDS was performed in 2003-2004, IVBSS in 2009-2010, and the Japan NDS in 2013. The sensor and software used in each of the NDS were likely different and more refined in recent years. The 10 year gap in the technology used in 100-Car may have resulted in lower quality data collection compared to the newer NDS data.

One argument that can be made from this research is that normal driving behavior is dynamic, and LDW systems should be designed to account for this if manufacturers want to see higher acceptance rates and larger benefits from these active safety technologies. Every driver has a different lane keeping profile, and every driver has different expectations from these LDW systems. The ellipsoid method provides a valuable tool for charting normal lane keeping behavior and could be extended in multiple ways. The purpose of the ellipse visualization of the NDS data was to identify a normal driving region and examine what might be causing false positive warnings leading to driver annoyance. One example of a behavior likely resulting in premature warnings is the conclusion that as drivers approach lane boundaries, lateral velocity decreases. LDW systems that rely on a lateral rate based intervention timing algorithm may be tripped at high lateral rates even if the driver planned to approach the lane edge and then hold that position with no lateral movement. Drivers who frequently drive close to the lane boundary would still be within the normal driving region at this point and likely become annoyed. A dynamic LDW system may be able to recognize the behavior is not yet abnormal and delay the warning until the driver actually departs the normal lane keeping region. The percentage of data captured in the normal driving region for these studies were set at 99%. However, this percentage could be increased or decreased for drivers who need a more

aggressive or lenient warning system based on driving behavior. It could even be adapted as a dynamic boundary where the software constantly monitors driving behavior and updates intervention timing based on current driving behavior.

2.6 CONCLUSIONS

This chapter analyzed normal lane keeping behavior through NDS data to characterize common drift out of lane departures. Both the IVBSS and 100-Car NDS data showed that driving behavior changes with road curvature. As roads become more sharply curved, drivers tend to maintain a trajectory further from the lane center—sometimes departing the lane. Both datasets also showed that lateral velocity decreased as drivers approached the lane boundary. However, only the 100-Car data found that lane width was a factor in normal lane keeping behavior as in the previous study [35]. Drivers tended to deviate further from the lane center as lanes became narrower. The center of the normal driving distribution was found to be around 0.8 m between the leading edge of the vehicle and the lane boundary for these two studies as well. This distribution center places drivers in the center of the lane for the majority of the data collected.

There are still many limitations with lane tracking devices such as weather, presence of lane lines, and differentiation of intentional maneuvers. These limitations affect both collection of NDS data and development of production LDW systems. It is clear, however, that normal driving behavior varies with factors like road demographics and it should be approached as a dynamic behavior. The methodology from this research should be extended to more NDS datasets and investigate additional factors that may alter driving behavior such as time of day, roadway type, and traffic density. It would also be interesting to investigate the idea of driver specific distributions, since every driver has a different profile that may change among trips, and potentially within a single trip.

3 CHARACTERIZING ROAD DEPARTURE CRASHES THROUGH REAL-WORLD CRASH DATA

3.1 BACKGROUND

Characterizing lane departure parameters from naturalistic driving studies provides a better understanding of normal driving and lane keeping behavior. However, actual departure crashes are rarely captured in NDS data. A crucial perspective in evaluating and improving LDW and LDP systems are the departure parameters of crashes. Since LDW and LDP systems need to effectively recognize departure situations and differentiate between normal driving and impending crashes to avoid false alarms, it is essential to identify differences in departure characteristics of minor drift out of lane departures and severe departures that lead to crashes.

One source used to investigate real world crash data is the NASS Crashworthiness Data System (CDS). NASS/CDS collects detailed information from a probability sample of about 5,000 police reported, tow-away crashes each year in the U.S. [41]. Trained crash investigators photograph the scene and vehicle, measure vehicle damage, review occupant injury outcome, and take measurements of the crash scene and vehicle trajectory to generate accurate scene diagrams. All of the data entered into NASS/CDS is extremely useful for many aspects of traffic safety research; however, details about road configuration and roadside safety features at the site of departure crashes are not recorded. There is a need for additional investigation and crash reconstructions to obtain key departure characteristics in traditional crash databases like NASS/CDS.

The National Cooperative Highway Research Program (NCHRP) Project 17-22 [42] was an investigation of serious road departure crashes involving roadside objects that aimed to identify impact conditions and crash environment details. The NCHRP 17-22 project consisted of 890 road departure crashes investigated as a part of NASS/CDS cases from 1997-2001 and 2004. Cases involved single passenger vehicle road departure crashes where speed limits were above 72 kph and

complete vehicle inspection, vehicle trajectory, and occupant injury data were available in NASS/CDS. In addition to collecting crash site characteristics, NCHRP 17-22 developed methods to estimate departure parameters such as departure angle and speed. While the NCHRP 17-22 project obtained supplemental roadside data lacking in NASS/CDS, the database is dated and was in need of an update to account for changes and improvements in roadway design, roadside safety features, and vehicle fleet safety technology.

NCHRP 17-43 Lite is a follow-up on the older NCHRP 17-22 database that contained a subset of NASS/CDS 2012 road departure crashes. The database is under development at Virginia Tech. Our development of the NCHRP 17-43 Lite database expanded the crash data collection protocol and refined reconstruction protocol used in NCHRP 17-22 [43]. The NCHRP 17-43 Lite database was developed exclusively from NASS documentation. The eventual goal is to generate a comprehensive roadside database from crash site inspection, which will be the full NCHRP 17-43 database as opposed to the Lite version discussed in this thesis. The main purpose of the database development is to supplement NASS/CDS and provide additional information that can be used to research vehicle safety, specifically in road departure crashes.

This chapter describes our development and use of the NCHRP 17-43 Lite database to characterize the problem of road departures resulting in real-world crashes to better understand road departure crash scenarios. One hypothesis which the research aimed to validate was that departure characteristics such as departure angle were much more severe in road departure crashes than in the unintentional drift out of lane departures observed in normal driving as seen in Chapter 2.

3.2 DATA SOURCE

The NCHRP 17-43 Lite database was composed of 567 NASS/CDS 2012 cases involving a single vehicle road departure. The departure crashes involved impacts with roadside objects and

roadside features such as concrete barriers, embankments, and guardrails. The most frequent events were rollover events and impacts with poles, trees and other narrow objects. Development of NCHRP 17-43 Lite was divided into two phases. In Phase I, supplemental roadside information, not typically recorded in NASS/CDS, was documented and vehicle trajectories were measured. Phase II used the vehicle trajectory measurements and a number of energy based methods to reconstruct departure and impact speeds.

Although the NCHRP 17-43 Lite database contained 567 cases, data was not collected from all of them. Sixty-two (62) cases did not have a scene diagram drawn to scale or were missing information about the case. No data was collected for these cases since the accuracy of vehicle trajectory and roadside characteristics was compromised. Also, one case was removed from this analysis due to high NASS/CDS case weight above 5,000, a practice conducted in previous studies [44]. Data was collected from the remaining 504 cases including measurements describing vehicle trajectory and roadside characteristics, as well as details about the departure and impact events. However, only 151 cases had a complete vehicle inspection. The reason the restriction of only using cases with complete vehicle inspection was placed on NCHRP 17-22 data was to ensure necessary measurements related to vehicle damage were available to perform speed reconstructions. Rollover event speed reconstructions only required basic vehicle information such as body type and roll distance, so some NASS/CDS cases with only partial inspections or even no inspection could be used as long as the scene diagram was accurate. There were 203 partial inspection cases, 148 no inspection cases, and 2 cases where the vehicle was repaired prior to inspection. A total of 275 cases were found to have enough evidence to perform speed reconstructions in Phase II and collect all supplemental roadside information performed in Phase I. Of the 275 reconstructed cases, 128 were single impact event cases.

3.3 METHODS

3.3.1 PHASE I: DATA COLLECTION

The data in the NCHRP 17-43 Lite tables were collected by reviewing scene photographs, crash summaries, and the scene diagrams. The first phase of the NCHRP 17-43 Lite project involved collecting data for the 504 cases with valid scene information. The database was organized into the following tables: Road, Bad, Roadside, Trajectory, Final Rest, and 7 additional tables describing the impacted object categories. Impacted object categories included metal barriers, concrete barriers, poles/trees/narrow objects, embankments, crash cushions, rollovers, and other object types that could not be classified. Tables were linked through unique NASS/CDS case identifiers. Figure 22 illustrates the organization and flow of the NCHRP 17-43 Lite database. Note that the Bad table consists of unique NASS/CDS case identifiers for the 62 cases with not-to-scale scene diagrams or missing information where roadside and trajectory data was not collected.

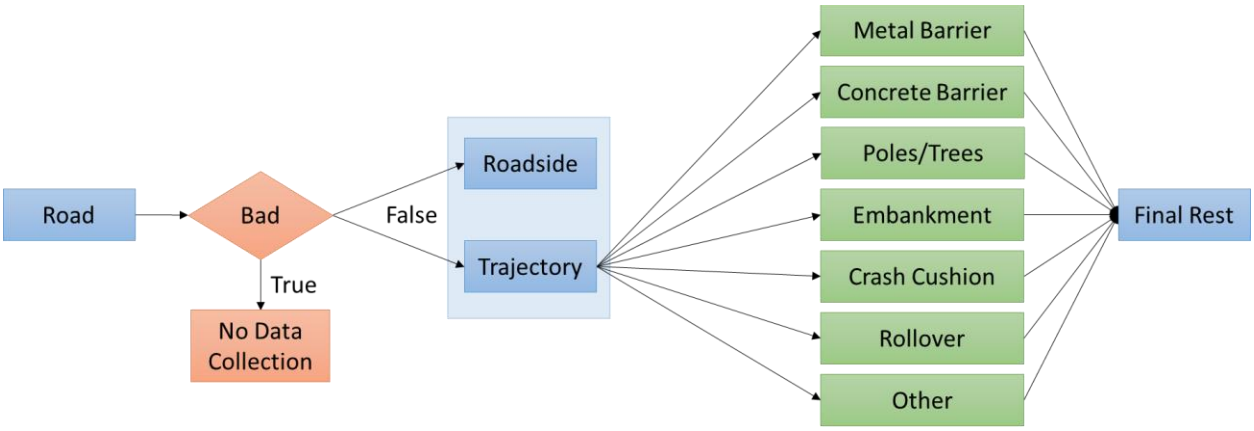

Figure 22. Flowchart of NCHRP 17-43 Lite Data Tables

Each NASS/CDS case contained one entry in the Road table to describe road demographics such as road alignment, number of lanes, and lane and median with. The Roadside table described departure events. Each NASS/CDS case had one entry per departure/re-entry from the roadway

edge. The Roadside table contained data elements such as departure side and curb or shoulder type. The Trajectory table contained one entry for every impact event in a case. Each impact event had data elements including impact location and impact event type. The impact event type determined which impacted object table additional information about the event would be collected for. For example, if a vehicle departed the road and impacted a concrete barrier, an entry would be placed in the Concrete barrier table to record elements such as the type of concrete barrier, barrier size, and extent of barrier damage. The last table was the Final Rest table, which every NASS/CDS case had a single entry describing the location of the vehicle and distance traveled from the last impact event to final rest. For more detail about the organization/definitions of data elements in each table and the data collection process, refer to the NCHRP 17-43 Lite Coding Manual and Data Collection Forms [45][46].

The scene diagram was the primary source of measurements and road characteristics. Of particular interest to this study was the vehicle trajectory. The trajectory in our study was defined to be a sequence of points of the vehicle center of gravity (CG) location. A sample scene diagram with annotations is shown in Figure 23 for NASS/CDS Case ID 500015136. The points of interest on the diagram included the vehicle CG trajectory between the point of departure (POD) and final rest. The vehicle CG was estimated as a point along the centerline of the vehicle, roughly between the driver and passenger seat location. CG points are marked by a red target and connected by blue lines to form trajectory segments in Figure 23. The POD was defined where the vehicle CG trajectory first crossed the edge of the roadway. The POD was used as the origin to base all measurements from, as seen by the green longitudinal distances annotated in Figure 23. Measurements were based on the Cartesian coordinate system. The y-axis was defined to be the tangent to the road edge at the POD. Final rest was defined where the vehicle stopped moving, or the last trajectory point. Additional measurements such as vehicle orientation and lane width were taken to further describe the crash scenario.

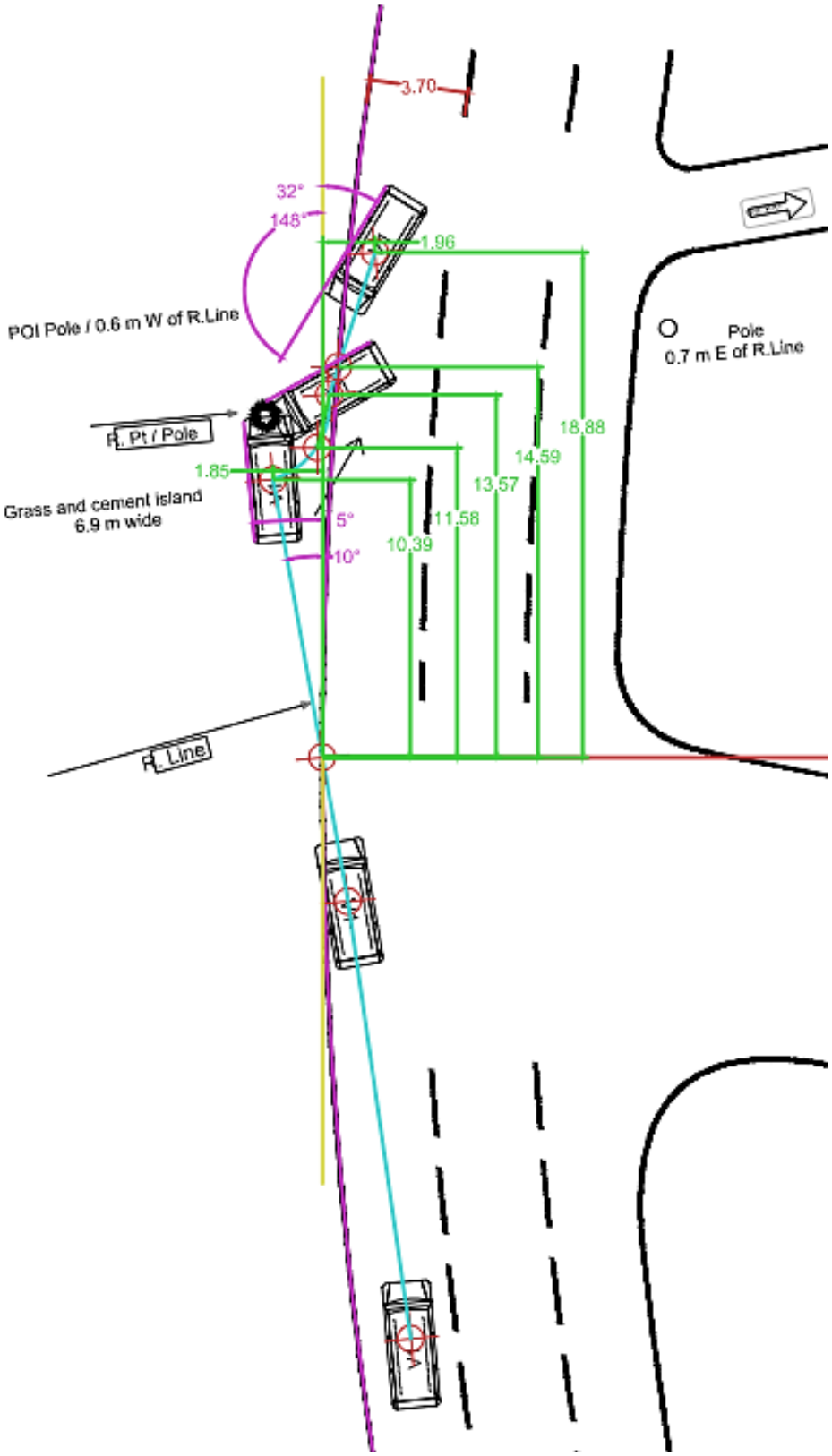

Figure 23. Sample NASS/CDS Scene Diagram with Measurements

The general process for data collection from the scene diagram is illustrated in Figure 23 and outlined below:

- Mark points of interest and connect trajectory segments
- Measure longitudinal and lateral distance from the POD to each trajectory point
- Measure vehicle heading and trajectory angles with respect to the road edge tangent
- Measure additional roadway characteristics of interest (e.g., lane width)
- Record measurements in the appropriate NCHRP 17-43 Lite data table

3.3.2 PHASE II: CRASH RECONSTRUCTIONS

The second phase of the NCHRP 17-43 Lite database development involved reconstructing departure and impact speeds. Our approach was to adapt the energy based techniques used in NCHRP 17-22 to the NCHRP 17-43 Lite data and supplement these techniques with EDR data. Reconstruction of the vehicle speeds required complete case information from NASS/CDS and careful consideration of assumptions and limitations. As previously discussed, only 275 of the NCHRP 17-43 Lite cases were eligible for speed reconstructions. This section outlines the techniques used to estimate departure and impact speed for each type of impacted object.

3.3.2.1 Kinematics and Energy Reconstruction Methods

The general process for reconstructing speed was to work backwards from the point of final rest where the vehicle speed and crash energy were known to be zero. At this point of final rest on the scene diagram, it was assumed all energy had been dissipated through either friction/braking or impact resulting in deformation/fracture of either the vehicle or the object impacted.

The kinematic relationship in Equation 7 was used to step back to each trajectory point from final rest, where V_f is the final velocity, E is any additional energy considered in the system while

traversing the segment, m is vehicle mass, and V_i is the initial or previous step velocity being estimated.

$$V_i = \sqrt{2\left(\frac{E}{m}\right) + V_f^2} \qquad \textbf{Equation 7}$$

In most of the trajectory segments, no additional energy was considered. Energy was only considered when there was a change in elevation (potential energy), a yielding impacted object, or substantial crush to the vehicle that NASS reported as ΔV (estimated change in speed based on a measured crush profile). These exceptions will be discussed in more detail in the following sections.

3.3.2.2 Drag Factors

In addition to impact energy and potential energy from elevation changes, energy dispersed through friction between the vehicle and the traveled surface for each segment was estimated. Drag factors used in the NCHRP 17-22 project [42] for various surfaces are shown in Table 2. When selecting drag factors, the minimum and maximum were selected based on surfaces traversed, and an average was taken for the segment.

Table 2. Estimated Drag Factors

Asphalt and Concrete Pavement		Dirt, Grass, or Gravel	
Surface Condition	**Drag Factor**	**Surface Condition**	**Drag Factor**
Dry, broken-in	0.6-0.8	Crushed grass	0.3
Dry, new	0.9	Torn grass	0.5
Wet	0.45-0.7	Torn grass roots	0.7
Icy	0.1-0.25	Soil surface tear-up	0.9
Loose snow	0.1-0.25	Deep furrowing/plowing	1.0-1.5
Packed snow	0.3-0.55	Gravel	0.4-0.8

In some cases, drag factors for a segment were adjusted based on evidence from the scene, case narrative, or other evidence in NASS/CDS. If a driver was said to have fallen asleep or been distracted prior to crashing and there was no evidence of braking or evasive maneuver, it was

assumed that the vehicle speed at the POD was equivalent to the speed at the first point of impact. Thus, no drag factors were used between these two points. If a vehicle was in yaw or lateral skid, the friction coefficients were assumed to be higher than when the vehicle is tracking. Drag factors were increased by 10-20% based on the amount of yaw for each segment as seen in NCHRP 17-22 reconstructions. If a vehicle lost one wheel during the crash, the drag factors were reduced by 25% to account for the reduction in tire-ground contact.

To estimate the speed at the beginning of each segment, Equation 8 was used, where Δx is the length of the linear segment, g is the acceleration due to gravity, and μ is the average drag factor for the various surfaces traveled across. Trajectory points were added to cases where scene diagrams were sparse and the vehicle trajectory appeared to curve. An example of this is shown in Figure 23 when the vehicle rotates around the impacted pole. These additional points helped reduce error between the projected curve length and the linear approximation.

$$V_i = \sqrt{2g(\Delta x \mu) + V_f^2} \qquad \textbf{Equation 8}$$

3.3.2.3 Poles, Trees, and Narrow Objects

Upon impact with a pole, tree, or other narrow object, there are typically two possible outcomes. The first possibility is that the object remains undamaged and the vehicle absorbs most of the energy in the form of structural crush or deformation. The second possible outcome that could happen, usually in combination with the first, is that the object will fully or partially fracture, absorbing additional energy.

When vehicle crush occurs, crash scene investigators often measure a crush profile which can be used to estimate the energy required to deform the vehicle that amount. NASS/CDS uses this crush profile, along with vehicle stiffness values from crash tests, to quantify the impact severity in terms of the effective change in velocity, or ΔV [47][48]. In many cases, ΔV was not available, so barrier

equivalent speed (*BES*) was used to estimate impact energy. *BES* is derived from vehicle crash tests into rigid barriers, and provides a speed estimate comparable to ΔV. To estimate the added energy as previously discussed, Equation 9 was used, where *KE* is the added kinetic energy and *m* is the mass of the vehicle.

$$\Delta KE = \frac{1}{2} m(BES)^2 \qquad \textbf{Equation 9}$$

If the pole, tree, or narrow object impacted did not deform or fracture, these objects were assumed to act like a rigid barrier and absorb no energy. If the object was wood (tree or utility pole) and partially fractured (e.g. splinters or bends, but still standing) or fully fractured (e.g. completely severed from base or knocked over), the equations shown in Table 3 estimate Breakaway Fracture Energy (BFE) based on pole circumference, *C*, in centimeters [49]. Previous research developed these equations from empirical data.

Table 3. Breakaway Fracture Energy for Wooden Poles [49]

Pole Circumference (cm)	Extent of Fracture	Breakaway Fracture Energy (kJ)
<= 66.04	None	0
	Partial	$0.00135582*1/2*(20{,}000 - (1.4*10^{-2})*(C/2.54)^{4.38})$
	Full	0.00135582*20,000
> 66.04	None	0
	Partial	$0.00135582*1/2*((1.4*10^{-2})*(C/2.54)^{4.38} - 20{,}000)$
	Full	$0.00135582*1/2*((1.4*10^{-2})*(C/2.54)^{4.38})$

If the object was not composed of wood, another study [50] estimated BFE for other common roadside poles including luminaires and metal signal poles with breakaway bases. Values for these devices are illustrated in Table 4.

Table 4. Breakaway Fracture Energy for Non-Wooden Poles [50]

Pole Type	BFE (ft-lb)	BFE (kJ)
Nonbreakaway Luminaire Support	30,000	40.67
Breakaway Luminaire Support		
Case-Aluminum Transformer Base	9,000	12.20
Progressive Shear Base	7,500	10.17
Slip Base	7,500	10.17
Nonbreakaway Sign Support		
Large	30,000	40.67
Small	2,250	3.05
Breakaway Sign Support		
Large	750	1.02
Small	750	1.02

If no vehicle inspection or crush profile was performed by investigators or there was overlapping damage from a later impact, the case could typically not be reconstructed. However, if the pole completely fractured and was not a breakaway pole, it was reasonable to assume the vehicle crush energy was equal to the pole breakaway fracture energy. This assumption was based on a sample of 30 NCHRP 17-43 Lite cases where both the vehicle crush energy and pole configuration were known. As shown in Figure 24, the energies are in relatively good agreement. BFE tended to be less than 20% higher than vehicle crush energy.

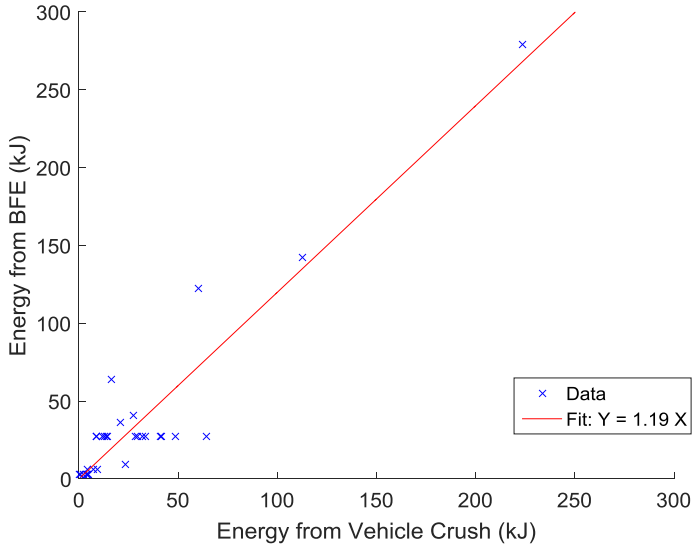

Figure 24. Comparison of Vehicle Crush Energy and BFE

3.3.2.4 Rollovers

Rollover cases used the drag factor methodology applied to poles, trees, and narrow objects. Although pole impacts often dissipate a large portion of energy through impact and crush quantified in NASS by ΔV or *BES*, rollovers dissipate energy through rotation and interaction between the rolling vehicle and the ground. Energy dissipated would be expected to increase with roll distance. A previous study [51] developed the so-called Kildare curves to estimate a ΔV equivalent based on roll distance. The Kildare curves assume a final velocity of zero and estimate the vehicle speed at trip based on total roll distance. There are separate curves for trucks/SUVs, sedans, and small cars, since different vehicle classes have different inertial properties. Figure 25 illustrates these curves.

For NCHRP 17-43, the trip point was defined as the first point where the vehicle was drawn on its side in the scene diagram. This was the point closest to where the vehicle CG passed or tripped over the outside edge of the leading wheels. In NCHRP 17-22, however, the trip point was typically taken as the last trajectory point where the vehicle was still on all 4 wheels in the scene diagram just

before the rollover event. The different definitions of vehicle trip point in the two NCHRP datasets may contribute to any discrepancies seen when comparing the reconstructed rollover speeds.

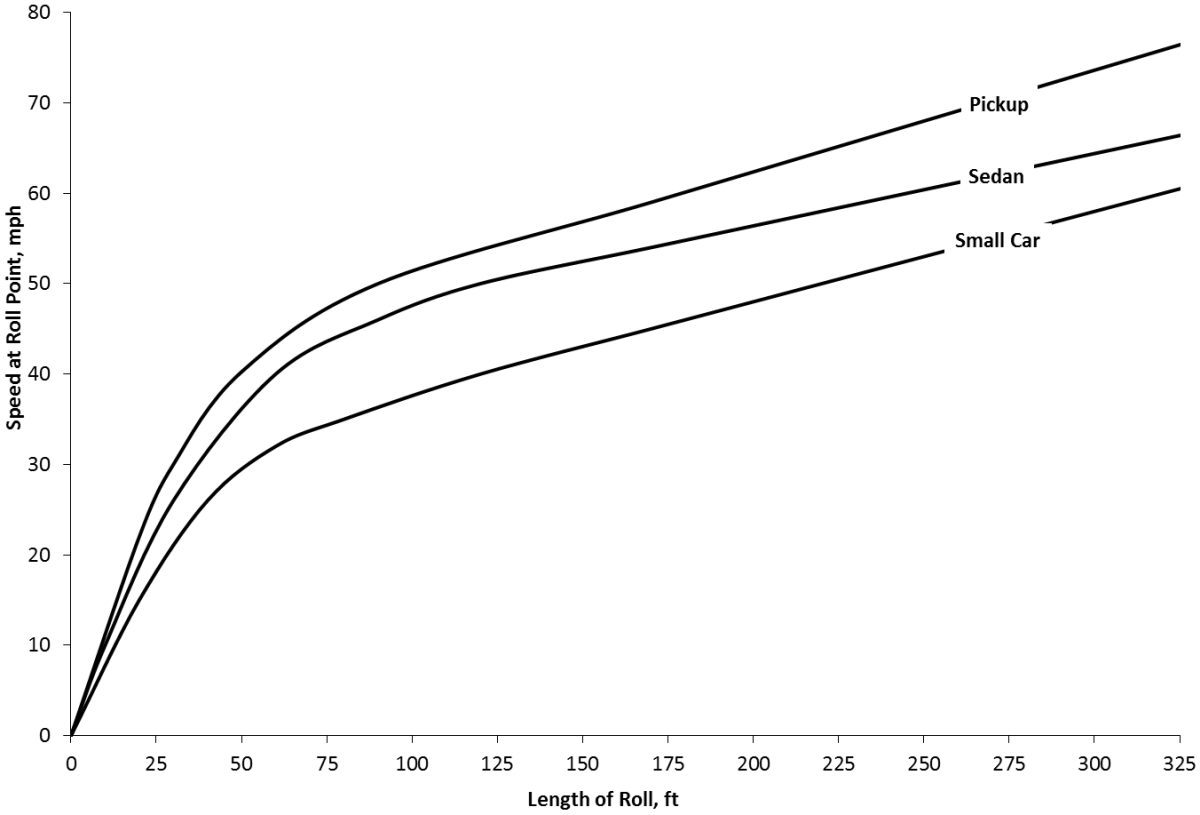

Figure 25. Kildare Curves for Rollover Cases [51]

3.3.2.5 Longitudinal Barriers

Guardrail Reconstructions

Fifteen (15) of the reconstructed impact events involved collisions with guardrails. For these cases, the general process for reconstructing rollover and narrow object cases was followed, but an additional step was added to account for any deflection of the longitudinal barrier or any vehicle-barrier frictional interaction. The methodology was adopted from the Longitudinal Barrier Special Study [52] and the NCHRP 17-22 reconstruction approach outlined in [53][54].

For impacts with a guardrail face, the velocity and energy (KE_{depart}) of the vehicle at departure or separation from the beam face was estimated based on the conventional method of back-tracking from the point of final rest using Equation 10.

$$KE_{depart} = \frac{1}{2} m\, V_{depart}^2 \qquad \textbf{Equation 10}$$

An initial guess of initial vehicle speed at the point of impact with the guardrail was made to calculate an initial energy guess as in Equation 11.

$$KE_{initial_{guess}} = \frac{1}{2} m\, V_{initial_{guess}}^2 \qquad \textbf{Equation 11}$$

Energy dissipated from factors including post deflection/fracture (E_{posts}), beam deformation (E_{beam}), vehicle damage and tire-ground friction ($E_{vehicle}$), and vehicle-barrier friction ($E_{friction}$) was estimated based on models developed in [53]. The models were derived from simulations and validated with full-scale crash test results estimated the amount of initial energy loss as a function of vehicle body type, impact angle, and vehicle speed.

Energy lost through vehicle-barrier friction ($E_{friction}$) was estimated using Equation 12, where θ is the impact angle in degrees. The product of the 1.45 term and θ gives the percent of original energy dissipated by friction.

$$E_{friction} = \frac{1.45 * \theta}{100} * KE_{initial_{guess}} \qquad \textbf{Equation 12}$$

Energy lost through post deflection/fracture (E_{posts}) was estimated using post force-deflection characteristics and information about the ground in which the post was embedded. Frozen ground, for example, acts as a rigid anchor and absorbs less energy than a post that is able to rotate in the soil. Using the force-deflection curve for a standard W150 X 13.5 steel post to generate an energy-deflection curve, the study [53] found that the rate of energy dissipated was 0.46 kJ/cm. Therefore,

if a post was shifted 10 cm from the original upright position, the energy absorbed would be 4.6 kJ. The sum of absorbed energy for each post equals E_{posts}. The slope of 0.46 kJ/cm was used for both wood and steel posts since post material has been found to not greatly affect guardrail performance [53].

It is important to note that NASS/CDS scene pictures often do not adequately document damage such as post deflection, so this method is prone to error. If post deflection was visible but not explicitly measured, the deflection was estimated based on surrounding elements in the photographs. The maximum effective deflection associated with post energy dissipation as shown in [53] was 38 cm. If the posts were buckled, fractured, or replaced and only the new posts were pictured, the average failure energy reported in [53] was used. Cases where no posts were documented or no deflection was visible from the NASS/CDS scene pictures were assumed to have no post movement.

Energy lost through barrier/beam deflection (E_{beam}) was estimated using the absorbed energy ratio of beam/posts. Again, this ratio is a function of vehicle body type, impact speed, and impact angle. For higher speed impacts, the ratio is generally 1. However, for lower speed impacts, the posts typically do not absorb as much energy and the ratio is greater than 1.

Energy lost through vehicle crush and ground friction ($E_{vehicle}$) was estimated using a vehicle body type model based on impact speed and angle. If a pickup truck impacted a guardrail at 20 degrees along a highway (speed ~100kph), for example, the energy loss due to vehicle crush and tire friction is about 5.5% of the initial kinetic energy. Therefore, $E_{vehicle} = \frac{5.5}{100} * KE_{initial_{guess}}$.

Based on the summation of these energies as shown in Equation 13, an initial kinetic energy was calculated.

$$KE_{initial} = KE_{depart} + E_{friction} + E_{posts} + E_{beam} + E_{vehicle}$$ **Equation 13**

The initial velocity was then computed using Equation 14 based on the calculated initial kinetic energy.

$$V_{initial} = \sqrt{2 * \frac{KE_{initial}}{m}}$$ **Equation 14**

If the calculated impact velocity ($V_{initial}$) was approximately the same as the initial guess ($V_{initial_{guess}}$), then that velocity was used to continue stepping back to the POD. If the guessed and calculated velocities were not close, the calculated speed was set equal to the next initial speed guess and $KE_{initial_{guess}}$ was computed for the next iteration. All of the energy losses were computed again and the process was repeated until $V_{initial}$ and $V_{initial_{guess}}$ converged.

Concrete and Bridge Rail Barrier Reconstructions

Fifteen (15) of the reconstructed events involved collisions with concrete barriers. Three (3) events involved bridge rail barriers. These traffic barrier impact reconstructions followed a somewhat different approach than guardrail reconstructions. Since concrete and bridge rail barriers act more like rigid fixed objects, there is typically no deformation of the barrier or posts to account for. The vehicle-barrier friction energy, vehicle crush energy, and tire-ground friction energy are the only sources of energy loss during impact. In NCHRP 17-22 reconstructions, it was common practice to use the standard reconstruction procedure of estimating crush energy from ΔV or BES and estimate ground friction using drag factors, but then increase the drag factors by 20-50% for the contact segment to account for the vehicle-barrier interaction. The more conservative end of this method was used for NCHRP 17-43 Lite. An inflation of the drag factors by 20% was used unless there was significant scraping/gouging along the barrier face. For example, dry asphalt has a drag factor

range of 0.6-0.8. If a vehicle impacted a concrete barrier and slid along its face for 3 m, the drag factors would be increased to 0.72-0.96 for the 3 m segment.

Cable Barrier Reconstructions

One (1) of the reconstructed cases involved a cable barrier event as the last coded NASS/CDS event. Although there are currently no energy reconstruction methods for cable barriers to our knowledge, this one case was reconstructed based on a simplifying assumption. The case involved a vehicle that contacted/landed on top of the barrier as it was coming to final rest. There was no damage or deformation to the cable barrier and only minor indentations on the vehicle, so it was assumed negligible energy was absorbed by the barrier. Without simplifying assumptions like this, cases involving cable barriers cannot be reconstructed through formal energy-based methods.

Guardrail End Terminal Reconstructions

Four (4) of the reconstructed events involved collisions with Extruder Terminal (ET-2000 PLUS), Flared Energy Absorbing Terminal (FLEAT-350), or Sequential Kinking Terminal (SKT-350) guardrail end terminals. For guardrail end terminal impacts, methods from [54] were used. The departure or separation energy was calculated using Equation 10 as with guardrail face impacts, but conservation of momentum was used to compute initial velocity (V_i). End terminal configurations were outlined in [54] including parameters such as terminal head mass, size, and average force required to crush/move the terminal down the beam.

The energy absorbed by the rail (E_{rail}) was determined using Equation 15, where F_{avg} is the average force required to displace the head along the rail determined from empirical data, and d is the distance the head is displaced. Since the average force required to slide the end terminal was determined from full-scale testing, the energy required to fracture the posts and crush other components of the rails were included in the parameter and did not need to be accounted for separately.

$$E_{rail} = F_{avg} d \qquad \textbf{Equation 15}$$

The initial energy (KE_c) was calculated as the sum of the departing and rail energies as shown in Equation 16.

$$KE_c = KE_{depart} + E_{rail} \qquad \textbf{Equation 16}$$

Equation 17 shows the calculation of the end terminal velocity (V_c) based on the combined mass of the vehicle and end terminal head.

$$V_c = \sqrt{2 * \frac{KE_c}{(m_{vehicle} + m_{head})}} \qquad \textbf{Equation 17}$$

Equation 18 shows the conservation of momentum calculation used to estimate vehicle initial velocity (V_i) based on the assumption that the impact was perfectly inelastic.

$$V_i = \frac{V_c(m_{vehicle} + m_{head})}{m_{vehicle}} \qquad \textbf{Equation 18}$$

3.3.2.6 Embankments and Other Objects

All other single impact cases were evaluated on a case-by-case basis. Impacts with embankments, building walls, and drainage structures typically resulted in damage only to the vehicle. Rigid objects like these were assumed to absorb no energy and were reconstructed based on ΔV or BES estimated from vehicle crush measurements. Curb strikes were assumed to involve negligible energy loss. Some of these other object impacts resulted in yielding objects. Minor impacts, such as a small fractured plastic delineator post, were assumed to absorb negligible energy through fracture or vehicle crush if not measured. However, in one case the subject vehicle impacted the side of an apartment building and traveled through the wall. Until better methods are developed for estimating the energy required to break through these odd/unknown objects, reconstructions could not be performed for these cases.

3.4 RESULTS AND VALIDATION

3.4.1 NCHRP 17-43 LITE RECONSTRUCTIONS

Using the methodology outlined above, departure and impact speed estimates were generated for 275 of the 504 cases. Several of the cases had incomplete or unknown details in the NASS database essential for reconstruction. The primary reason a case could not be completed was because the crash investigator did not fully inspect the vehicle and conduct crush profile measurements. Of the 229 cases not reconstructed, 135 had no inspection performed, 63 had only a partial inspection performed (e.g., photographs only), and 2 had vehicles that were repaired prior to inspection. Complete vehicle inspections were not performed if the vehicle involved in the crash was more than 10 years old. Without a crush profile, ΔV or *BES* could not be estimated. Since all energy must be accounted for, large amounts of energy dissipated when the vehicle was crushed upon impact could not be ignored. Other reasons cases could not be completed included unknown roll distances and missing details about the impacted object. In some cases, the impacted object damage was repaired before crash scene investigators visited the site, or the damage was inadequately documented in NASS/CDS for energy estimates to be made. If a guardrail was severely damaged along a sharp curve in the roadway where there is a high potential for additional road departures, it may need to be repaired or replaced quickly after the crash to maintain a safe driving environment for other vehicles. Twenty-nine (29) of the cases fell into this category of unknown energy absorbing characteristics or reconstruction protocol, even though complete inspections were performed.

Table 5. Reasons Cases were not Reconstructed

Reason	Case Count
No Inspection	135
Partial Inspection	63
Vehicle Repaired Prior to Inspection	2
Unknown Energy/Reconstruction Procedure	29

One concern with not being able to reconstruct nearly half of the original NCHRP 17-43 Lite caselist was that bias may be introduced in analyses if the reconstructed and non-reconstructed case groups were significantly different. Chi-squared tests for independence were performed using a significance level of 5% for variables characterizing the road departure crashes. Vehicle model year and inspection type were found to be significant, which means the proportions of reconstructed cases by inspection type and vehicle model year were different than the proportion of non-reconstructed cases. This confirms the statement previously made about complete vehicle inspections not being performed for vehicles over 10 years old, making it difficult to reconstruct. Other comparisons including road alignment at departure, total number of impact events, vehicle body class, and general area of damage (GAD) did not meet the 5% significance level. This means that whether or not a case could be reconstructed was independent of these crash characteristics. One variable that did show a potential bias was impact event type. There was a significantly higher proportion of rollover cases in the reconstructed group compared to the non-reconstructed group. As discussed in the reconstruction methods, rollover cases only required roll distance and the vehicle body type to be reconstructed. Therefore, it was more common for rollover cases to be completed, even if the vehicle was more than 10 years old and no inspection was performed.

3.4.2 NCHRP 17-43 LITE COMPARISON TO NCHRP 17-22

Our first question was how departure characteristics might have changed from the NCHRP 17-22 study conducted based on 1997-2004 crashes to the NCHRP 17-43 Lite study based on 2012 crashes. The following figures show weighted departure and impact characteristics of NCHRP 17-43 Lite compared to the NCHRP 17-22 cases separated by impact type. For multiple event cases, only the first impact was considered when analyzing impact speeds. It does not make sense to compare similar impact types for multiple event crashes after the first impact since each crash scenario is unique depending on vehicle and object response after the initial impact. Departure parameters for

the two databases were also compared combining all impact event types. As previously discussed with NCHRP 17-43 Lite, cases in NCHRP 17-22 with NASS/CDS weighting factors greater than 5,000 were excluded in this analysis. There were 14 of the 890 NCHRP 17-22 cases with high weights.

3.4.2.1 Pole Impacts

Figure 26 shows the cumulative distribution of departure angle in pole impact cases for both NCHRP datasets. The median departure angle for NCHRP 17-22 was 11 degrees, while the NCHRP 17-43 Lite median was slightly higher at 14 degrees. Note that N_{wgt} in the following figures represents the weighted sample size of each database subset, and N_{raw} represents the number of cases. These sample sizes for departure parameters are not always equal within the impact categories. Departure angle was always available based on the scene diagram vehicle trajectory. However, as mentioned in the reconstruction methods, there was often missing data in NASS/CDS which did not permit speed reconstructions. In NCHRP 17-22, some cases were coded as unknown for departure and/or impact speed.

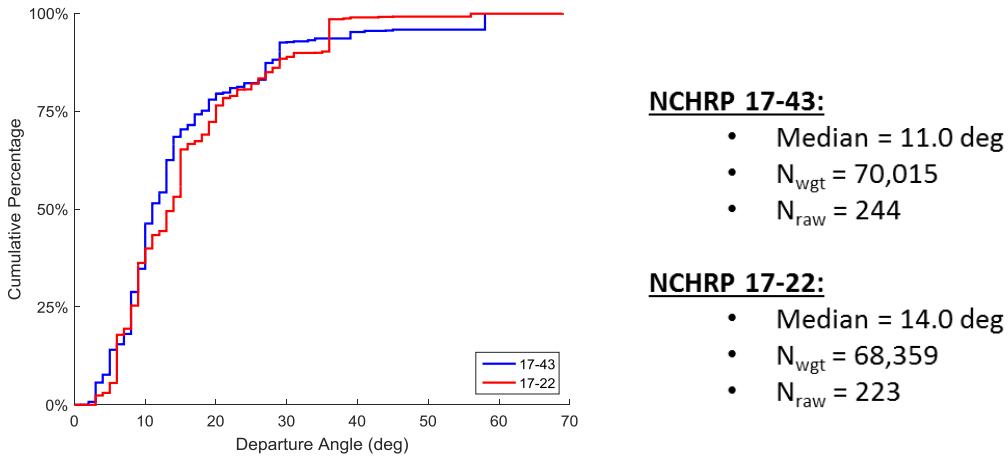

Figure 26. Departure Angle Distributions for Tree and Pole Impacts

Figure 27 shows the cumulative distribution of departure speeds for cases involving a pole impact. The median departure speed in NCHRP 17-22 was 58.3 kph compared to 69.9 kph for NCHRP

17-43 Lite. The sample size for NCHRP 17-43 Lite was decreased significantly because 118 of the 244 cases did not have a Δ*V* or *BES* reported in the NASS/CDS database needed to estimate vehicle crush energy.

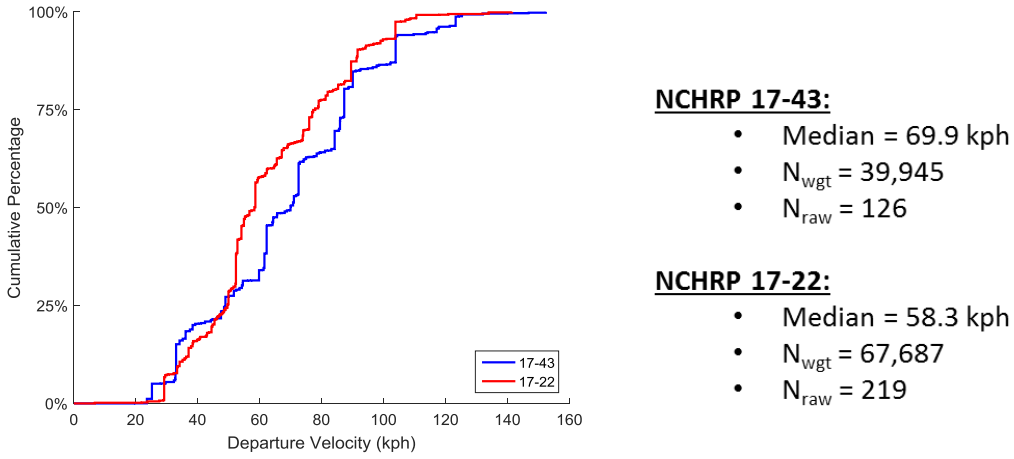

Figure 27. Departure Speed Distribution for Tree and Pole Impacts

Figure 28 shows the distribution of tree and pole impact speed. The NCHRP 17-22 dataset had a median impact speed of 40.2 kph while the NCHRP 17-43 Lite dataset had a median of 40.5 kph.

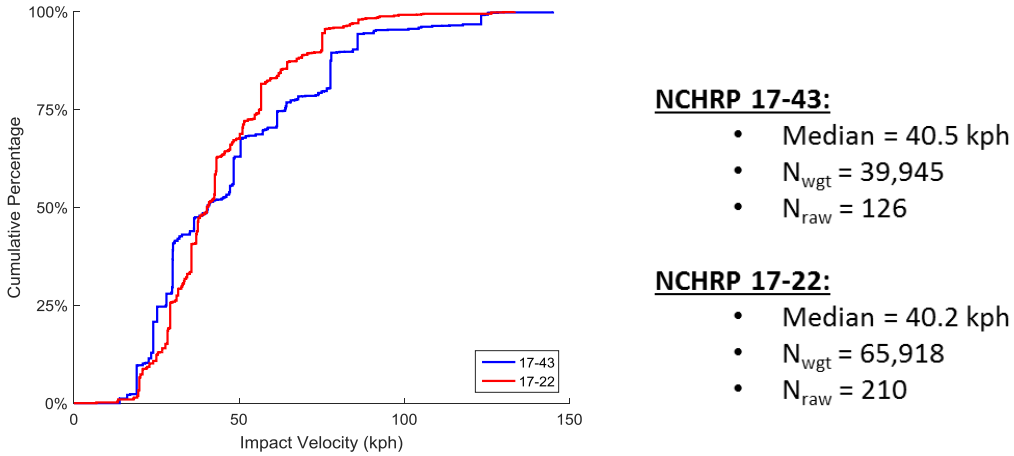

Figure 28. Impact Speed Distribution for Tree and Pole Impacts

In tree and pole impacts, the distributions for departure angle, departure speed, and impact speed were in relatively good agreement for the two NCHRP databases.

3.4.2.2 Rollovers

Figure 29 shows the distribution of departure angle in rollover event cases for both NCHRP datasets. The median departure angle for NCHRP 17-22 was 15 degrees, while the NCHRP 17-43 Lite median was close at 16 degrees. Note that 5 of the 54 cases account for 56% of the total weighted sample size.

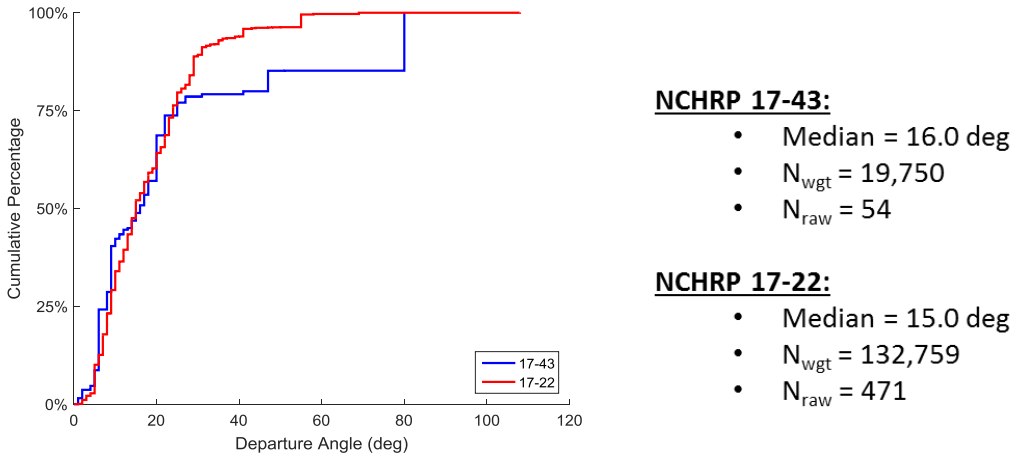

Figure 29. Departure Angle Distributions for Rollover Events

Figure 30 shows the cumulative distribution of departure speeds for cases involving a rollover event. NCHRP 17-22 had a lower median at 77.2 kph compared to 97.8 kph for NCHRP 17-43 Lite. The median speeds for the rollover cases are much higher than the median departure speeds for pole impact cases. One rollover case in the NCHRP 17-43 Lite subset had an unknown roll distance and the speeds could not be reconstructed for this case. The other 7 cases were multi-impact event cases where a full reconstruction was not possible. The 5 cases previously mentioned accounting for a large proportion of the total weighted sample size contribute 59% of the total weight in this reduced sample of 46 cases.

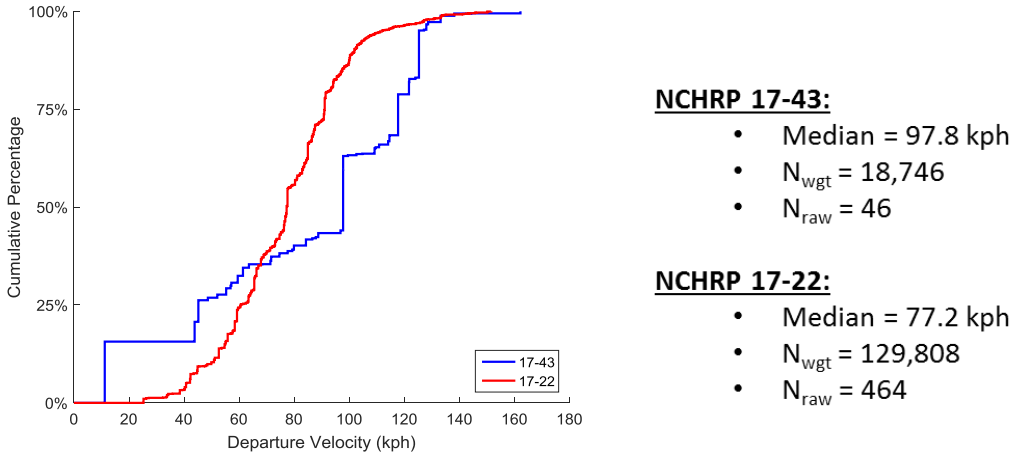

Figure 30. Departure Speed Distribution for Rollover Events

Figure 31 shows the distribution of rollover event trip speeds. NCHRP 17-22 had a median trip speed of 57.9 kph, while NCHRP 17-43 Lite had a much lower median of 29.8 kph. Recall, the two NCHRP datasets had slightly different definitions of vehicle trip point, which may contribute to a large portion of the low agreement between rollover departure and impact speed. Also, 4 of the 5 cases accounting for 59% of the total case weight had lower trip speeds and contributed to the low NCHRP 17-43 Lite median.

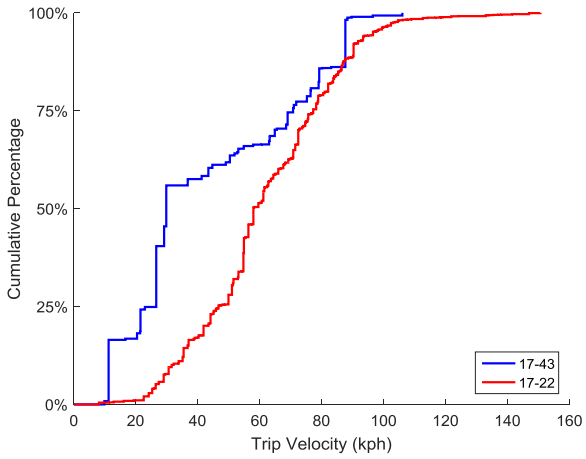

NCHRP 17-43:

- Median = 29.8 kph
- N_{wgt} = 18,746
- N_{raw} = 46

NCHRP 17-22:

- Median = 57.9 kph
- N_{wgt} = 123,984
- N_{raw} = 456

Figure 31. Trip Speed Distribution for Rollover Events

The different definitions of vehicle trip point in NCHRP 17-22 and NCHRP 17-43 Lite likely contributed to poor agreement in departure and trip speed distributions due to the shift in trajectory segments used to complete speed reconstructions. Two distances were compared in this chapter to investigate differences in the two NCHRP datasets. The first was the distance between the POD and the trip point. The second was the distance between the trip point and final rest, or roll distance. The NCHRP 17-22 dataset contained lateral coordinates (x) for every point on the scene diagram. However, longitudinal coordinates (y) were only recorded for key points such as the POD, trip point, and final rest. The NCHRP 17-43 Lite dataset contained a lateral and longitudinal pair (x, y) for each trajectory point. Therefore, to make equal comparisons, a linear distance approximation was made using the distance formula and coordinates for the two points of interest. Figure 32 illustrates a sample rollover case where the vehicle departs to the right, enters a counterclockwise yaw, trips, and rolls 8 quarter turns before coming to final rest. In this example, the linear roll distance, *d*, would be estimated as $d = \sqrt{\left(x_{Final\ Rest} - x_{Trip\ Point}\right)^2 + \left(y_{Final\ Rest} - y_{Trip\ Point}\right)^2}$. Note that the true roll distance would be the sum of the individual segment lengths and slightly longer than the linear approximation. The same approach was applied for the POD to trip distance.

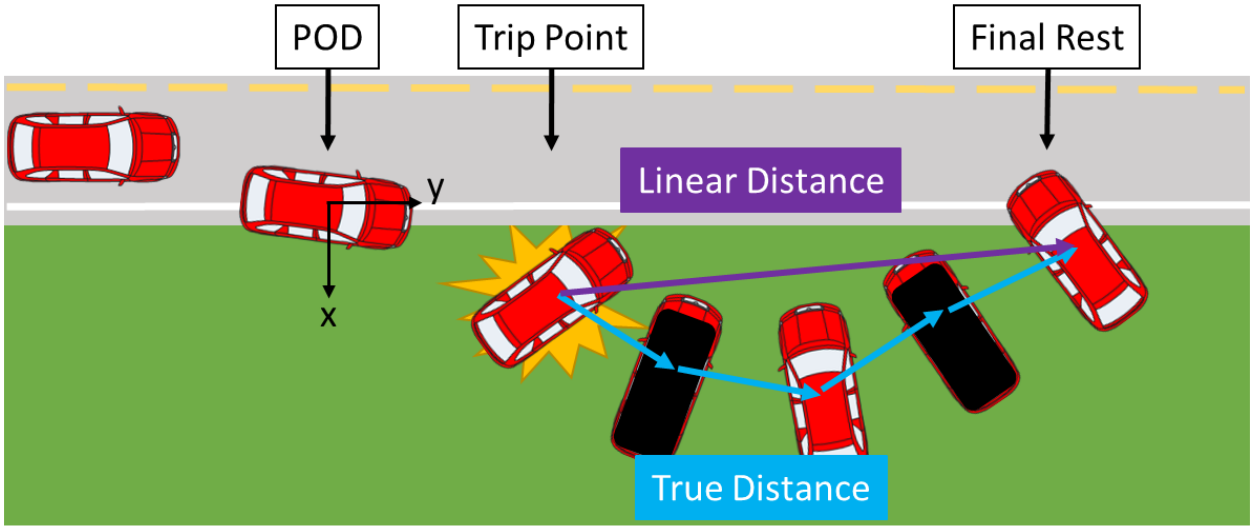

Figure 32. Sample Case to Explain Rollover Distance Calculations

Figure 33 shows the cumulative distribution of how far the vehicle traveled after departing the roadway before tripping and initiating rollover as described above. The median distance to trip for NCHRP 17-22 was 15.5 m, while the median for NCHRP 17-43 Lite was higher at 34.2 m. This means vehicles in NCHRP 17-43 Lite traveled much further off road before rollover was initiated. The distribution illustrates the effect of NCHRP 17-43 Lite having a trip point defined later in the series of trajectory points. The 5 cases with high weight proportions for the rollover subset tended to have longer POD to trip distance, shifting the 17-43 Lite distribution to a higher median.

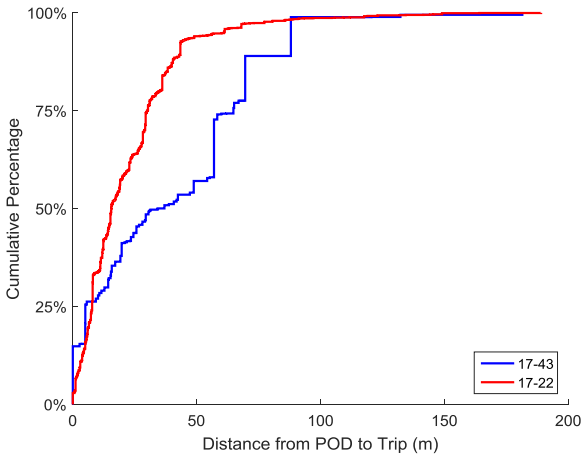

NCHRP 17-43:

- Median = 34.2 m
- N_{wgt} = 19,750
- N_{raw} = 54

NCHRP 17-22:

- Median = 15.5 m
- N_{wgt} = 131,249
- N_{raw} = 465

Figure 33. Distance between POD and Trip for Rollover Events

Figure 34 shows the distribution of distance between rollover initiation and the end of the rollover event. Again, NCHRP 17-22 only provided longitudinal coordinates for the point of trip and point at the end of the rollover event, so the linear estimate was used. NCHRP 17-22 had a median roll distance of 14.0 m—more than twice the 5.9 m median for NCHRP 17-43 Lite. This is consistent with the difference in trip point definition. Opposite of the POD to trip distance, the 5 cases accounting for 56% of the sample weight were at the low end of the distribution. This held the roll distance median to a lower value for NCHRP 17-43 Lite.

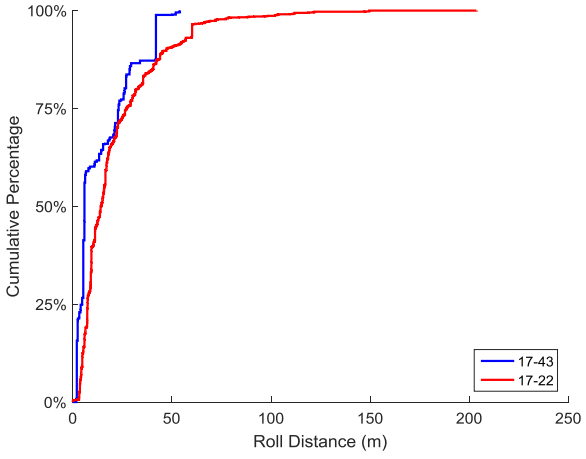

NCHRP 17-43:

- Median = 5.9 m
- N_{wgt} = 19,750
- N_{raw} = 54

NCHRP 17-22:

- Median = 14.2 m
- N_{wgt} = 132,577
- N_{raw} = 468

Figure 34. Distance between Trip and End of Roll for Rollover Events

3.4.2.3 Traffic Barrier Impacts

Figure 35 shows the cumulative distribution of vehicle departure angle in crashes involving a traffic barrier such as a guardrail or concrete median divider. The median departure angle for both NCHRP 17-22 and 17-43 Lite was 14 degrees. Note that one case weight accounted for nearly 20% of the total sample size.

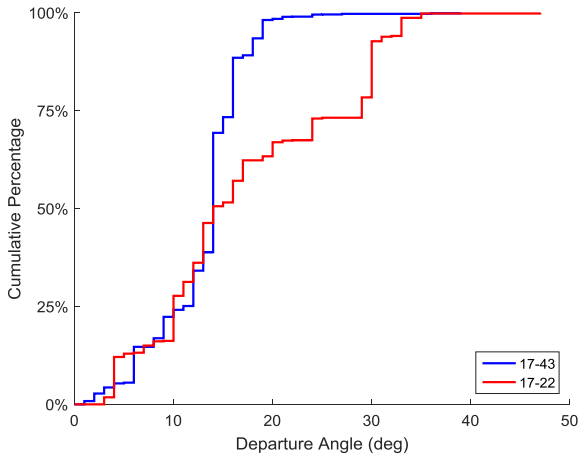

NCHRP 17-43:

- Median = 14.0 deg
- N_{wgt} = 13,157
- N_{raw} = 46

NCHRP 17-22:

- Median = 14.0 deg
- N_{wgt} = 35,569
- N_{raw} = 63

Figure 35. Departure Angle Distributions for Traffic Barrier Events

Of the 46 cases in NCHRP 17-43 Lite with the first impact being a traffic barrier, only 21 had a ΔV or *BES* from which to estimate departure and impact speed. Figure 36 shows the distribution of departure speed in single event traffic barrier cases. The median departure speed for NCHRP 17-22 was 52.9 kph, which was almost 30 kph lower than the NCHRP 17-43 Lite median of 79.0 kph. This was likely due to the distribution bias caused by the single case with a high weight proportion for the traffic barrier reconstructed subset.

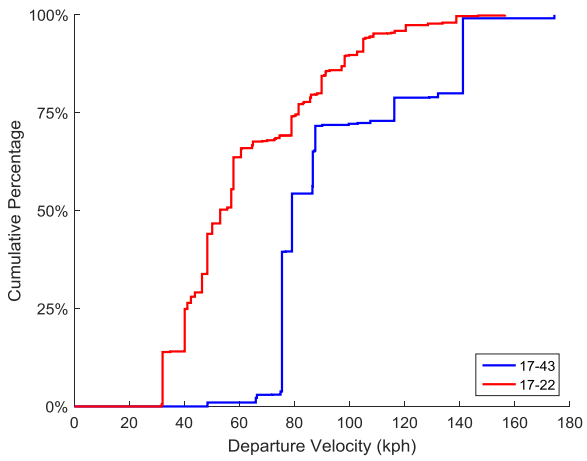

NCHRP 17-43:

- Median = 79.0 kph
- N_{wgt} = 6,993
- N_{raw} = 21

NCHRP 17-22:

- Median = 52.9 kph
- N_{wgt} = 35,243
- N_{raw} = 59

Figure 36. Departure Speed Distributions for Traffic Barrier Events

The distribution of impact speed in these traffic barrier cases are shown in Figure 37. NCHRP 17-22 had a median impact speed of 49.6 kph and the NCHRP 17-43 Lite median was 79.0 kph. Again, the one case with high weighting factor pushed the NCHRP 17-43 Lite distribution to higher speeds.

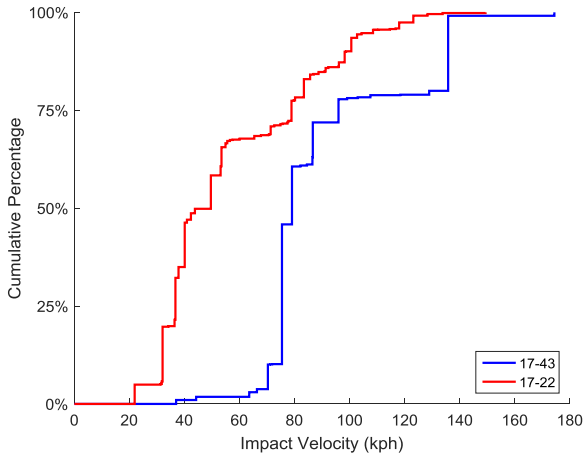

NCHRP 17-43:

- Median = 79.0 kph
- N_{wgt} = 6,993
- N_{raw} = 21

NCHRP 17-22:

- Median = 49.6 kph
- N_{wgt} = 33,740
- N_{raw} = 57

Figure 37. Impact Speed Distributions for Traffic Barrier Events

3.4.2.4 Embankment Impacts

Figure 38 shows the distribution of vehicle departure angle in cases impacting an embankment as the first event. The median departure angle for NCHRP 17-22 was 19 degrees, which is nearly double the median departure angle for NCHRP 17-43 Lite at 10 degrees.

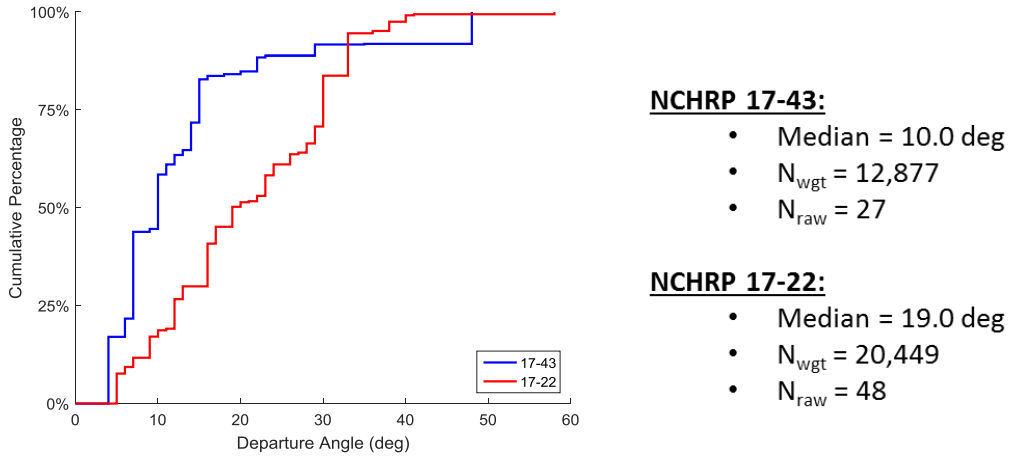

Figure 38. Departure Angle Distributions for Embankment Cases

The case count for the embankment category is even smaller than traffic barriers. Only 19 of the possible 27 cases in NCHRP 17-43 Lite had a ΔV or *BES* from which to estimate departure and impact speed. Figure 39 shows the cumulative distribution of departure speed in the embankment impact cases. The median departure speed for the NCHRP 17-22 dataset was 61.8 kph. The NCHRP 17-43 Lite median was slightly higher at 63.6 kph. Note that 2 of the reconstructed cases account for 50% of the total 17-43 Lite weighted distribution.

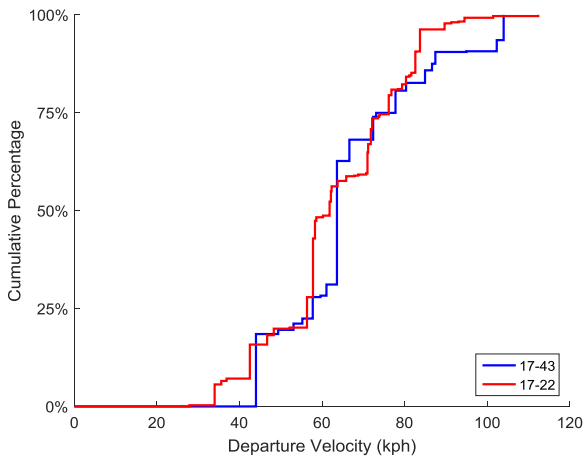

NCHRP 17-43:

- Median = 63.6 kph
- N_{wgt} = 5,672
- N_{raw} = 19

NCHRP 17-22:

- Median = 61.8 kph
- N_{wgt} = 20,154
- N_{raw} = 47

Figure 39. Departure Speed Distributions for Embankment Cases

The distribution of impact speed in embankment crashes are shown in Figure 40. NCHRP 17-22 had a median impact speed of 49.6 kph, and the NCHRP 17-43 Lite median was lower at 44.6 kph. The 2 cases with a high weight proportion had lower impact speeds.

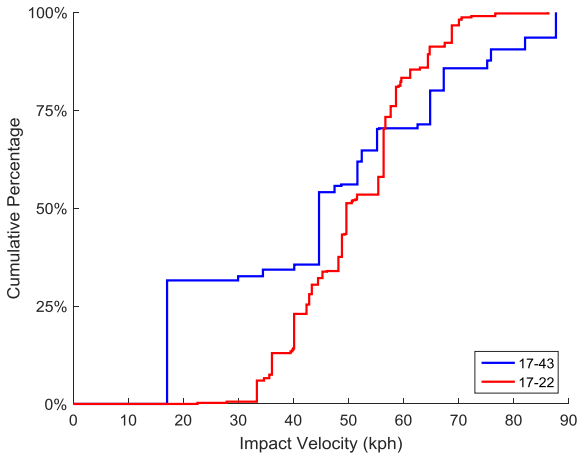

NCHRP 17-43:

- Median = 44.6 kph
- N_{wgt} = 5,672
- N_{raw} = 19

NCHRP 17-22:

- Median = 49.6 kph
- N_{wgt} = 19,909
- N_{raw} = 46

Figure 40. Impact Speed Distributions for Embankment Cases

3.4.2.5 Other Object Impacts

The common types of other objects impacted in each database are outlined in Table 6. Other objects were handled on a case-by-case basis for reconstructions, often resulting in assumptions being made to avoid throwing out more cases.

Table 6. Counts of Other Objects Impacted

Object Description	NCHRP 17-43 Lite	NCHRP 17-22
Advertisement Sign	1	-
Animal	1	-
Boulder/Rock/Ground	8	4
Bridge/Bridge Support	9	3
Building/Wall	4	4
Curb	43	6
Delineator/Other Small Post	2	9
Demarcation Box	-	1
Ditch/Culvert	12	15
Dumpster/Storage Container	3	-
Fence/Post	14	9
Fire Hydrant	5	-
Guide Wire	3	-
Hay Bales	1	-
Mailbox	6	11
Phone/Utility Terminal	1	1
Shrubbery/Bush/Stump/Branch	14	7
Stone Column	2	-
Vehicle/Trailer	1	-
Water Well Casing	-	1
Total	**130**	**71**

Figure 41 shows the distribution of departure angle in cases with initial impacts involving other objects for both NCHRP datasets. The median departure angle for both datasets was 11 degrees.

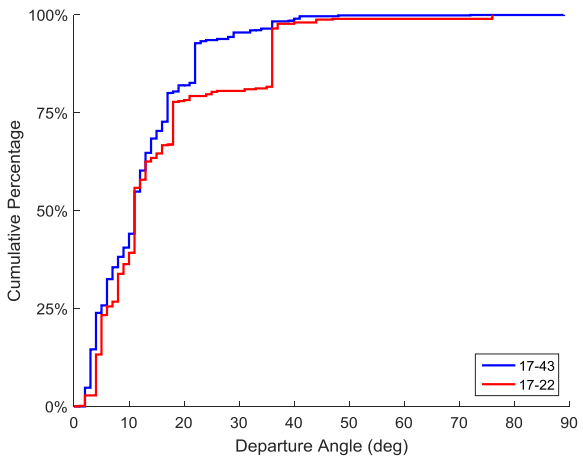

NCHRP 17-43:

- Median = 11.0 deg
- N_{wgt} = 48,314
- N_{raw} = 130

NCHRP 17-22:

- Median = 11.0 deg
- N_{wgt} = 23,881
- N_{raw} = 71

Figure 41. Departure Angle Distributions for Other Object Events

Only 71 of 130 other object cases had a ΔV or *BES* from which to estimate departure and impact speed in NCHRP 17-43 Lite. Figure 42 shows the cumulative distribution of departure speeds for other object events. NCHRP 17-22 had a median of 67.4 kph compared to 69.7 kph for NCHRP 17-43 Lite.

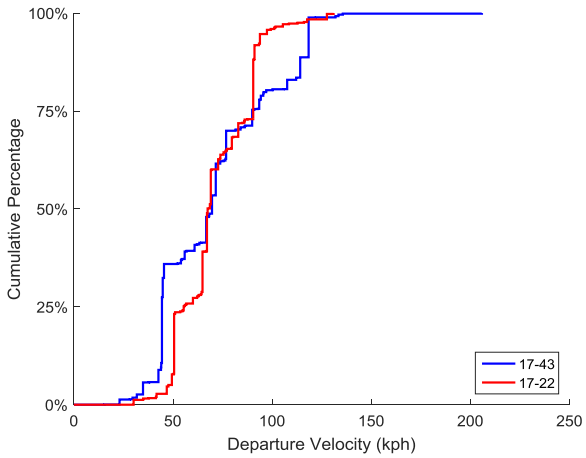

NCHRP 17-43:

- Median = 69.7 kph
- N_{wgt} = 28,315
- N_{raw} = 63

NCHRP 17-22:

- Median = 67.4 kph
- N_{wgt} = 23,339
- N_{raw} = 67

Figure 42. Departure Speed Distribution for Other Object Events

Figure 43 shows the distribution of other object event impact speeds. The NCHRP 17-22 dataset had a median impact speed of 60.7 kph. NCHRP 17-43 Lite had a median of 56.8 kph.

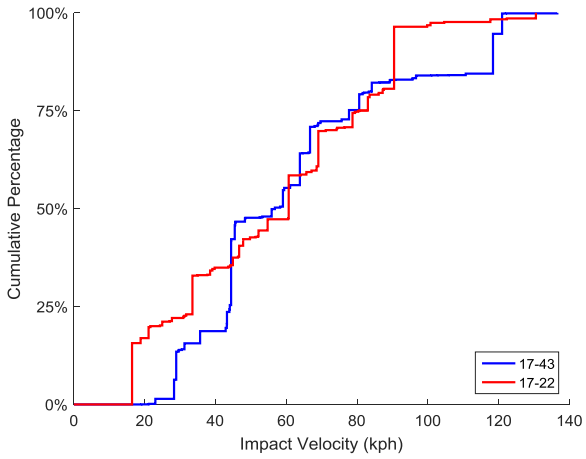

NCHRP 17-43:

- Median = 56.8 kph
- N_{wgt} = 28,315
- N_{raw} = 63

NCHRP 17-22:

- Median = 60.7 kph
- N_{wgt} = 22,675
- N_{raw} = 64

Figure 43. Impact Speed Distribution for Other Object Events

Although the other impacted object category was the most diverse subset of the two datasets compared in this analysis, departure angle, departure speed, and impact speed were all in good agreement.

3.4.2.6 All Impacts

Figure 44 shows the overall distribution of departure angle for all cases, single and multi-event, in the databases. The angle used for cases with multiple departures was the trajectory angle at the first POD. The median departure angles were in good agreement, with a NCHRP 17-22 median of 15 degrees and a NCHRP 17-43 Lite median of 11 degrees.

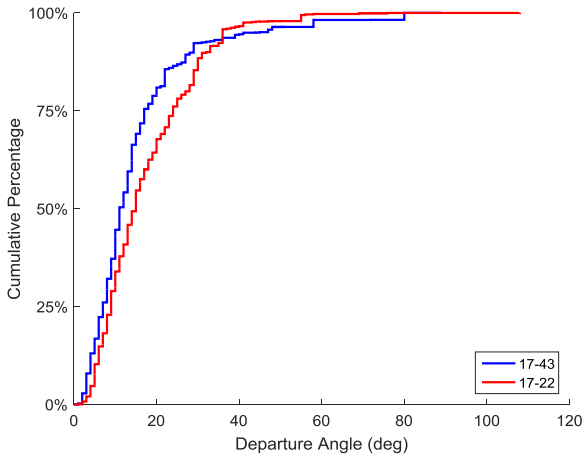

NCHRP 17-43:

- Median = 11.0 deg
- N_{wgt} = 164,883
- N_{raw} = 504

NCHRP 17-22:

- Median = 15.0 deg
- N_{wgt} = 281,018
- N_{raw} = 876

Figure 44. Departure Angle Distribution for All Cases

Figure 45 shows the distribution of departure speeds for all cases in NCHRP 17-22 and NCHRP 17-43 Lite. Only the speed at the first POD was used for cases with multiple departure events. The median departure speed for all cases in 17-22 was slightly lower at 67.9 kph compared to 72.3 kph for 17-43 Lite.

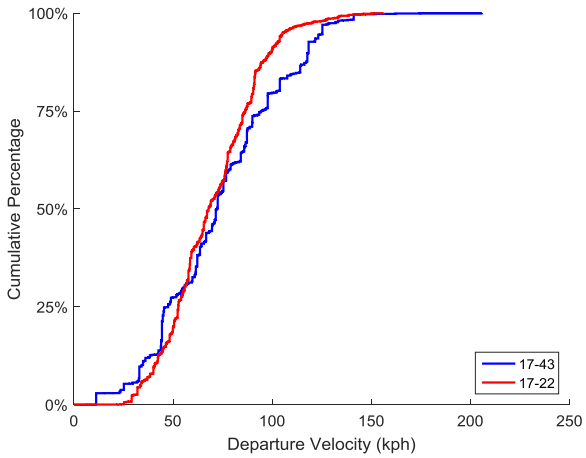

NCHRP 17-43:

- Median = 72.3 kph
- N_{wgt} = 99,671
- N_{raw} = 275

NCHRP 17-22:

- Median = 67.9 kph
- N_{wgt} = 276,231
- N_{raw} = 856

Figure 45. Departure Speed Distribution for All Cases

Figure 46 shows the impact speed cumulative distributions for all cases. Only the impact speed at the first event was used for comparison, as crash characteristics and vehicle dynamics

widely vary after initial impact depending on what objects are impacted and vehicle trajectory. In contrast to departure speed, the median impact speed for NCHRP 17-22 was higher at 54.7 kph compared to 47.2 kph for NCHRP 17-43 Lite.

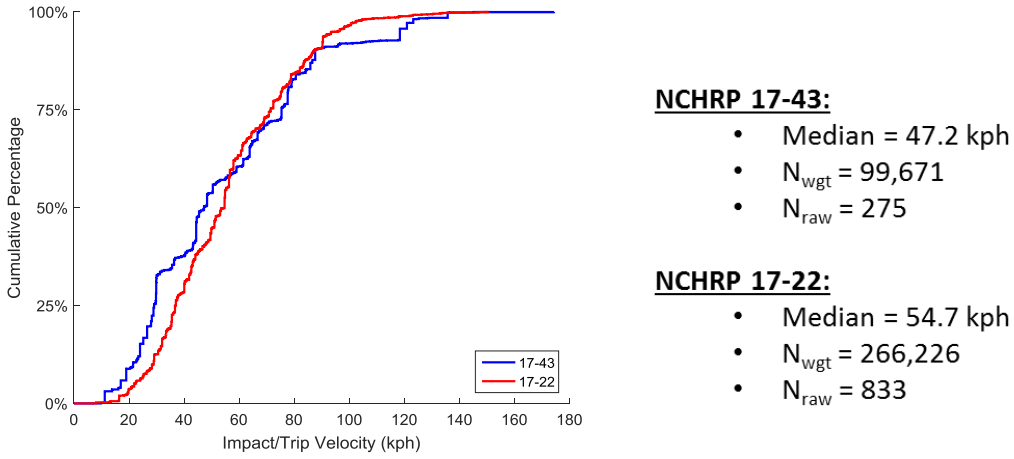

Figure 46. Impact/Trip Speed Distribution for All Cases

Figure 47 shows the distribution of distance between POD and point of first impact/trip for all cases in NCHRP 17-22 and NCHRP 17-43 Lite. The same methodology used to estimate linear distances for the rollover cases was applied to all cases, substituting coordinates of the trip point with coordinates of the first impact point. The median distance to impact/trip for 17-43 Lite was 9.4 m. The median distance for 17-22 was 13.5 m. This distance was more than 40% further than the median distance traveled in NCHRP 17-43 Lite. Note that 22% (N_{raw} = 91) of the 17-43 Lite weighted sample had a distance to impact of 0 m, while only 10% (N_{raw} = 50) had a 0 m distance in 17-22. This means that more crashes in 17-43 Lite were initiated with roadway features at the POD. Removing these cases with 0m travel distances shifts the medians of the 17-22 and 17-43 Lite distributions to a more agreeable 15.0 m and 13.4 m, respectively.

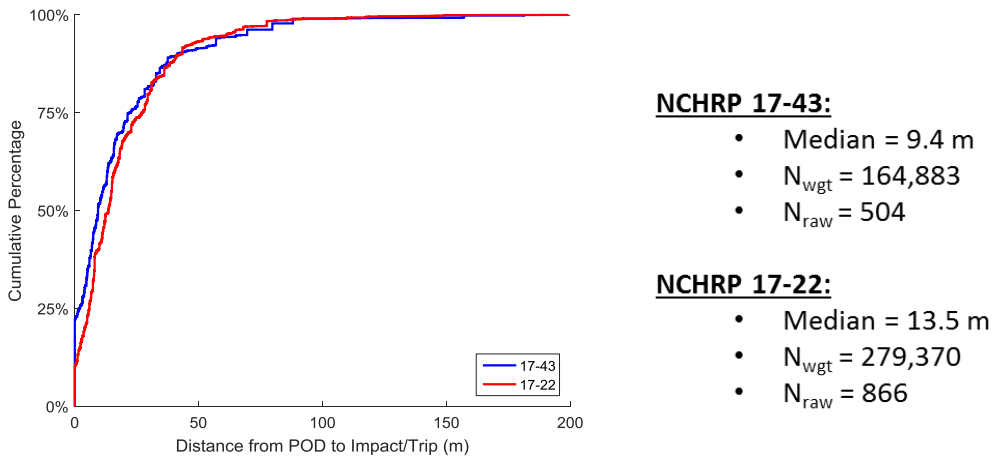

Figure 47. Distance between POD and Impact/Trip Point for All Cases

Figure 48 shows the distribution of linear distance between POD and point of final rest for all cases in NCHRP 17-22 and NCHRP 17-43 Lite. The median linear distance to final rest from POD for 17-43 Lite was 21.7 m. The median distance for 17-22 was 28.3 m. This distance was about 30% further than the median distance traveled in NCHRP 17-43 Lite. In some cases, the linear distance may underestimate the total distance traveled if there were segments that followed more of a curved path.

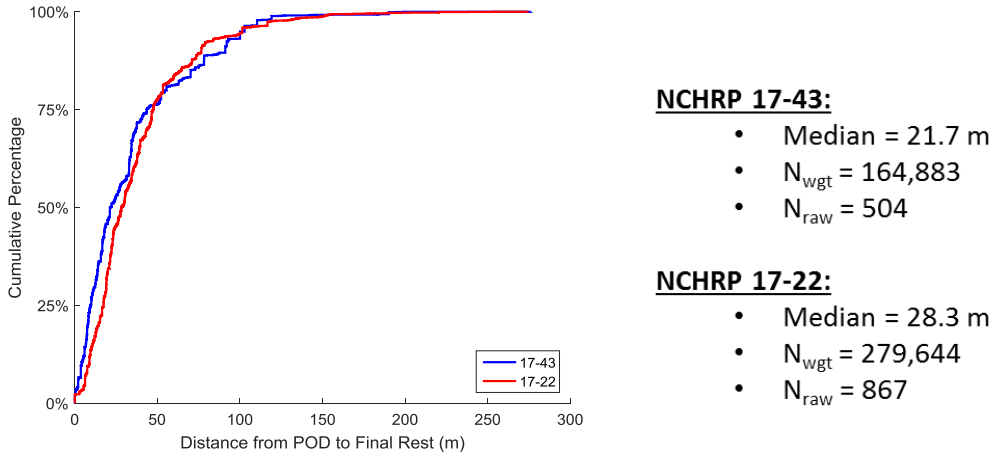

Figure 48. Distance between POD and Final Rest for All Cases

3.4.3 VALIDATION OF NCHRP 17-43 LITE USING EDR DATA

To validate the reconstruction methodology and speeds derived in this chapter, the reconstructions were compared with event data recorder (EDR) data. EDRs record up to 5 seconds of data before a crash occurs. Data elements recorded include vehicle speed, throttle/brake application, and airbag deployment status. The information downloaded from EDRs can be used to understand crash causation, performance of safety systems, and driver action prior to the crash [55][56][57]. One key parameter measured by these devices is ΔV. As previously discussed in the methods, ΔV is the most commonly used crash severity measure and has been shown to correlate well to injury [47][48][58]. However, the NASS/CDS estimation of ΔV using algorithms relying on vehicle crush profile and properties such as stiffness has been found to underestimate ΔV by about 13-15% [48]. EDR ΔV is an objective measure that can be used to validate the estimated values in NASS/CDS, but the sample size of crashes with available EDR data is small.

Out of the entire NCHRP 17-43 Lite dataset, only 107 cases had EDR data downloaded in NASS/CDS. However, many of the EDR files associated with these cases contained invalid or unusable data (*ptime* or *pvalue* = –999x), or it was impossible to match EDR events with the NASS/CDS case event (typically in complex multiple event crashes). Invalid EDR data was defined as records containing time or data values of –999X, where X can be any integer. To ensure accurate EDR data was being used for this validation, only EDR events triggered by an airbag deployment or EDR events classified as non-deployment with a ΔV over 5 mph were used. Also, the first event coded in NASS had to be the most severe event (highest ΔV) to improve the certainty that the events matched. These restrictions filtered the 107 case sample to 38 cases.

Step I of the validation was to compare NASS/CDS and EDR ΔV. For this portion of the validation, 22 of the remaining 38 cases were found to have valid EDR ΔV data and a NASS/CDS ΔV. One (1) case was removed because it involved a rollover event, and 2 additional cases were manually

removed because the NASS/CDS and EDR event sequence did not match. Step II of the validation was to compare the reconstructed NCHRP 17-43 Lite departure and impact speeds to the EDR pre-crash speeds. Of the 38 filtered cases, 31 were found to have valid EDR pre-crash speed, but only 25 were also reconstructed in the 17-43 Lite database. Table 7 outlines the cases included in the validation sample of Step I and Step II.

Table 7. Cases Available to Validate Reconstructed Speed and ΔV with EDR Data

Case List Description	Case Count
In NCHRP 17-43 Lite and EDR Present	107
NCHRP 17-43 Lite Cases with Complete and To-Scale Scene Diagrams	96
EDR Data with Deployment Event or Triggered by Non-Deployment with ΔV > 5 mph	71
First Event Coded in NASS/CDS was Most Severe Event	38
STEP I:	
EDR Data Contained Vehicle Δ*V* (i.e., *pcode* = 1010)	35
EDR Data Contained Valid *ptime* and *pvalue* (i.e., not -999X)	26
NASS/CDS Data Contained ΔV Estimate	22
Non-Rollover Cases	21
Manually Inspected for Correct NASS/CDS Event Matchup	**19**
STEP II:	
EDR Data Contained Vehicle Pre-Crash Speed (i.e., *pcode* = 1040)	33
EDR Data Contained Valid *ptime* and *pvalue* (i.e., not -999X)	31
Reconstructed in NCHRP 17-43 Lite using NASS/CDS Data	**25**

The first validation step compared NASS/CDS and EDR Δ*V* values. Figure 49 illustrates this comparison. For EDRs, the maximum Δ*V* was used as the objective measure. Note that only 19 cases were validated. NASS/CDS tended to under-predict Δ*V* by 11% compared to EDR data, similar to the 13-15% underestimation reported in [48].

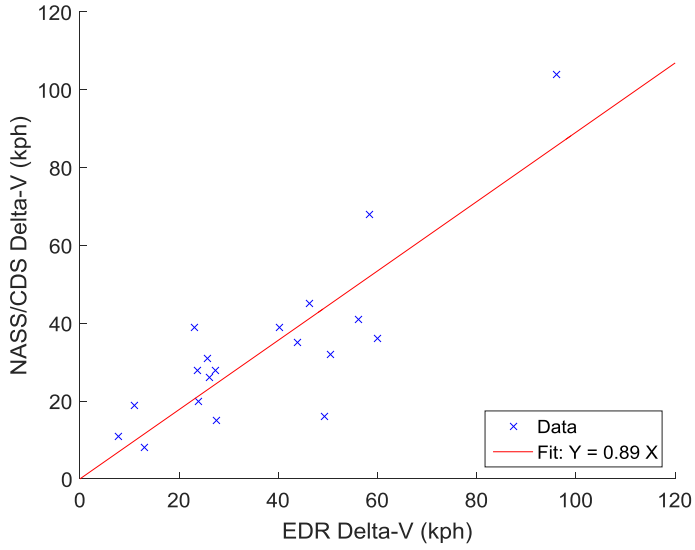

Figure 49. Validation of NASS/CDS ΔV with EDR ΔV

The second validation step involved comparing the reconstructed departure and impact speeds in NCHRP 17-43 Lite to EDR velocity profiles. The velocity profile of EDRs typically record pre-crash speed several seconds prior to impact. Depending on the vehicle manufacturer, EDRs may record data every 0.1, 0.5, or 1 second. In some EDRs, the last sampled data point is at impact for time step 0 (t_0). The more common practice, however, is that impact occurs at or within one time sample after time step -1 (t_{-1}). For the latter, there is a potential 1 time step bias since true impact could have occurred anywhere between t_{-1} and t_0. To account for this bias, cases that only provided pre-crash data up to t_{-1} were linearly interpolated to t_0.

Figure 50 shows the cumulative distribution of reconstructed impact speeds and EDR impact speeds for both time points in each of the 25 cases. The median NCHRP 17-43 Lite impact speed was lower than both the EDR medians at 48.4 kph. This suggests the NCHRP 17-43 Lite reconstruction methods slightly underestimated impact speed, which is consistent with the underestimation of ΔV. Of the 25 cases, 19 involved a pole, tree, or narrow object, 1 involved a metal barrier, 1 involved an embankment, 2 involved rollovers, and 2 involved impacts with other roadside objects.

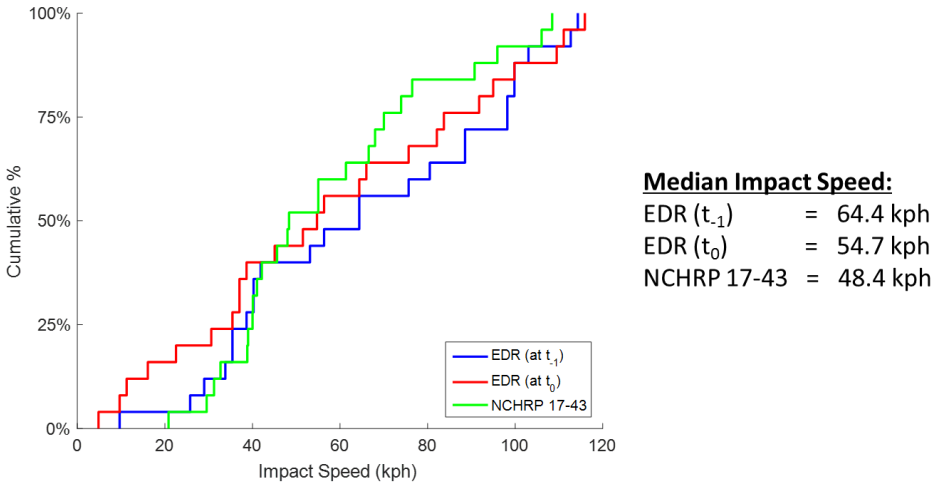

Figure 50. Distribution of NCHRP 17-43 Lite and EDR Impact Speeds

Figure 51 illustrates the comparison of NCHRP 17-43 Lite impact speeds to EDR impact speeds assuming true impact occurred at time step t_{-1}. The regression fit shows a 17% underestimation of speed using the reconstruction methods.

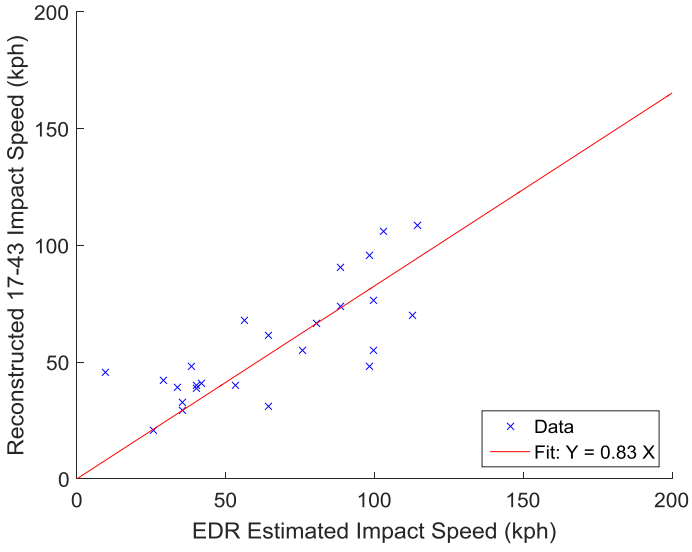

Figure 51. Validation of NCHRP 17-43 Lite Impact Speed with EDR speed at t_{-1}

Similarly for true impact assumed at EDR time step t_0, the regression fit shown in Figure 52 estimates a 16% under-prediction of impact speed following the NCHRP 17-43 Lite reconstruction methods, but with more variation.

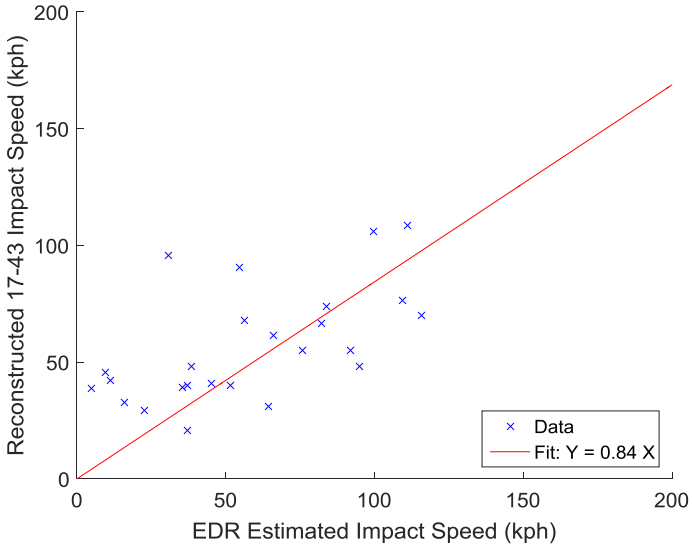

Figure 52. Validation of NCHRP 17-43 Lite Impact Speed with EDR speed at t_0

Comparing departure speeds required additional computation of the EDR speed profile to align with vehicle position on the scene diagram. Using the NCHRP 17-43 Lite vehicle trajectory points, a cumulative segment distance between the point of impact (POI) and POD was calculated. The EDR speed profile was then integrated using trapezoidal integration to work back from impact. The cumulative distance from this integration was used to determine which time-velocity point corresponded to an equivalent distance traveled to the POD. Again, this integration was performed twice—assuming true impact at t_{-1} and t_0—to account for EDR sampling bias. One case involved a vehicle that traveled a significant distance off road before impact, so the EDR did not capture enough pre-crash data to integrate back to the POD. Therefore, only 24 cases were compared for departure speed.

Figure 53 shows the cumulative distribution of departure speeds for the NCHRP 17-43 Lite reconstructions and the two EDR integrations. The NCHRP 17-43 Lite departure speed median was 67.3 kph, which was closer to the EDR median values compared to the impact speed distribution.

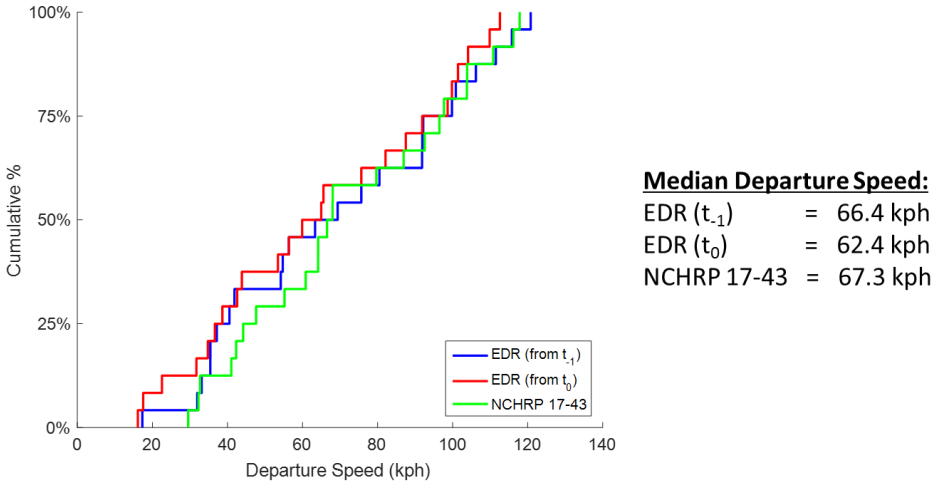

Figure 53. Distribution of NCHRP 17-43 Lite and EDR Departure Speeds

The validation of NCHRP 17-43 Lite departure speeds and EDR speeds estimated from t_{-1} is shown in Figure 54. Compared to impact speed, the departure speeds are in much higher agreement. The fit suggests a 0.5% underestimation of departure speed in the NCHRP 17-43 Lite reconstructions.

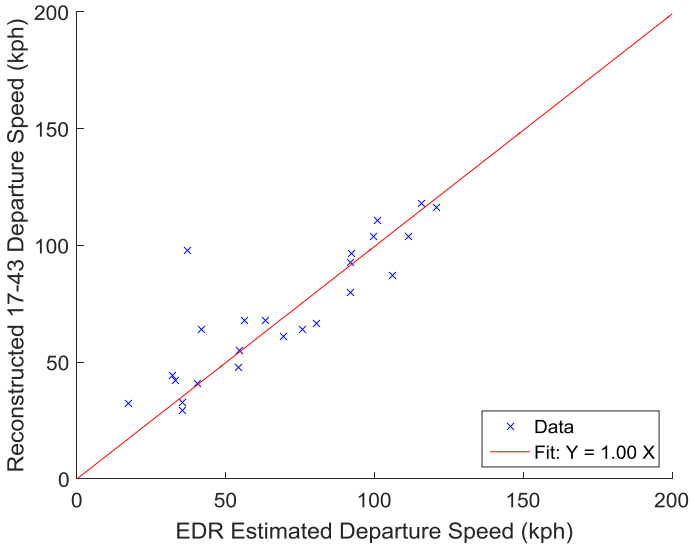

Figure 54. Validation of NCHRP 17-43 Lite Departure Speed with EDR Speed from t_{-1}

Similarly for EDR true impact assumed at t_0, Figure 55 shows high agreement between NCHRP 17-43 Lite reconstructed departure speeds and EDR integrated departure speeds. The regression expresses a 5% overestimation of departure speed using the NCHRP 17-43 Lite methods.

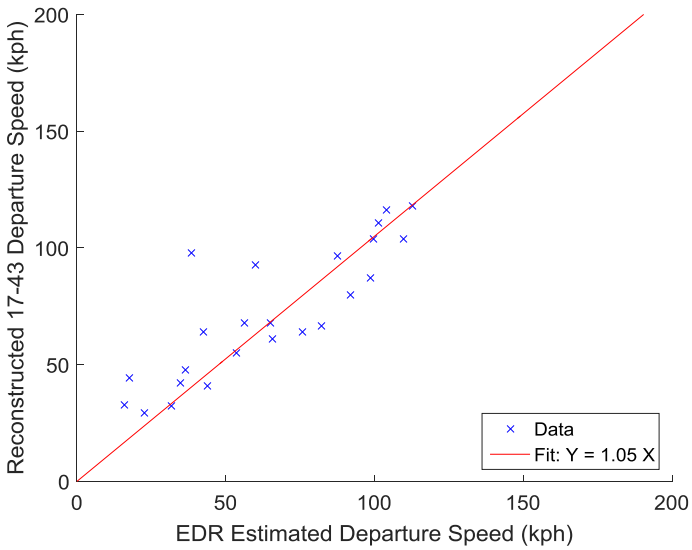

Figure 55. Validation of NCHRP 17-43 Lite Departure Speed with EDR Speed from t_0

One outlier identified in the departure speed distributions highlights a limitation in the NCHRP 17-43 Lite reconstruction methods: the influence of driver action. Figure 56 shows the scene diagram of NASS/CDS Case ID 773015315. The vehicle crossed the median dividing oncoming traffic in an intersection and continued over some distance before contacting a tree. Following the reconstruction methods outlined in NCHRP 17-43 Lite, constant drag factors were assumed from the POD to impact. However, the EDR record shows a constant pre-crash speed up to 5 seconds prior to impact. This indicates the driver was not decelerating as assumed with the drag factors. Unknown driver action prior to impact for the majority of the NASS/CDS cases may be a significant limitations to some of the reconstructions.

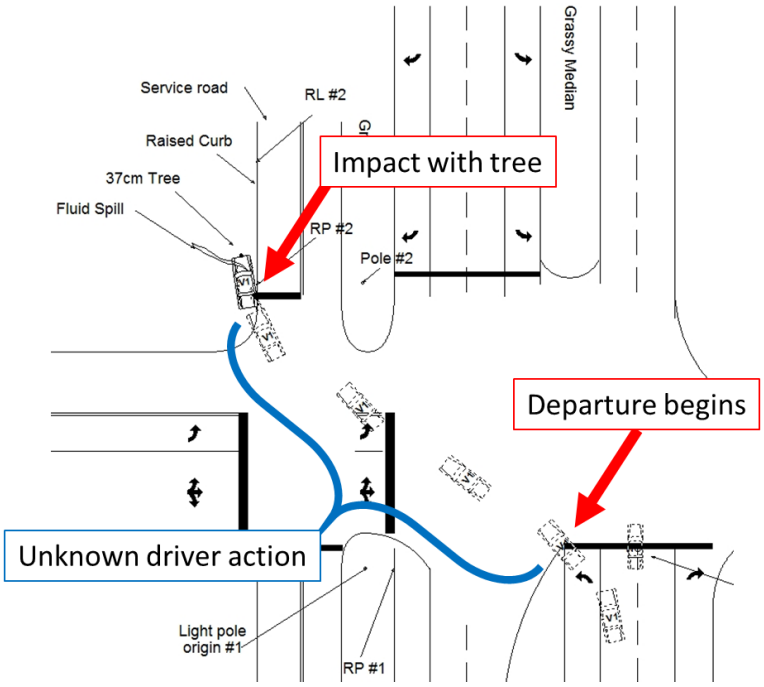

Figure 56. Example Outlier Case where Driver Action is Unknown

3.5 Discussion

Overall, the results from this chapter show the NCHRP 17-43 Lite reconstructed departure and impact parameters were in reasonably good agreement with the previous NCHRP 17-22 and EDR

data. The departure angle of 11 degrees was close to the 15 degrees for 17-22. The larger departure angles also confirm the hypothesis that compared to the NDS drift out of lane departures, with departure angles around 0.5 degrees as seen in chapter 2, road departure crashes occur at much steeper departure angles. These steeper departure angles are more difficult for drivers to recover from and safely return to the initial lane of travel. Also note that the NCHRP 17-43 Lite median departure and impact speeds for these real-world crashes were much lower—around 72 kph and 47 kph, respectively—than the vehicle speeds of over 100 kph seen in the NDS data from chapter 2. The NDS data was collected primarily on well-marked highways with high speed limits. In contrast, the NCHRP dataset contained more diverse road characteristics such as local and collector roads containing more curved segments and lower speed limits.

The rollover cases in NCHRP 17-43 Lite displayed sizable differences in departure and impact speed from the NCHRP 17-22 study. Two factors likely contributed to these differences: high case weight proportions and differences in reconstruction protocol. In the rollover subset, 5 of the 54 cases accounted for 56% of the total weighted sample. These high proportion weights biased the distribution medians to higher departure speeds and lower impact speeds. The second factor accounting for some of the shift in reconstructed speeds is related to the differences illustrated in distance to trip and roll distance. While NCHRP 17-43 Lite was largely modeled after NCHRP 17-22, there was a slight difference in the definition of vehicle trip point during a rollover event. In 17-22, the trip point was defined as the last trajectory point on the scene diagram where the vehicle was still drawn on all 4 wheels. In 17-43 Lite, however, the first vehicle drawn on its side was defined as the trip point. The analysis found that NCHRP 17-43 Lite crashes traveled further off road from the POD before rollover initiation, but rolled for less distance compared to NCHRP17-22 crashes. This is consistent with the trip point convention and partially explains why 17-43 Lite departure speeds were higher and impact speeds lower. Working from the end of a crash back to the point of vehicle trip, further roll distances result in higher trip speeds according to the Kildare curves. However,

working back from rollover initiation to the POD, drag factors increase departure velocity as they are applied over longer distances. Some of the other discrepancies in this comparison came from the influence of high proportion weighting factors in distributions where only a small number of cases were reconstructed, such as the single case accounting for 35% of the total weighted sample in traffic barrier departure and impact speed distributions.

One concern and limitation with the reconstruction methods used in both NCHRP databases was that calculating departure and impact speeds relied heavily on the ΔV or *BES* estimates provided in NASS/CDS. The validation of reconstructed speeds and EDR pre-crash data helped alleviate some of the concern. As previous studies have shown, the NASS/CDS method for computing change in velocity tends to underestimate by about 13-15% compared to EDR records for passenger vehicles [48]. The validation completed for the small sample of 19 cases in this analysis confirmed the NASS/CDS values were low by 11%. The primary parameter this underestimation directly influenced was the impact velocity, as it decreased the assumed energy absorbed by the vehicle upon impact. However, the analysis showed that the under-prediction of departure and impact speeds were similar at 17% and 16%, respectively.

Although the validations suggest the reconstruction methods for estimating departure parameters used in NCHRP 17-43 Lite were generally valid, there were several limitations and assumptions made that should be noted. For the EDR comparisons, linear interpolation and extrapolation of the time series data was a crude method. The method amplified any error or bias in the EDR data since it relied on the slope of the surrounding speed profile segment. The further from the recorded data time point, the less accurate calculations for a case would be. Also, most EDRs have low recording rates. For the last pre-crash data point prior to impact, t_{-1}, impact could have occurred anywhere between that last point and one time step later. Few manufacturers claim to record true impact at t_0.

Other limitations related to the reconstruction methods include the assumptions made for energy dissipated through vehicle-ground friction after departure. Drag factors were selected based on the traversed surface types and conditions. These drag factors assumed a constant deceleration for each segment. However, driver and vehicle characteristics during a crash are dynamic. Distracted, drowsy, or impaired drivers may not realize they are in a crash scenario until impact. In cases like these, assuming constant drag factors from the POD to impact could inflate the reconstructed departure speed. Similarly, brake and throttle application, as well as other driver actions, are often unknown and could lead to error in the reconstruction methods.

In addition to the drag factor assumptions, other limitations in the reconstruction methods involve the NASS/CDS data available. Scene evidence is typically collected several days to weeks after the crash occurred. By the time the case is investigated, the vehicle and roadside features may have been repaired. Other scene evidence may no longer be available. Surface conditions may be masked by snow, damaged property may have been repaired or replaced, or the crash location may be too dangerous for an investigator to take photographs and measurements. Reasonable assumptions were often made about characteristics such as pole diameter and elevation change.

3.6 CONCLUSIONS

This chapter outlined our development and validation of the NCHRP 17-43 Lite database. The data collected and reconstructions performed in this dataset were validated using EDR data and compared with NCHRP 17-22 data. The comparison of EDR data showed NASS/CDS tended to underestimate ΔV by 11% in the 17-43 Lite dataset. However, the comparisons of departure angle, departure speed, and impact speed were in good agreement with the 17-22 departure conditions. Through this characterization of single vehicle road departure crashes, it is apparent that the departure conditions, such as departure angle, are much more severe compared to the minor drift out of lane departures seen in the NDS normal lane keeping data of Chapter 2.

One way to significantly improve on the results from this characterization of road departure crashes would be to increase the sample size. Over half of the original NCHRP 17-43 cases were discarded due to a lack of complete NASS/CDS data and established reconstruction methods. Future extensions should continue to add more recent NASS case years to the database to increase the number of cases that can be fully reconstructed and validated. Also, for some cases that could not be fully reconstructed using NASS/CDS data, it may possible to use EDRs to perform departure and impact speed reconstructions as shown in the EDR validation section.

4 IMPROVEMENTS TO THE LANE DEPARTURE WARNING SYSTEM FLEETWIDE SAFETY BENEFITS MODEL

4.1 BACKGROUND

The final portion of the research objective for this thesis was to investigate how lane departure safety systems could help avoid, or at least mitigate, single vehicle run-off-road departure crashes. The hope with these systems is that if a driver is alerted to an impending crash at or near the point of departure (POD), the driver may have adequate time to react and correct the vehicle trajectory.

4.1.1 THE ORIGINAL LDW BENEFITS MODEL

Kusano et al. (2014b) developed a simulation model to estimate the benefits of lane departure warning (LDW), assuming every vehicle in the U.S. fleet was equipped with this system. The study used a subset of NASS/CDS 2012 cases involving single vehicle road departure crashes to perform simulations. Two scenarios were considered for each case: 1) the crash occurred exactly as depicted in NASS/CDS, and 2) the crash occurred as depicted, but a LDW was delivered the instant the leading edge of the vehicle crossed the lane boundary. Comparing the outcome of simulation condition 2) to condition 1) allowed estimation of crash and injury reduction. The benefits model predicted LDW could potentially prevent 29% of all drift out of lane road departure crashes, and could reduce the number of serious driver injuries, or injuries with a Maximum Abbreviated Injury Score of 3 or greater (MAIS 3+), by 24% [59][60]. The AIS scale ranges from 1 to 6, with higher values correlating to an injury with a higher threat to life [61].

In the driver reaction model, it was assumed that there was some delay between when the LDW was delivered to the driver and when the driver took evasive action. A steering radius, R, was defined as $R = v^2/\mu g$, where v is vehicle speed at the POD, μ is the roadside surface coefficient of friction, and g is the acceleration of gravity. A coefficient of friction of 0.5 was selected, which was in

the middle of the range of values used in NCHRP 17-22 and 17-43 Lite reconstructions, and resulted in similar steering angles reported by Mazzae et al. (1999) in a driver avoidance behavior test track study [62]. In simulations where the vehicle was not equipped with LDW, the driver was assumed to be alerted to the departure once the vehicle departed the paved roadway. In simulations with LDW, the driver was assumed to be alerted when LDW was delivered, which was assumed to occur the instant the leading wheel first touched the lane line. For both simulation scenarios, the driver was assumed to steer back toward the road at the estimated steering radius after prescribed reaction times. The driver model did not account for any braking and assumed a constant velocity throughout the simulated trajectory.

For the trajectory model, the roadside was divided into discrete zones parallel to the road edge. The simulated trajectory was broken into three segments. The first segment was based on a straight line trajectory of vehicle speed and angle at departure. At the point of driver reaction to the departure, the driver reaction model contributed a curved segment to steer the vehicle back towards the roadway. In most simulations, the vehicle returned to the road during this curved segment. However, if the vehicle was still in one of the roadside zones, a third segment was added. This third segment was a straight line continuation at the end of the steering input and ensured the vehicle return angle was no greater than 45 degrees. Figure 57 shows an illustration of this trajectory model. The further into each zone and the more distance traveled in each zone, the higher the probability was of a crash occurring. Measurements from NCHRP 17-22 of lateral distance between impacted roadside objects and roadway edge were used to predict the probability of impact or crash in each zone. Driver injury outcome was the product of this probability that a crash occurred and the probability of injury given the crash occurred. [59][60]

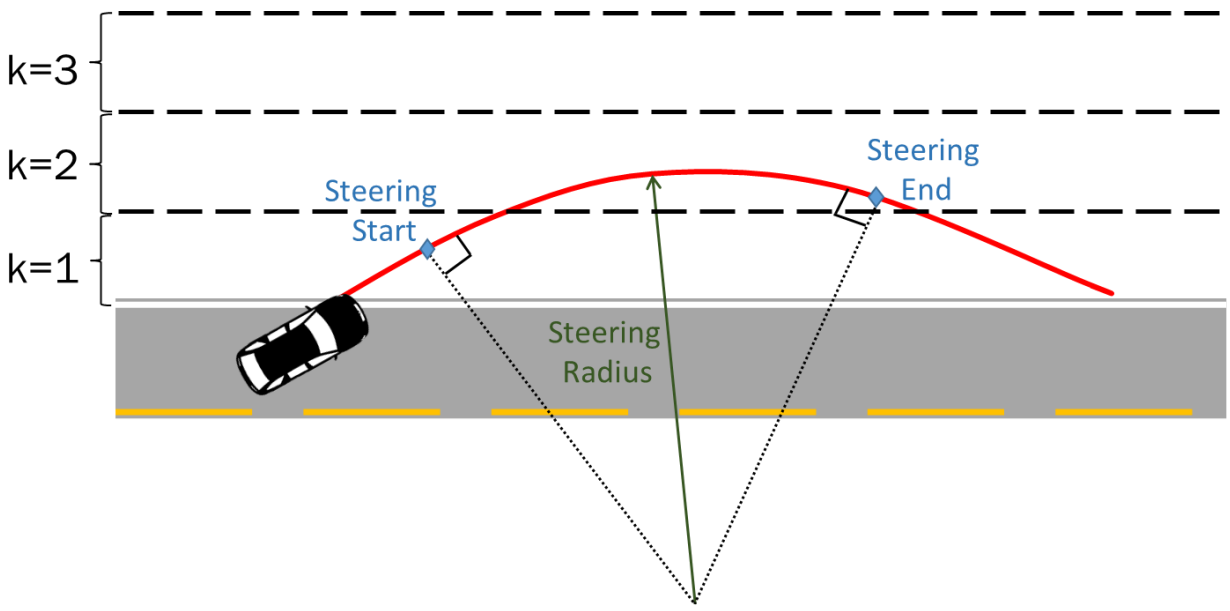

Figure 57. Original LDW Benefits Trajectory Simulation Model

In the original LDW benefits model, several key factors such as vehicle departure angle and speed, and departure ROC were not known. These parameters were instead estimated using statistical regression models—not measured values. The original LDW benefits model [59] was developed before completion of NCHRP 17-43 Lite, so the older NCHRP 17-22 dataset was utilized to estimate departure parameters and injury risk [59][60]. Kusano et al. (2014b) performed one-way analysis of variance (ANOVA) to identify significant predictors for departure speed, departure angle, and departure radius of curvature. Then, models were developed maximizing the goodness of fit statistic, adjusted-R^2. Assuming a normal probability distribution, three values divided the normal distribution into three equal portions of area. The 17th, 50th, and 83rd percentiles were computed for each departure parameter for each simulation case.

For injury risk, the probability of an injured driver given a crash was modeled using logistic regression. The two predictors used to determine serious MAIS 3+ driver injury outcome were departure velocity, *v*, and seat belt use, *belted*. The relationship is defined in Equation 19. For seat belt use, a value of 1 indicates the driver is belted and 0 indicates the driver is unbelted. Departure

velocity is in kph. It is important to note that NCHRP 17-22 data was used to generate this injury risk function, which consisted of much older vehicles. These older vehicles likely had much different occupant protection systems and injury outcome than vehicles in the NCHRP 17-43 Lite dataset.

$$P_{injured} = \frac{1}{1 + \exp\left(-(-3.0257 + 0.0277 * v - 1.910 * belted)\right)} \qquad \textbf{Equation 19}$$

While departure speed, angle, and ROC relied on regression models, roadway shoulder width was estimated based on a manual review of scene photographs. For each case, the shoulder width was classified into one of four ranges: less than 0.3 m (zero-width), 0.3 to 1 m, 1 to 3.6 m, or above 3.6 m. The minimum and maximum value of the selected range accounted for the simulation conditions for shoulder width.

Reaction times were obtained from driving simulator studies [63][64]. Kozak et al. (2006) conducted a driver simulator study of the effect of drowsiness on driver reaction time during lane departure scenarios. The 32 test subjects were sleep-deprived for 23 hours and then sent into a driving simulator to complete an approximately 3 hour test drive. During the test drive, lane departures were randomly induced by the simulator operator. With LDW, the average reaction time of drowsy drivers was 0.62 seconds. Without LDW, reaction times were as high as 2.36 seconds, with an average of 1.17 seconds [64]. A similar simulator study by Suzuki et al. (2003) on non-drowsy drivers analyzed 54 departure events from 24 drivers. Departures were induced by giving drivers a secondary task to focus on while driving. The study found driver response times ranged from 0.38 to 1.36 seconds depending on waring modality and whether or not the driver was informed of the LDW system function [63]. The study consisted of 24 drivers and a total of 54 departure events. The two extremes from this study were used as a fast and slow response time in the LDW benefits simulation model since the range also captured average reaction times from [64].

In total, each NASS/CDS crash could have up to 108 simulations (3 angles * 3 speeds * 3 ROCs * 2 reaction times * 2 shoulder widths = 108 simulations). Further details about the methodology behind the mathematical predictive models of departure parameters can be found in [59] and the corresponding supplemental material. While the original LDW benefits model was comprehensive, there are several areas that could be enhanced to improve the model value and accuracy. The original model relied on statistical regression for departure input parameters, used an injury risk function based on departure velocity and outdated safety technology, and did not model the benefits of LDP.

4.1.2 Needed Improvements to the Original LDW Benefits Model

The outcome of each case—crash or no crash, injury or no injury—was highly dependent on the simulated vehicle trajectory, driver reaction time, and roadway characteristics. While the statistical models derived in [59] were based off a real-world crash dataset, NCHRP 17-22, the models carried extremely low R^2 values ranging from 0.04 to 0.48. The NCHRP 17-43 Lite database has since been completed and departure parameters for more recent real-world crashes are known. As discussed in the previous chapter, real-world crash databases such as NASS/CDS do not collect complete roadside details needed to study road departure crashes in this manner. However, the supplemental data collection and crash reconstructions from the NCHRP 17-22 and NCHRP 17-43 Lite projects were developed to provide the data for these types of analyses. In particular, departure parameters such as vehicle angle and speed, road radius of curvature (ROC), and shoulder width can be used to characterize a crash scenario and determine whether or not drivers would have been able to avoid a crash if a LDW was delivered.

There is a need for three main improvements to the original LDW benefits model. The first area of improvement involves the input departure parameters discussed above. The reconstructed departure speeds, angles, and ROCs in the NCHRP 17-43 Lite dataset have potential to enhance the original LDW benefits model. Replacing the original simulated departure parameters with measured

17-43 Lite values would reduce reliance on statistical model predictions, improve accuracy, and limit the number of simulations required for each case. The second enhancement involves utilizing the reconstructed impact speeds in 17-43 Lite to modify the injury risk function and the trajectory simulation model. In the original LDW benefits model, injury was assessed based on a function of departure velocity and belt use. Although ΔV is the standard parameter used to correlate crash severity to injury [47][48], it is not typically reconstructed in collisions with roadside objects. However, one hypothesis is that impact speed may prove to be a better injury predictor than departure speed and more closely relate to the ΔV correlation. Vehicle speed is likely to change based on roadside surface conditions and driver action between the POD and point of impact where injury would occur. Also, the steering radius calculated to input into the trajectory model relies on departure velocity as previously discussed. Since there is a delay between the POD and the start of steering, a proposed improvement is to add a deceleration term for the first segment. This would account for changes in vehicle speed after departure and provide a more accurate steering response. The third weakness of the original lane departure benefits model was that the model did not incorporate an algorithm for automated steering of LDP systems. The LDW model assumes drivers take action after the specified reaction time. However, adding a LDP system would likely increase the effectiveness since LDW could begin steering input before the driver reacts or if the driver fails to react.

The objective of this chapter was to target the first two enhancements of the original LDW benefits model. This was done by integrating real-world road departure crash data from the more recent NCHRP 17-43 Lite database into the previously developed LDW model to provide more accurate fleetwide estimates of crash and injury reduction.

4.2 METHODS

4.2.1 IMPROVED DEPARTURE CONDITIONS

The original LDW benefits model contained 478 cases from NASS/CDS 2012. All of the cases were classified as LDW applicable ran-off-road departure crashes, which excluded control loss, end departures, multisided departures, and high case weights (> 5000). The NCRHP 17-43 Lite database was composed of 567 NASS/CDS 2012 cases, which were also single vehicle road departure crashes. However, 17-43 Lite contained cases involving control loss, swerving to avoid an animal, and end departures. NCHRP 17-43 Lite also contained 62 cases which had missing or incorrect data. These were cases where the NASS/CDS scene diagrams were not to scale or important event or vehicle trajectory information was missing and no data could be collected.

The general approach for the first portion this update to the LDW benefits study was to 1) investigate how accurate the original statistical models for departure parameters were, and 2) replace the estimated departure parameters with the measured and reconstructed parameters from NCHRP 17-43 Lite. Of the 567 cases in NCHRP 17-43 Lite, only 275 had sufficient information to perform full crash reconstructions estimating departure speed. Only 202 of these fully reconstructed cases were in the original LDW benefits caselist of 478. When re-running the benefits model with the NCHRP 17-43 Lite measured parameters, 4 of the original 478 cases were flagged by the original algorithm for having high departure angles above 45 degrees. Two of these cases were identified as intersection end departure scenarios, which should have been excluded in the original caselist of 478 but were not. One constraint of the original LDW benefits trajectory model was that the departure angle could not be greater than 45 degrees to simplify the geometric simulations. The other two high departure angle cases were removed due to this constraint. These 4 cases with high departure angles were removed from this update of the LDW benefits, resulting in a total LDW applicable case count of 474 and 200 fully reconstructed cases.

To investigate the accuracy of the regression models estimating departure angle, departure speed, and departure ROC, the measured departure parameters in NCHRP 17-43 Lite were directly compared to the 50th percentile simulated values from the original models. The 17th percentile value was used as a lower bound and the 83rd percentile as an upper bound as a measure of the model accuracy. If the 17-43 Lite recorded value fell within this range, the statistical models were said to have correctly captured the true value of the departure parameter. Otherwise, the regression model was deemed to have failed to predict the correct departure speed, angle, or ROC and likely produced incorrect crash and injury probabilities for the simulation case. For this validation, all 474 cases were considered. However, only departure parameters measured in NCHRP 17-43 Lite were analyzed. For example, if a case was not reconstructed for departure speed, but still had a departure angle recorded, only a comparison between the measured and simulated departure angle would be investigated. For ROC comparisons, NCHRP 17-43 Lite was assumed to be the true measured value, and only curved roads were compared. The general interpretation of ROC is that smaller values represent more sharply curved roads, and larger values indicate straighter roads. For the datasets and models in this study, a completely straight road was coded as a ROC of 0 m.

4.2.2 Improved Injury Model

The approach for the second enhancement of the original LDW benefits model was to incorporate the reconstructed impact speeds from NCHRP 17-43 Lite into the injury criteria and trajectory model. The original injury model was a logistic regression fit using departure speed and seat belt use as predictors for driver injury outcome (MAIS3+). NCHRP 17-22 cases were used, excluding cases with high weights (> 5000), unknown belt use, and unknown departure speed. For the updated injury risk function, a similar approach was used. However, in addition to excluding cases with high weights and unknown belt use and speed, cases where the vehicle was not equipped with an airbag were not included. The simulations performed with the benefits model assume

fleetwide installment of LDW systems, so it is safe to assume that every vehicle would also be equipped with an airbag. Also, impact speed was used as a predictor instead of departure speed. The 17-22 data was used in this enhancement instead of the 17-43 Lite data because the sample size was too small to develop a robust model.

In addition to re-defining the injury regression with impact speed, the simulation trajectory model was enhanced using impact speed. The original model assumed a constant speed from the point of departure to the point of return to the roadway. Vehicle speed in the LDW benefits model primarily impacts injury outcome through the calculation of driver input or turning radius. Turning radius increases with departure speed, which means longer segments in each roadside zone and a higher probability of crash and injury. Since vehicle speed likely changes between the POD and start of steering input, the proposed improvement was to add a deceleration term to the model and compute turning radius based on the vehicle speed at start of steering—not POD. The deceleration rate was estimated through the kinematic relationship shown in Equation 20. Here, a is the deceleration rate, v_{imp} is the first event impact speed, v_{dep} is the departure speed, and d is the segment distance. The speeds and segment length were taken from the NCHRP 17-43 Lite reconstructions.

$$a = \frac{v_{imp}^2 - v_{dep}^2}{2d} \qquad \textbf{Equation 20}$$

The speed at the start of steering was then calculated as shown in Equation 21, where v_s is the speed at steering start and t_r is the simulated driver reaction time. The enhanced steering radius was then computed as previously described by replacing departure speed with this new speed at the start of steering input.

$$v_s = v_{dep} + a * t_r \qquad \textbf{Equation 21}$$

4.2.3 *Enhanced LDW Benefits*

The re-calculation of fleetwide LDW benefits involved simply replacing departure conditions from the statistical models with NCHRP 17-43 Lite values and adding the acceleration term into the trajectory model. However, since only 200 of the cases in the original benefits caselist were fully reconstructed, two different approaches were taken. The first iteration involved estimating benefits for only the 200 cases with reconstructed departure and impact speeds to obtain the most accurate results. The second iteration involved including all 474 LDW applicable cases from the original benefits study to maximize sample size. Departure angle, departure speed, and ROC were substituted when possible. For simulation cases where departure speed was unknown or not reconstructed, the statistical models were used. For the injury model enhancement, when impact speed was unknown or not reconstructed, the regression model prediction for departure speed was used since there was no regression fit for impact speed developed in the original study. Also, since impact speed was missing for these cases, the deceleration magnitude could not be computed. The median rate from the cases that were reconstructed was used to fill in these missing parameters.

In both iterations, shoulder width and driver reaction time simulations remained consistent with the original ranges. These revisions resulted in improved accuracy and a reduction in simulation size and time. A case that was fully reconstructed, for example, would only have 1 angle * 1 speed * 1 ROC * 2 reaction times * 2 shoulder widths = 4 simulations total compared to 108.

4.3 Results

4.3.1 *Validation of Previous Models*

The following plots compare the original regression models with the NCHRP 17-43 Lite data. Figure 58 illustrates the relationship between the reconstructed NCHRP 17-43 Lite departure speeds and the predicted 50th percentile speeds from the statistical model. The plot shows departure speed

was underestimated by about 22% using the mathematical models in the original LDW benefits analysis. The average difference between the predicted 17th and 83rd percentile departure speed was 38 kph. Based on the lower and upper bound defined by the 17th and 83rd percentile values, the model captured the reconstructed departure speed 56% of the time.

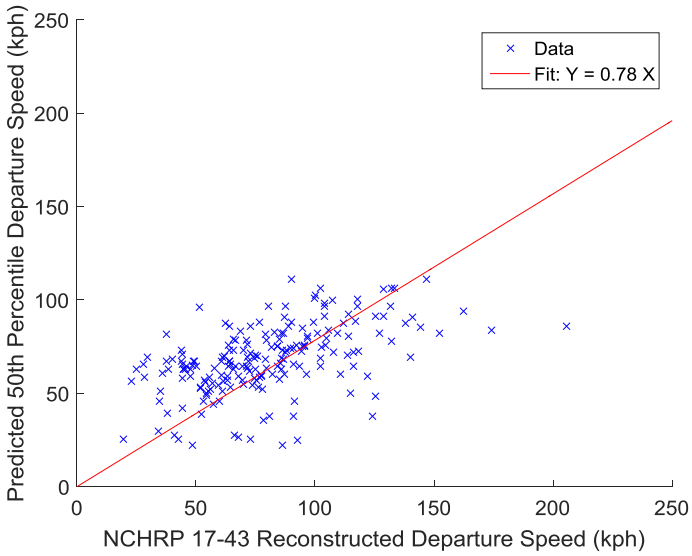

Figure 58. Departure Speed Validation using NCHRP 17-43 Lite Values (n = 200)

The validation of departure angle is shown in Figure 59. The 50th percentile departure angle underpredicted the measured NCHRP 17-43 Lite departure angle by 55%. The average difference between the 17th and 83rd percentile for departure angle was only 1 degree. Due to this narrow range and the underestimation, the measured 17-43 Lite departure angle was between the lower and upper bound in only 6% of the cases.

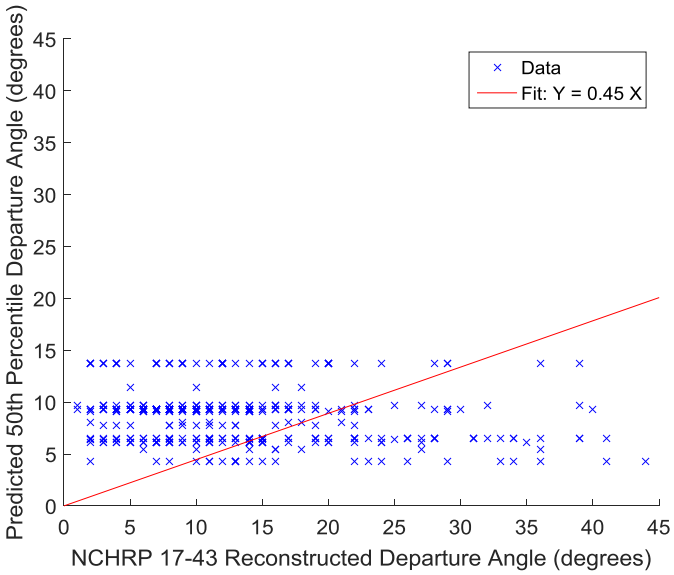

Figure 59. Departure Angle Validation using NCHRP 17-43 Lite Measured Values (n = 413)

Figure 60 shows the comparison of ROC between the statistical model predictions and measured 17-43 Lite values. ROC had the worst agreement of the three departure parameters, showing almost no correlation or trend. The mathematical models did not correctly predict any of the ROC values based on the 17th and 83rd percentile range. Over half (62%) of the cases contained straight roads. The plot shows 39 cases along the x-axis, where the model predicted a straight road (0 m), but NCHRP 17-43 Lite measured a curved road at departure. Many of these discrepancies are likely due to interpretation error during data collection of roadway alignment, especially for transition cases where the vehicle departed as it was entering a curve from a straight section, or exiting a curve to a straight section. For the cases where the regression models predicted a non-zero ROC, the measured 17-43 Lite ROC was overestimated 89% of the time.

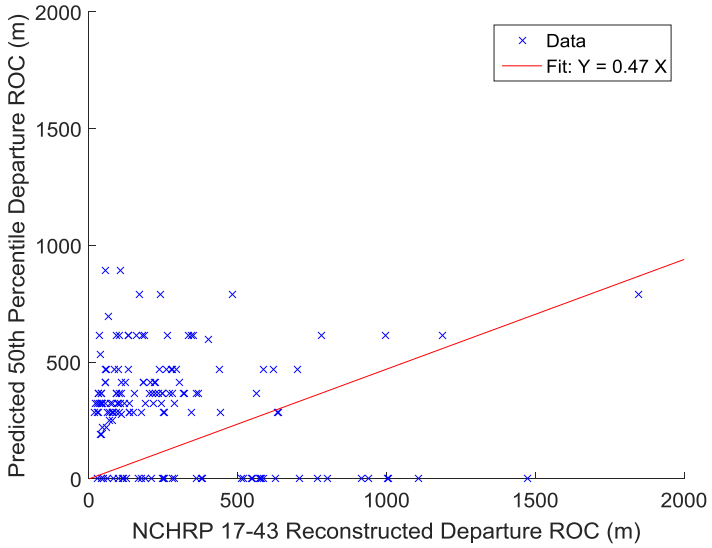

Figure 60. Departure ROC Validation using NCHRP 17-43 Lite Measured Values (n = 155)

4.3.2 IMPROVED INJURY MODEL

The enhanced injury model used belt use and impact speed as predictors for serious MAIS3+ driver injury given a crash occurred. The model equation is shown in Equation 22, where p is the probability of serious driver MAIS3+ injury given a crash, v_{imp} is the first impact speed, and *belt* is the belt use. As in the original regression, a value of 1 indicates the driver was belted and 0 indicates the driver was unbelted.

$$p = \frac{1}{1 + \exp\left(-\left(-1.5061 + 0.0156 * v_{imp} - 1.3333 * belt\right)\right)} \qquad \textbf{Equation 22}$$

The fit statistics and data summary of this enhanced injury model showed it was an improvement to the original model using departure velocity. The c-statistic, or the area under the Receiver Operator Characteristic curve, is a measure of model discrimination with a value between 1 and 0. A value of 1 indicates a perfect fit, while a value of 0.5 indicates the model prediction is no better than a random guess. The original model had a c-statistic of 0.71, while the improved model

had a statistic of 0.73. Also, the fit summary showed all three coefficients in the new model had higher statistical significance compared to the levels of the original model.

4.3.3 Updated Benefits Integrating Real-World Crash Data

The first iteration of the revised LDW benefits involved using only 200 cases that were fully reconstructed and common between the original benefits caselist and the NCHRP 17-43 Lite caselist. This produced more accurate effectiveness estimates for each of these cases since all of the departure parameters besides shoulder width and reaction time were a single measured value. However, this also limited the sample size to less than half of the original case count. Without LDW, the simulation dataset accounted for a weighted 67,024 road departure crashes. The simulation estimated 9,287 of these could have been prevented if the vehicles were equipped with LDW. This resulted in a 10.9% effectiveness. Similarly for injury, 2,099 of the estimated 18,989 serious driver injuries (MAIS 3+) could have been potentially avoided with LDW—an 11.1% reduction. The benefits model also estimated that, given a LDW, drivers would have had enough time and space to correct the vehicle trajectory without ever leaving the paved surface in 4,338 of the crashes. These non-departure simulations accounted for 59.6% of the total LDW effectiveness. These predicted benefits using only the 200 common and fully reconstructed cases were significantly lower than the original LDW benefits stated in [59] of 28.9% of all crashes and 24.3% of all seriously injured drivers (MAIS 3+). Although these percentages from the original study were based on the full 478 caselist, re-running the original model using the same 200 cases resulted in similar effectiveness values—28.2% reduction in crashes and 26.5% in seriously injured drivers (MAIS 3+).

The second simulation used all but 4 of the original benefits cases due to end departures and non-applicable high angle departures. The effectiveness of LDW systems in the U.S. fleet was re-evaluated. The drawbacks of this second iteration were that 274 of the cases relied on the original departure speed regression model, 61 relied on the departure angle model, and 25 relied on the ROC

model. Since the validation showed that the regression model predictions generally resulted in less severe departure parameters, the simulation effectiveness would be skewed towards the estimates of the original LDW benefits analysis. The total number of weighted crashes for this second iteration of the update was 146,099. After running the simulations assuming LDW was equipped, 16.1% of these crashes were avoided. For seriously injured drivers (MAIS 3+), 6,519 of the estimated 44,588 injuries were prevented when simulating the crashes with LDW. This resulted in a 14.6% reduction of injuries. As with the first iteration using only 200 cases, a large percentage of the benefits came from cases where the vehicle would have never departed the paved surface given a LDW. This second iteration found that in 16,224 of the total crashes prevented, the driver would have been able to react to the warning and retain the vehicle on the roadway, accounting for 68.9% of the overall effectiveness.

Table 8 summarizes the predicted fleetwide LDW benefits for each of the described methods. As hypothesized, the more severe departure parameters measured in NCHRP 17-43 Lite resulted in significantly lower overall effectiveness compared to the original study relying entirely on the statistical regression models.

Table 8. Fleetwide LDW Benefits based on NASS/CDS 2012 Simulation Cases

Measure	Original Benefits (n = 478)	Updated Benefits (n = 200)	Updated Benefits (n = 474)
Crashes without LDW	147,662	67,024	146,099
Crashes with LDW	105,050	59,737	122,548
Effectiveness, Crashes	28.9 %	10.9 %	16.1 %
Injured drivers (MAIS 3+) without LDW	30,337	18,989	44,588
Injured drivers (MAIS 3+) with LDW	22,972	16,890	38,069
Effectiveness, Injuries	24.3 %	11.1 %	14.6 %

4.4 DISCUSSION

It is important to note some of the assumptions and limitations of this study and the simulation approach. One key assumption made in regard to LDW was at what point in the departure event the system delivered warnings to the drivers. As seen in the NCAP test discussed previously, a LDW system can pass if the warning is delivered anywhere between 0.75 m prior to crossing the lane boundary and 0.3 m after crossing. However, for the benefits model, it was assumed that LDW was delivered the instant the leading edge of the vehicle crossed the lane boundary. In production systems, if there was variability in when the warning is delivered, there may be an increase or decrease in effectiveness compared to the predicted values of this analysis. Also, the LDW is only effective if the driver takes adequate action to correct the vehicle trajectory. If a driver is too slow or fails to react to a LDW, a departure and crash are inevitable. The simulation model assumes drivers take sufficient action within published reaction times for drivers in avoidance situations.

Other assumptions include driver acceptance and road conditions. As discussed with the NDS studies, drivers are not always accepting of active safety systems if they are prone to false alarms or the drivers determine they are unnecessary. The fleetwide benefits model assumes every vehicle in the U.S. will be equipped with LDW and the system will remain activated. Drivers who disable the system due to annoyance will gain no benefits. Also, the effectiveness relies on the ability to detect lane boundaries. If there are no lane lines or the road is covered in snow, the LDW system will have difficulties determining when the vehicle is departing the roadway.

One important factor in determining whether or not a crash could have been avoided was the number of lanes crossed and shoulder width. The two updates estimated approximately 60-70% of the overall LDW effectiveness came from cases where LDW was delivered upon lane departure, and there was sufficient adjacent roadway space for the driver to react and prevent a road departure from occurring. Additional lateral area provides the driver more time to correct the trajectory before

leaving the paved lanes or shoulder. However, as with the original study, this update assumed that no vehicles or objects were present in adjacent lanes to inhibit the use of the additional lateral paved space beyond the marked lane of travel.

It is not surprising the effectiveness of LDW systems decreased when incorporating NCHRP 17-43 Lite parameters into the original benefits simulations. The injury risk and simulation models were based on the input departure parameters such as departure and impact speed, departure angle, and ROC. The validation of the regression models showed NCHRP 17-43 Lite road departure crashes occurred at higher departure speeds and steeper departure angles than previously predicted. Also, the roads were more curved at the POD. Integrating these three parameters into the benefits model resulted in the simulation of much more severe road departure crashes compared to the original benefits model simulations. Since the original LDW benefit models were underestimating the severity of the crashes, the number of serious driver injuries (MAIS 3+) and crashes were certain to increase. This is portrayed in Table 8. For the updated benefits column using all but 4 of the same 478 cases in the original benefits study, the number of injured drivers with and without LDW actually increased even though fewer cases were analyzed.

An alternate perspective to these LDW fleetwide benefits is to analyze the ineffectiveness of these systems. The original model estimated that in over 70% of single vehicle road departure crashes, LDW active safety systems would be completely ineffective and provide no benefits in terms of avoiding crashes or mitigating driver injury. According to the updated model, this ineffectiveness would be over 80%. One argument that could be made based on the characterizations of lane and road departures in this thesis is that LDW systems are not the solution for ran-off-road departure crashes. In the drift-out-of-lane departures analyzed in Chapter 2, the median departure angle was about 0.5 degrees. However, the median departure angle for the road departure crashes analyzed in Chapter 3 was closer to 11 degrees. The other departure characteristics also suggest a higher severity

of road departure crashes. In departures with more severe departure parameters, the driver may not have been able to react appropriately, regardless of whether or not LDW was delivered. Even when considering LDP, the automated steering input may not be strong enough to correct the vehicle trajectory. For both LDW and LDP systems, it is uncertain whether or not a steep departure angle would register as a valid departure. In these scenarios, the lane tracking system could potentially perceive this high angle as a false positive and decide not to intervene.

4.5 CONCLUSIONS

This update identified three weaknesses in the original LDW U.S. fleetwide benefits model. The first weakness was that the model inputs, or departure parameters, were predicted from regression models with low correlation. The second portion of the model that could be improved was the injury criteria and trajectory model. Finally, the original LDW model did not incorporate the impact of LDP on fleetwide benefits. The improvements made in this chapter target the first two possible enhancements. Future research should also aim to add a LDP model to the benefits computation.

Enhancements made to the original LDW model in this thesis resulted in a sharply reduced estimate of LDW effectiveness. The NCHRP 17-43 Lite data used to replace mathematical regression models of departure parameters arguably increased the accuracy of the predicted benefits, and certainly reduced the simulation size and time. However, the validation of predicted and measured departure parameters suggests that the original models substantially underestimated the severity of these road departure crashes. Higher departure velocities, steeper departure angles, and more sharply curved roads make it more difficult for drivers to recover and avoid a crash and serious injury, even with a LDW.

The two iterations of the LDW benefits update aimed to strike a balance between using the most accurate departure input parameters and maintaining a large case count. The first iteration of

using only 200 completely reconstructed and common cases with the original benefits caselist resulted in a 10.9% reduction in road departure crashes, and an 11.1% reduction in seriously injured drivers. The second iteration of using all 474 LDW applicable crashes resulted in a higher 16.1% crash and 14.6% injury effectiveness. While the second iteration of the update resulted in benefits closer to the original study, this was to be expected since the original departure parameter models were used to fill in missing measurements in NCHRP 17-43 Lite.

5 CONCLUSIONS

5.1 RESEARCH CONCLUSIONS

5.1.1 RESEARCH INTRODUCTION

Lane and road departure crashes remain a large threat to the U.S. driving population. Road departure crashes alone account for nearly 1/3rd of traffic fatalities each year in the U.S. In response, automakers have been developing and installing lane departure warning (LDW) and prevention (LDP) safety systems into the vehicle fleet. However, driver acceptance of LDW and LDP systems has been lower than expected and opportunities exist to improve both systems.

This thesis aimed to better understand the implications of lane departure safety systems in the U.S. vehicle fleet through the characterization of lane and road departures. The research had three specific objectives: 1) the characterization of normal lane keeping behavior and lane departures using naturalistic driving study (NDS) data, 2) the characterization of real-world road departure crashes, and 3) the enhancement of a LDW benefits model using real-world crash data.

5.1.2 CHARACTERIZING LANE DEPARTURES THROUGH NATURALISTIC DRIVING STUDY DATA

This thesis used two separate NDS datasets to quantify normal driving through the relationship of lateral velocity and DTLB. It was determined that lane keeping behavior changes with road characteristics. As roads become more sharply curved and lanes become narrower, drivers tend to deviate further from the lane center. However, as drivers approach the lane boundary, lateral velocity tends to decrease. These results suggest lane departure systems should consider dynamic algorithms that account for changes in road features and driver behavior.

The studies helped identify some of the characteristics of LDW systems which may cause driver annoyance. Our analysis of normal lane keeping behavior distributions showed that some

drivers frequently drive in close proximity to the lane boundary, and occasionally drift out of lane unintentionally. These minor lane excursions may be perceived by the driver as normal behavior, but the LDW system may identify the lateral drift as a potentially dangerous situation and deliver a warning. These nuisance alarms may encourage the driver to disable the system, resulting in no benefits.

5.1.3 Characterizing Road Departure Crashes through Real-World Crash Data

In contrast to normal lane keeping and minor lane departures, Chapter 3 characterized road departure crashes using real-world crash data. Many in depth crash databases such as NASS/CDS do not collect details about the roadside or impacted objects in single vehicle ran-off-road departure crashes. There is a need for supplemental roadside documentation to understand road departure crashes. This research project developed and validated a supplemental road departure database, called the NCHRP 17-43 Lite database, including reconstruction methods for impact and departure speeds. The 17-43 Lite dataset contains over 500 single vehicle road departure crashes and has great potential to supplement NASS/CDS in the analysis of road departure crashes.

Characterizing the road departure crashes in this dataset illustrated how different these scenarios are from the minor drift out of lane departures analyzed in normal driving. The departure conditions were much more severe, as reflected by the reported crash and injury outcome. Analysis of the NCHRP 17-43 Lite parameters demonstrated the differences in crash characteristics for various types of impact events, such as poles/trees and rollovers. Although the 17-43 Lite dataset contains 567 NASS/CDS 2012 cases, fewer than half of them could be fully reconstructed due to a lack of complete post-crash scene and vehicle inspection by NASS/CDS investigators. Expanding this dataset to more NASS case years would increase the sample size and allow for more detailed analyses on the road departure crashes by impact type.

Regardless of the small sample size, comparison of the NCHRP 17-43 Lite departure data with the older NCHRP 17-22 data showed good agreement between departure speed, departure angle, and impact speed. One concern was that the reconstruction methods in both NCHRP datasets relied on NASS/CDS reconstructed ΔV, which has been found to underestimate true ΔV by about 15% [48]. Our validation with event data recorder (EDR) data confirmed a similar underprediction of 11% using cases from the 17-43 Lite dataset. Despite this bias, comparing EDR pre-crash speed profiles to the reconstructed NCHRP 17-43 Lite departure and impact speeds showed relatively good agreement. Our comparison of the 17-43 Lite and 17-22 data, combined with our validation of 17-43 Lite with EDR cases gave us confidence that the reconstruction methods used were valid.

5.1.4 Improvements to the LDW System Fleetwide Safety Benefits Model

The development of NCHRP 17-43 Lite dataset was critical in developing enhancements to the original LDW fleetwide safety benefits model. The original model relied heavily on mathematical regression models to approximate critical roadside parameters, e.g. radius of curvature and departure velocity. The direct measurement of these parameters in NCHRP 17-43 Lite meant that these parameters could be greatly improved. Two of the three components of the original LDW model identified in this chapter as areas in need of enhancement were completed.

The dependence of the original LDW fleetwide benefits model on statistical regression models to predict departure parameters was the first to be corrected. These models with low correlation coefficients were replaced with measured NCHRP 17-43 Lite departure parameters when possible. This improved the model accuracy and reduced the number of simulations required for each case. The second update involved improvements to the injury criteria. Impact speed was hypothesized to be a better predictor of injury than departure speed, since vehicle speed can change significantly between the POD and impact. A new injury logistic regression was developed to predict the probability of serious MAIS3+ driver injury given a crash based on impact speed and belt use. In

addition to a new regression, impact speed was used to better predict the steering radius input and simulated vehicle trajectory.

These two enhancements alone sharply reduced simulation time and improved accuracy of the predicted benefits by replacing a large portion of the predictive models with measured values from real-world crashes. However, the enhancements also significantly decreased the predicted effectiveness of LDW systems. This can largely be attributed to the significant underestimation of departure angle, speed, and road radius in the original benefits as shown in the validation of the statistical models. The more severe crash characteristics resulted in a higher number of crashes and serious injuries in the LDW simulations. The crash prevention dropped from 29% to 11-16% with the enhancements. For seriously injured drivers, the reduction rate declined from 24% to 11-15% with the modifications. Although a model of LDP was not added in this thesis, the automated steering would certainly increase benefits by beginning steering input before some drivers could react to LDW.

5.2 Publication Plan

A portion of the research in this thesis was published in a peer-reviewed conference publication and journal publication. The two papers are listed below:

- "Investigation of Driver Lane Keeping Behavior in Normal Driving based on Naturalistic Driving Study Data." *SAE Int. J. Trans. Safety* [65]
- "Driver lane keeping behavior in normal driving using 100-car naturalistic driving study data." IEEE Intelligent Vehicles Symposium [66]

5.3 Future Directions

Each chapter of this thesis contains content that could be readily extended to additional studies and datasets. The methodology established to track normal lane keeping could be applied to

any NDS study with lane tracking data available. As lane tracking systems and software become more developed, it would be interesting to analyze data with more diverse road and driver demographics. The normal driving and lane keeping behavior analysis primarily focused on the effect of lane width and road curvature. However, there are numerous other factors such as sex, age, time of day, road type, and traffic density that could be investigated to determine how driving behavior changes. These studies on normal lane keeping behavior could help guide development of future LDW systems. By understanding how normal driving behavior dynamically changes with various factors, automakers can better predict departures outside of normal lane keeping to reduce the number of false alarms and driver annoyance.

As previously discussed, the NCHRP 17-43 Lite dataset is a powerful tool for supplementing road departure analyses. The restriction to a single case year, however, restricts the number of road departures available for data collection and reconstructions. The data collection and reconstruction process should be extended to more recent years, and continuously updated to ensure vehicles being used in analyses are equipped with more recent safety technologies.

The older safety systems and vehicle crash characteristics of the NCHRP 17-22 dataset may not be the most relevant data to use for studies such as the LDW benefits algorithm. Automakers are looking to the future for predictions and insight on where vehicle safety will be in 5, 10, 20 years down the road. Appropriate assumptions should be made when developing predictive models. If an algorithm is developed to determine potential fleetwide benefits of an advanced safety system, it should be assumed that basic safety features such as airbags will be equipped in every vehicle.

To complete the update to the original LDW fleetwide benefits model, the third enhancement of adding LDP to the vehicle trajectory model should be completed. LDP would reduce the probability a crash or injury occur because the system could intervene and provide automatic steering earlier

than the driver could respond. The main considerations when adding a LDP model should be when the steering begins, what the magnitude is, and the shape of the signal.

6 REFERENCES

[1] "Traffic Safety Facts 2014." National Highway Traffic Safety Administration, Washington, D.C., Report Number DOT HS 812 261, 2016.

[2] Kusano, K. D., Gabler, H. C. "Comprehensive Target Populations for Current Active Safety Systems Using National Crash Databases," *Traffic Injury Prevention*, 15:7, 753-761, 2014a. doi: 10.1080/15389588.2013.871003

[3] Gabauer DJ and Gabler HC, "Comparison of Roadside Crash Injury Metrics Using Event Data Recorders", Accident Analysis and Prevention, Vol. 40/2 pp 548-558 (2008)

[4] "FMVSS No. 126 Electronic Stability Test." National Highway Traffic Safety Administration, Washington, D.C., March 2007.

[5] Lie, A., Tingvall, C., Krafft, M., Kullgren, A. "The Effectiveness of Electronic Stability Control (ESC) in Reducing Real Life Crashes and Injuries," *Traffic Injury Prevention*, 7:1, 38-43, 2006. doi: 10.1080/15389580500346838

[6] Johnson NS and Gabler HC, "Reduction in Fatal Longitudinal Barrier Crash Rate due to Electronic Stability Control", Transportation Research Record: Journal of the Transportation Research Board, Transportation Research Board of the National Academies, No. 2521, pp 79—85 (2015)

[7] "Distracted Driving 2014." National Highway Traffic Safety Administration, Washington, D.C., Report Number DOT HS 812 260, April 2016.

[8] Olson, R. L., Hanowski, R. J., Hickman, J. S., Bocanegra, J. "Driver distraction in commercial vehicle operations," Report No. FMCSA-RRR-09-042, 2009.

[9] Scanlon JM, Kusano KD, and Gabler HC, "A Preliminary Model of Driver Acceleration Behavior prior to Real-World Straight Crossing Path Intersection Crashes Using EDRs", Proceedings of the 2015 IEEE Intelligent Transportation Systems Conference, Canary Islands, Spain (September 2015)

[10] Scanlon J, Page K, Sherony R, and Gabler HC, "Using Event Data Recorders from Real-World Crashes to Evaluate the Vehicle Detection Capability of an Intersection Advanced Driver Assistance System," SAE Technical Paper 2016-01- 1457 (April 2016)

[11] Scanlon JM, Sherony R, and Gabler HC, "Predicting Crash-Relevant Violations at Stop Sign-Controlled Intersections for the Development of an Intersection Driver Assistance System", Traffic Injury Prevention (2016)

[12] Scanlon JM, Sherony R, and Gabler HC, "Preliminary Potential Crash Prevention Estimates for an Intersection Advanced Driver Assistance System in Straight Crossing Path Crashes", Proceedings of the 2016 IEEE Intelligent Vehicle Symposium, Gothenburg, Sweden (June 2016)

[13] Scanlon JM, Kusano KD, and Gabler HC, "The Influence of Roadway Characteristics on Potential Safety Benefits of Lane Departure Warning and Prevention Systems in the U.S.

Vehicle Fleet", Transportation Research Record: Journal of the Transportation Research Board, Transportation Research Board of the National Academies, (2017)

[14] Kusano KD and Gabler HC, "Comparison of Expected Crash and Injury Reduction from Production Forward Collision and Lane Departure Warning Systems", Traffic Injury Prevention, v16:sup2, pp. S109-S114, DOI: 10.1080/15389588.2015.1063619 (2015)

[15] Kusano KD, Gabler HC, and Gorman T, "Fleetwide Safety Benefits of Production Forward Collision and Lane Departure Warning Systems," SAE International Journal Passenger. Cars - Mechanical Systems, 7(2):2014, doi: 10.4271/2014-01-0166.

[16] Kusano KD and Gabler HC, "Safety Benefits of Forward Collision Warning, Brake Assist, and Autonomous Braking Systems in Rear-end Collisions", IEEE Transactions – Intelligent Transportation Systems, 13(4), pp. 1546 – 1555, doi 10.1109/TITS.2012.2191542 (2012)

[17] Kusano KD and Gabler HC, "Potential Occupant Injury Reduction in Pre-Crash System Equipped Vehicles in the Striking Vehicle of Rear-end Crashes", Annals of Advances in Automotive Medicine, v.54, pp. 203-214 (2010)

[18] Scanlon JM, Kusano KD, Sherony R, and Gabler HC, "Potential Safety Benefits of Lane Departure Warning and Prevention Systems in the U.S. Vehicle Fleet", Proceedings of the Twenty-Fourth International Conference on Enhanced Safety of Vehicles, Paper Number 15-0080, Gothenburg, Sweden (June 2015)

[19] Kusano KD, Montgomery J, and Gabler HC, "Methodology for Identifying Car Following Events from Naturalistic Data", Proceedings of the 2014 IEEE Intelligent Vehicle Symposium, Dearborn, MI (June 2014)

[20] Chen R, Kusano KD, and Gabler HC, "Driver Behavior during Overtaking Maneuvers from the 100-Car Naturalistic Driving Study", Traffic Injury Prevention, v16:sup2, pp. S176-S181, DOI: 10.1080/15389588.2015.1057281 (2015)

[21] Kusano KD, Chen R, Montgomery J, and Gabler HC, "Population Distributions of Time to Collision at Brake Application during Car Following from Naturalistic Driving Data", Journal of Safety Research, v, 54, p. 95-104, DOI:/10.1016/j.jsr.2015.06.011 (2015)

[22] Chen R, Sherony R, and Gabler HC, "Comparison of Time to Collision and Enhanced Time to Collision at Brake Application during Normal Driving," SAE Technical Paper 2016-01- 1448 (April 2016)

[23] Reagan, I. J., McCartt, A. T. "Observed activation status of lane departure warning and forward collision warning of Honda vehicles at dealership service centers," *Traffic Injury Prevention*, 17:8, 827-832, 2016. doi: 10.1080/15389588.2016.1149698

[24] Ponziani, R. "Turn Signal Usage Rate Results: A Comprehensive Field Study of 12,000 Observed Turning Vehicles," SAE Technical Paper, Detroit, Michigan, Paper Number 2012-01-0261, 2012.

[25] "IIHS Status Report." Insurance Institute for Highway Safety, Arlington, V.A., volume 47, December, 2012.

[26] Gabler HC and Hinch J, “Feasibility of using Event Data Recorders to Characterize the Pre-Crash Behavior of Drivers in Rear-End Collisions”, Proceedings of the Twenty-first International Conference on Enhanced Safety of Vehicles, Paper No. 09-0452, Stuttgart, Germany, 2009.

[27] Noble AM, Kusano KD, Scanlon JM, Doerzaph ZR, and Gabler HC, “Driver Approach and Traversal Trajectories for Signalized Intersections Using Naturalistic Data”, Proceedings of the 95th Annual Meeting of the Transportation Research Board, Paper No. 16-1490, Washington, DC (January 2016)

[28] “Lexus 2015 NX200T Owner’s Manual.” Toyota Motor Company, User Manual No. NX200t_U_OM78006U, 2015.

[29] “The New Car Assessment Program Suggested Approaches for Future Program Enhancements.” National Highway Traffic Safety Administration, Washington, D.C., Report Number DOT HS 810 698, January 2007.

[30] “Lane Departure Warning System Confirmation Test and Lane Keeping Support Performance Documentation.” National Highway Traffic Safety Administration, Washington, D.C., 2013.

[31] Kusano KD and Gabler HC, ”Field Relevance of the New Car Assessment Program Lane Departure Warning Confirmation Test,” SAE International Journal Passenger Cars - Mechanical Systems, 5(1), doi:10.4271/2012-01- 0284 (2012)

[32] “European New Car Assessment Programme Test Protocol – Lane Support Systems.” Euro NCAP, Brussels, Belgium, v.1.0, January 2016.

[33] Kusano KD, Chen R, Tsoi A, and Gabler HC, “Comparison of Event Data Recorder and Naturalistic Driving Data for the Study of Lane Departure Events”, Proceedings of the Twenty-Fourth International Conference on Enhanced Safety of Vehicles, Paper Number 15-0149, Gothenburg, Sweden (June 2015)

[34] Montgomery J, Kusano KD, and Gabler HC, “Age and Gender Differences in Time to Collision at Braking From the 100-Car Naturalistic Driving Study”, Traffic Injury Prevention, v15:sup1, pp. 15-20, DOI:10.1080/15389588.2014.928703 (2014)

[35] Fujishiro, R., Takahashi, H. “Research on Driver Acceptance of LDA (Lane Departure Alert) System,” In *Proceedings of the 24th International Technical Conference on the Enhanced Safety of Vehicles*, Gothenburg, Sweden, Paper No. 15-0222, June 8-11, 2015.

[36] Sayer, J. R., Bogard, S. E., Buonarosa, M. L., LeBlanc, D. J., Funkhouser, D. S., Bao, S., Blankespoor, A. D., Winkler, C. B. “Integrated Vehicle-Based Safety Systems Light-Vehicle Field Operational Test Key Findings Report,” Research and Innovative Technologies Administration, U.S. DOT, Washington, D.C., Report Number DOT HS 811 416, 2011.

[37] Neale, V. L., Dingus, T. A., Klauer, S. G., Sudweeks, J., Goodman, M. "An overview of the 100-car naturalistic study and findings," National Highway Traffic Safety Administration, Washington, D.C., Paper 05-0400, 2005.

[38] Toledo, T., Zohar, D. “Modeling duration of lane changes,” *Transportation Research Record: Journal of the Transportation Research Board*, No. 1999, pp. 71-78, 2007. doi: 10.3141/1999-08

[39] Chen, R., Kusano, K. D., Gabler, H. C. "Driver Behavior During Lane Change from the 100-Car Naturalistic Driving Study," In *Proceedings of the 24th International Technical Conference on the Enhanced Safety of Vehicles*, Gothenburg, Sweden, Paper No. 15-0423, June 8-11, 2015.

[40] "Policy on geometric design of highways and streets." American Association of State Highway and Transportation Officials, Washington, D.C., 2001.

[41] "Crashworthiness Data System Overview." National Highway Traffic Safety Administration, accessed 7 November 2016 <http://www.nhtsa.gov/Data/National-Automotive-Sampling-System-(NASS)/NASS-Crashworthiness-Data-System>

[42] Mak, K. K., Sicking, D. L. “Identification of Vehicular Impact Conditions Associated with Serious Ran-off-Road Crashes,” Transportation Research Board, National Cooperative Highway Research Program (NCHRP) Report 665, 2010.

[43] Gabler, H. C., Thomson, R., Daniello, A., Johnson, N., Kusano, K., Kusano, S. “Long-Term Roadside Crash Data Collection Program, Interim Report,” Report to the Transportation Research Board, National Academies of Science, NCHRP Project 17-43, March 2012.

[44] Kononen, D., Flannagan, C., Wang, S. "Identification and validation of a logistic regression model for predicting serious injuries associated with motor vehicle crashes," *Accident Analysis & Prevention*, 43:1, pp. 112-122, 2011.

[45] “NCHRP 17-43 Lite Roadside Database – Coding Manual.” Unpublished document, Virginia Tech, Blacksburg, VA, 2016.

[46] “NCHRP 17-43 Lite Roadside Database – Data Collection Forms.” Unpublished document, Virginia Tech, Blacksburg, VA, 2016.

[47] Niehoff, P., Gabler H. C. “The Accuracy of WinSmash Delta-V Estimates: The Influence of Vehicle Type, Stiffness, and Impact Mode,” *Annals of Advances in Automotive Medicine*, Vol. 50, pp. 1540-0360, 2006.

[48] Hampton, C. E., and Gabler H. C. “Evaluation of the Accuracy of NASS/CDS Delta-V Estimates from the Enhanced WinSmash Algorithm,” *Annals of Advances in Automotive Medicine*, Vol. 54, pp. 241-252, 2010.

[49] Labra, J. J., Mak, K. K. “Development of Reconstruction Procedure for Pole Accidents,” National Highway Traffic Safety Administration, Washington, D.C., Final Report No. SWRI-11-8090, 1980.

[50] Mak, K. K., Mason, R. L. “Accident analysis – Breakaway and nonbreakaway poles including sign and light standards along highways volume III,” National Highway Traffic Safety Administration, Washington, D.C., Report Number DOT HS 805 606, 1980.

[51] Ivey, D. L., Adamson, K. S. “Speed Losses During Vehicle Overturning, Influence of Body Shape and Tripping Mechanism,” Texas: Scientific Inquiry, Inc., 2006.

[52] Erinle, O., Hunter, W., Bronstad, M., Council, F., Stewart, R. “An Analysis of Guardrail and Median Barrier Accidents Using the Longitudinal Barrier Special Studies (LBSS) File,” Federal Highway Administration, McLean V A, Final Report, Volumes 1 and 2, FHWA Publication No. FHW A-RD-92-098, 1994.

[53] Coon, B. A., Reid, J. D. "Crash reconstruction technique for longitudinal barriers," *Journal of Transportation Engineering*, 131:1, 2005. doi: 10.1061/(ASCE)0733-947X(2005)131:1(54)

[54] Coon, B. A., Reid, J. D. "Reconstruction techniques for energy-absorbing guardrail end terminals," *Accident Analysis & Prevention*, 38:1, 2006. doi: 10.1016/j.aap.2005.06.016

[55] Kusano KD and Gabler HC, “Characterization of Lane Departure Crashes Using Event Data Recorders Extracted from Real-World Collisions,” SAE International Journal Passenger. Cars - Mechanical Systems 6(2):2013, doi: 10.4271/2013-01-0730 (2013)

[56] Scanlon JM, Kusano KD, and Gabler HC, “Analysis of Driver Evasive Maneuvering prior to Intersection Crashes Using Event Data Recorders”, Traffic Injury Prevention, v16:sup2, pp. S182-S189, DOI: 10.1080/15389588.2015.1066500 (2015)

[57] Gabler HC, Hinch J, and Steiner J, Event Data Recorders: A Decade of Innovation, SAE International, Warrendale, PA (2008)

[58] Johnson NS and Gabler HC, “Evaluation of NASS-CDS Side Crash Delta-V Estimates using Event Data Recorders”, Traffic Injury Prevention, v. 15, no. 8, pp. 827-834, DOI:10.1080/15389588.2014.88199516 (2014)

[59] Kusano, K. D., Gorman, T. I., Sherony, R., Gabler, H. C. "Potential occupant injury reduction in the US vehicle fleet for lane departure warning–equipped vehicles in single-vehicle crashes," *Traffic injury prevention*, 15:sup1, 2014b. doi:10.1080/15389588.2014.922684

[60] Gorman TI, Kusano KD, and Gabler HC, “Model of Fleet-wide Safety Benefits of Lane Departure Warning Systems”, Proceedings of the 2013 IEEE Intelligent Transportation Systems Conference, The Hague, Netherlands (October 2013)

[61] Gabler HC, Weaver A, and Stitzel J, “Automotive Field Data in Injury Biomechanics”, Accidental Injury, Third Edition, Edited by Yoganandan N, Nahum AM, and Melvin JW, eds., Springer, New York, NY (2015)

[62] Mazzae E., Barickman F., Baldwin G., Forkenbrock G. “Driver Crash Avoidance Behavior With ABS in an Intersection Incursion Scenario on Dry Versus Wet Pavement,” SAE Technical Paper, Warrendale, PA, Paper Number 1999-01-1288, 1999.

[63] Suzuki, K., Jansson, H. “An analysis of driver’s steering behaviour during auditory or haptic warnings for the designing of lane departure warning system.” *JSAE Review*, 24:1, pp.65–70. 2003. doi: 10.1016/S0389-4304(02)00247-3

[64] Kozak, K., Pohl, J., Birk, W., Greenberg, J., Artz, B., Blommer, M., Cathey, L., Curry, R. "Evaluation of lane departure warnings for drowsy drivers," *Proceedings of the human factors and ergonomics society annual meeting*, Vol. 50. No. 22. Sage Publications, 2006.

[65] Johnson, T., Chen, R., Sherony, R., and Gabler, H. C. "Investigation of Driver Lane Keeping Behavior in Normal Driving based on Naturalistic Driving Study Data," *SAE Int. J. Trans. Safety*, 4(2):236-244, 2016, doi:10.4271/2016-01-1449.

[66] Johnson, T., Sherony, R., and Gabler, H. C. "Driver lane keeping behavior in normal driving using 100-car naturalistic driving study data," Intelligent Vehicles Symposium (IV), 2016 IEEE. IEEE, 2016. doi:10.1109/IVS.2016.7535390.